ISTANBUL TECHNICAL UNIVERSITY ★ GRADUATE SCHOOL OF SCIENCE ENGINEERING AND TECHNOLOGY

MULTI-SCALE SELF-HEALING NANOCOMPOSITE SHIELDING MATERIAL FOR AEROSPACE

Ph.D. THESIS

Tayfun BEL

Department of Metallurgical and Materials Engineering

Metallurgical and Materials Engineering Programme

JANUARY 2018

ISTANBUL TECHNICAL UNIVERSITY ★ GRADUATE SCHOOL OF SCIENCE ENGINEERING AND TECHNOLOGY

MULTI-SCALE SELF-HEALING NANOCOMPOSITE SHIELDING MATERIAL FOR AEROSPACE

Ph.D. THESIS

Tayfun BEL
(506102417)

Department of Metallurgical and Materials Engineering

Metallurgical and Materials Engineering Programme

Thesis Advisor: Prof. Dr. Cüneyt ARSLAN
Thesis Co-Advisor: Prof. Dr. Nilgün BAYDOĞAN

JANUARY 2018

ISTANBUL TEKNİK ÜNİVERSİTESİ ★ FEN BİLİMLERİ ENSTİTÜSÜ

HAVACILIK VE UZAY İÇİN KENDİNİ ÇOK BOYUTTA ONARABİLEN NANOKOMPOZİT ZIRH MALZEMESİ

DOKTORA TEZİ

Tayfun BEL
(506102417)

Metalurji ve Malzeme Mühendisliği Anabilim Dalı

Metalurji ve Malzeme Mühendisliği Doktora Programı

Tez Danışmanı: Prof. Dr. Cüneyt ARSLAN
Eş Danışman: Prof. Dr. Nilgün BAYDOĞAN

OCAK 2018

Tayfun BEL, a Ph.D. student of İTU Graduate School of Science Engineering and Technology student ID 506102417, successfully defended the thesis entitled "MULTI-SCALE SELF-HEALING NANOCOMPOSITE SHIELDING MATERIAL FOR AEROSPACE", which he prepared after fulfilling the requirements specified in the associated legislations, before the jury whose signatures are below.

Thesis Advisor :	**Prof. Dr. Cüneyt ARSLAN** İstanbul Technical University	.....
Co-advisor :	**Prof.Dr. Nilgün BAYDOĞAN** İstanbul Technical University	.....
Jury Members :	**Prof. Dr. İsmail DUMAN** Istanbul Technical University	.....
	Doç. Dr. Hüseyin KIZIL Istanbul Technical University	.....
	Prof.Dr. Ayben KİLİSLİOĞLU Istanbul University	.....
	Doç.Dr. Serco Serkis YEŞİLKAYA Yıldız Technical University	.....
	Yrd.Doç.Dr. Pelin Sarıtepe OTANSEV Istanbul University	.....

Date of Submission : 29 December 2017
Date of Defense : 15 January 2018

To my FATHER and FAMILY,

FOREWORD

Tayfun BEL thanks to his proffessors Prof. Dr. Cüneyt ARSLAN and Prof. Dr. Nilgün BAYDOĞAN for their constant suport.

Tayfun BEL thanks to BIDEB (Bilim Insani Destekleme Daire Baskanlıgı) 2211-C program of The Scientific and Technological Research Council (TUBITAK) of Turkey.

Tayfun BEL thanks to ARDEB for their support in 115R017 project of The Scientific and Technological Research Council (TUBITAK) of Turkey.

Tayfun BEL thanks to ITU BAP for their financial support.

Tayfun BEL thanks to Japan Aerospace Exploration Agency (JAXA) for their space qualification supports.

Tayfun BEL thanks to ITU Prof.Dr. Adnan Tekin Materials Science and Production Technologies Applied Research Center (ATARC) personel at the production and the characterization processes of the polymer.

December 2017 Tayfun BEL

TABLE OF CONTENTS

Page

ABBREVIATIONS

AFB : Air Force Base
AFOSR : Air Force Office of Scientific Research
ATRP : Atom Transfer Radical Polymerization
Bu4NBr : Tetra-n-butylammonium bromide
CMT : Colemanite
CNT : Carbon nanotubes
CuBr : Copper(I) bromide
DFRC : Dryden Flight Research Center
EBiB : Bromoisobutyrate
ERI : Eril Research, Inc.
GMA : Glycidyl methacrylate
HAP : High Alltitude Platform
HNTs : Halloysite clay nanotubes
HVL : Half-value layer
ISRL : The International Space Radiation Laboratory
LbL : Layer-by-Layer
LEO : Low Earth Orbit
MF : Melamine Formaldehyde
MK : GMA loaded microspheres
MMA : Methyl methacrylate
MMT : Montmorillonite clay nanoplates
NIRS : Japanese National Institute of Radiological Sciences
PAA : Poly(acrylic acid)
PAH : Polyallylamine hydrochloride
PGMA : Poly(glycidyl methacrylate)
PMDETA : Pentamethyldiethylenetriamine
PMMA : Poly(methyl methacrylate)
PS : Polystyrene
PVA : Poly(vinyl alcohol)
SDBS : Sodium Dodecyl Benzenesulfonate
SPEEK : Suffocated poly(ether ether ketone)
UAV : Uninhabited aerial surveillance vehicle

SYMBOLS

μ	: Attenuation Coefficient
μ_{mass}	: Mass Attenuation Coefficient

LIST OF TABLES

Page

LIST OF FIGURES

Page

MULTI-SCALE SELF-HEALING NANOCOMPOSITE SHIELDING MATERIAL FOR AEROSPACE

SUMMARY

In the past two decades, the attention of researchers shifted from intellectual to experimental studies that are appliance-directed (Portale, Hermida-Merino, & Bras, 2016). The area of polymeric radiation shielding materials is highly underrated as it has great application potential. Polymer shielding materials offer advantages such as enhanced homogenous shielding, flexibility, and lower weight relative to metallic shielding materials (Håkansson, Amiet, Nahavandi, & Kaynak, 2007). Such improvement is essential for the protection of astronauts, spacecraft, and payloads from radiation damage in long-term space missions (Emmanuel & Raghavan, 2016; Pohl & Britt; Slaba et al., 2017).

Poly(methyl) methacrylate (PMMA) is a thermoplastic polymer with exceptional mechanical properties. (PMMA) $(C_5O_2H_8)n$ is widely used in the automotive and aerospace industry. PMMA is used in aircraft windshields, radar screens, and telescope production (Hu et al., 2016). Polymer's functionality such as magnetic, optical, and mechanical properties can be enhanced through the incorporation of inorganic nanomaterials into the polymer matrix. Changes in properties of the polymer depend on filler type and preparation method of the nanocomposite (Chang et al., 2008).

One of the main reasons for polymer degradation is chain scission under radiation energy (I. H. Kim, Cho, Bae, Park, & Chung, 2003). This deterioration creates both new radicals and the macromolecules. The living polymer produced with the ATRP method has a potential advantage as the living matrix might allow self–healing from the damage induced by ionizing, ultraviolet, and electromagnetic radiation. The living polymer can induce recombination between new radicals and the macromolecular on the end of the matrix chain (Ming Qiu Zhang & Rong, 2011b; Zhu, Rong, & Zhang, 2015). For this reason, PMMA living polymer synthesized by ATRP was chosen as the matrix material of reinforced nanocomposites.

In this study, the content of GMA loaded microspheres (MK) and Halloysite clay nanotubes (HNTs), as well as Montmorillonite clay nanoplates (MMT) and Colemanite (CMT), were optimized in a living PMMA matrix to achieve maximum radiation-shielding capacity while keeping the mechanical properties and the self-healing capacity. For maximum efficiency, a multiphase autonomous self-healing approach was followed. First, the most promising nanocomposite compositions have been determined by applying the hardness, impact, flexural, and compression tests for mechanical shielding applications. Samples are tested for shielding gamma and neutron radiation for radiation shielding properties. Thus, it is determined how to produce a multiphase self-healing nanocomposite shielding material for aerospace.

HAVACILIK VE UZAY İÇİN KENDİNİ ÇOK BOYUTTA ONARABİLEN NANOKOMPOZİT ZIRH MALZEMESİ

ÖZET

Son yirmi yılda, araştırmacılar, çalışmalarını, teorik çalışmalardan deneysel çalışmalara dönüştürmeyi amaçlamışlardır (Portale, Hermida-Merino, & Bras, 2016). Polimerik radyasyon zırh malzemeleri, geniş bir uygulama potansiyeline sahip olmasına rağmen yeterince çalışılmamaktadır. Polimer radyasyon zırh malzemeleri, metalik zırh malzemlerine göre homojen zırhlama, esneklik ve daha düşük ağırlık gibi avantajlar sunmaktadır (Håkansson, Amiet, Nahavandi, & Kaynak, 2007). Bu tür iyileştirme astronotların uzun sürecek görevlerinde radyasyon hasarından uzay aracının ve yüklerin korunması için gereklidir (Emmanuel & Raghavan, 2016; Pohl & Britt; Slaba ve diğ., 2017).

Kendini onaran malzemeler dışardan bir müdahale ile (yamalama, yapıştırma, kaynaklama vb.) ihtiyaç duymadan oluşan hasarları onarma kapasitesine sahip malzemlerdir. Otonom kendini onaran malzemeler, dışardan bir müdahaleye ihtiyaç duymazlar. Otonom olmayan kendini onarma mekanizmalarıda mevcuttur. Bu tip otonom olmayan kendini onaran malzemlerde kendini onarma ışık veya ısı gibi bir tetik ile başlamakta ve malzeme kendini onarmaya tetiklendikten sonra başlamaktadır. Kendini onaran malzemeler dahil oldukları sistemin ömrünü uzatmakta, sistemin güvenliğini artırmakta ve bakım masraflarını düşürmektedir(Chang ve ark., 2008).

Poli (metil) metakrilat (PMMA) olağanüstü mekanik özelliklere sahip bir termoplastik polimerdir. (PMMA) $(C_5O_2H_8)_n$, otomotiv ve havacılık endüstrisi tarafından yaygın olarak kullanılmaktadır. PMMA, hava aracı ön cam panelde, radar ekranında ve teleskop üretiminde kullanılmaktadır (Hu ve diğerleri, 2016). Manyetik, optik ve mekanik özellikler; inorganik nanomalzemelerin polimer matrisine dahil edilmesiyle geliştirilebilir. Polimerin özelliklerinde meydana gelen gelişmeler, dolgu maddesi türüne ve nanokompozitin hazırlanma yöntemine bağlı olarak değişmektedir (Chang ve diğ., 2008).

Polimer yapının bozulmasının başlıca sebepleri arasında, çeşitli uygulamalardaki görevleri süresince, iyonizan radyasyona maruz kalan polymer zincirinin kopması sayılabilmektedir (IH. Kim, Cho, Bae, Park, & Chung, 2003). Polimerde oluşan bu bozulma, hem yeni radikaller ve makromoleküller yaratabilmektedir. Canlı polimer matris, iyonizan elektromanyetik radyasyon sonucu oluşan hasar karşısında da kendi kendine iyileşmeye izin verebilmektedir. Dolayısıyla, ATRP yönteminin kullanılması, bu doktora tez çalışması kapsamında üretilen canlı polimerin oluşrulmasında, potansiyel bir avantaj olarak kabul edilmiştir. Çünkü, ATRP yönteminin kullanılması, canlı polimer matriks zincirlerinin sonundaki makromoleküler ve yeni radikaller arasında rekombinasyonu etkileyebilmektedir (Ming Qiu Zhang & Rong, 2011b; Zhu, Rong, & Zhang, 2015). Bu sebeple, bu doktora tez çalışmasında, polimer matris malzemesi olarak, ATRP yöntemi ile sentezlenen, PMMA canlı polimer üretimi tercih edilmiştir.

Atom Transfer Radikal Polymerizasyon (ATRP) tekniği ile üretilen canlı polimerin diğer bir kendini onarma mekanizması, oluşan bir çatlağın etkisiyle kırılan monomer yüklü mikrokapsüllerin canlı polimer matris içinde kapiler etki ile yayılarak kendini onaramayı tetiklemesidir. Kendini onarma ajanının çatlak yüzeyini kaplamasıyla katılaşma başlar, çatlak bölgesi dolar ve nihai olarak, katılaşır. Sonuç olarak; çatlak onarılmış olur (Ming Qiu Zhang & Rong, 2011b; Zhu, Rong, & Zhang, 2015). Bu sebeple, bu doktora tez çalışmasında, polimer matris malzemesi olarak, ATRP yöntemi ile sentezlenen, PMMA canlı polimer üretimi tercih edilmiştir.

Bu çalışmada, canlı PMMA matrisinde optimize edilmiş, kendini onarma sıvısı Glycidyl Methacrylate (GMA) yüklü mikroküreler (MK) ve Halloysite kil nanotüpler (HNT'ler), Montmorillonit (MMT'ler) kil nanolevhalar ve Kolemanite (CMT) ilave edilmiştir. GMA, MK, HNTs ve MMTs olarak 4 farklı dolgu malzemesi kullanılarak, malzemeyi ağırlaştırmadan ve iyonizan radyasyonu zırhlama kapasitesinden ödün vermeden, mekanik özelliklerdeki geliştirilmeler mukayeseli olarak değerlendirilmiştir. Böylece, canlı polimerin kendini onarma özelliğinde, maksimum verimlilik elde etmek için, çok yönlü (3 boyutta), özgün, kendini iyileştirme kapasitesine sahip termoplastik yapılar incelenmiştir.

Öncelikle, mekanik özelliklerde en umut verici nanokompozit zırh kompozisyonu; sertlik, darbe, eğilme ve basma testleri uygulanarak belirlenmiştir. Seçilen kompozisyona, gama ve nötron transmisyon deneyleri yapılmış ve zırhlama

potansiyeli belirlenmiştir. Böylece, havacılık uygulamaları açısından cazip, dışarıdan herhangi bir müdahale olmaksızın çok yönlü (3 boyutta) kendi kendini iyileştirebilen, nanokompozit zırh malzemesinin üretim parametrelerine ilişkin detaylar belirlenmiştir.

1. INTRODUCTION

1.1 Literature Review

1.1.1 Satellite systems

Today low earth orbit satellite systems are becoming the primary satellite component of the third generation private mobile communication networks and military command and control infrastructure (Collier, 2008; Fadel, Tohme, & ieee, 2004; Mourad, Al-Bassiouni, Emam, & Al-Hussaini, 2001). The most significant workload of such networks is the real-time voice and data transfer services which requires keeping full bandwidth to be at service on demand (Fadel et al., 2004).

For the military perspective, there is an emerging term “Network Centric Warfare” which can be described as the warfare founded mainly on the information superiority established by linking sensors, fighters and the decision makers to maximize the situation awareness. Such network increases the combat power by providing the lethality, survivability, and degree of self-synchronization for the combatant troops. In such theatrical situation, each fighter is an independent node with a capacity to receive, evaluate and push information, which requires on-demand data transfer facilitators (Ferguson, 2001). These streaming data and voice demands of civilian and military are handled by Satellites and High Altitude Platforms.

Satellites are an essential part of the neoteric lifestyle and new battle zones; such that they provide all means of communications, data transfer, and geospatial information for civilians as well as for as the personnel under arms (Symolon, 2009). It is expected that within a few decades thousands of low earth orbit LEO satellites will be designed for global communications, military applications and other purposes (Helvajian, 1999).

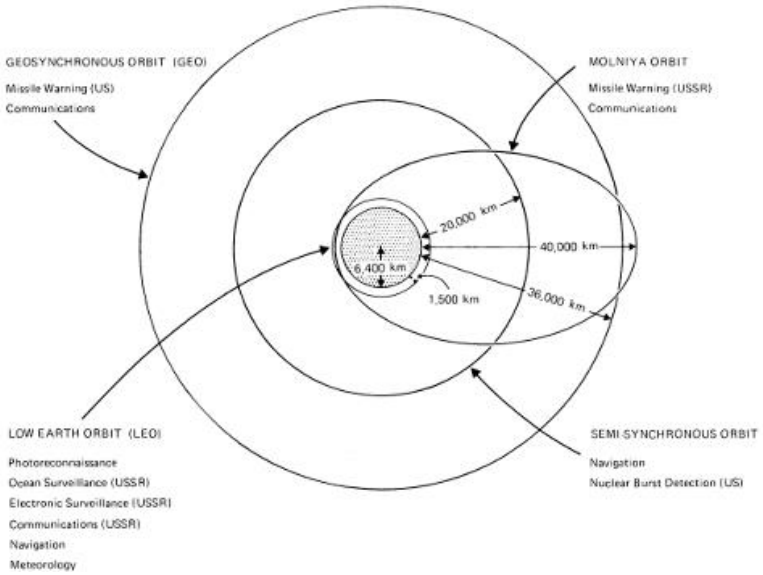

Figure 1.1 : Four Major Orbit Types (Carter, 1986).

Low earth orbit (LEO) is defined as 200km to 2000km while mid-earth orbit is defined the altitude between the 2000km to 35786km. Finally, the high orbit is defined as the 35786km and above (Figure 1.1) (Hamzah, Yaacob, Muthusamy, Hamzah, & Ghazali, 2013). LEO Low Earth Orbit (200km to 2,000km altitude) satellites have significant advantages over conventional geostationary satellites; they have better link quality, lower launching costs and shorter delay in transmission (L. H. Li, Heymsfield, Racette, Tian, & Zenker, 2004; S.-Y. Li & Wang, 2012). LEO satellites are quite fast as they have orbits from 90 mins to a few hours (Carter, 1986). LEO satellite systems pave the way to the correct global instantaneous communications and data transfer systems by facilitating inter-satellite links (ISLs) in addition to terrestrial links with better autonomy and the significant reduction in ground systems dependence (B. W. Kim, Min, Yang, & Kim, 2000). As a military capacity; LEO satellites can deploy space-based counteroffensive and microsatellites (space mines) opposing geosynchronous satellites (DeBlois, Garwin, Kemp, & Marwell, 2004).

1.1.2 High altitude airplanes and airships

Long-haul communications, remote sensing and surveillance capabilities are run mainly by satellite-based assets. This firm dependence on space-based assets is accepted as the Achilles heel of the currently advanced militaries. United States of America's Department of Defence has started High Altitude Platform (HAP) programs (Figure 1.2) to break this dependence and provide an alternative to both

geosynchronous and LEO satellites, even with better versatility and mission capability (Collier, 2008).

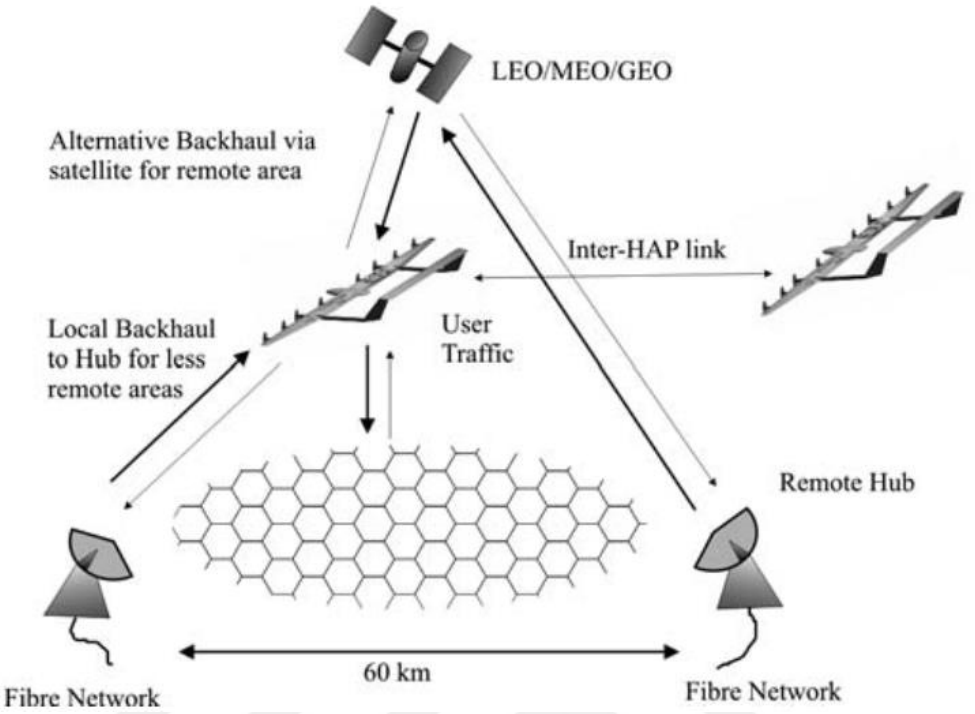

Figure 1.2 : Network Centric Warfare applications of LEO and High Altitude Planes (Aragón-Zavala, Cuevas-Ruiz, & Delgado-Penín, 2008).

Although both Airplanes and Airships provide high altitude solutions; they both have a very distinct difference. Airships generate lift through buoyancy effect while airplanes generate lift through aerodynamics as a result of the different mechanisms airships do not require to move steadily to a float while airplanes do (Figure 1.3) (Yu & Lv, 2010). The downside of the airships is that they are very slow, so their response time is very high.

Figure 1.3 : NASA's Helios prototype high altitude aircraft were taking off (Galante, 2001).

With a better response time, high altitude airplanes provide much better solution current demands of the civilian and military requirements. Thus there has been much research has been done to make high altitude flights economical and viable.

There has been global effort to determine exposed radiation dose during high altitude flights, in this context; The International Space Radiation Laboratory (ISRL) of the Japanese National Institute of Radiological Sciences (NIRS), Eril Research, Inc. (ERI), and the Flight Surgeon's Office at the NASA Dryden Flight Research Center (DFRC) use measurements with NASA ER-2 High Altitude plane (McElroy, 1995; Uchihori, Benton, Moeller, & Bendrick, 2003).

Er-2 have to lift off from Edwards Air Force Base (AFB) in Southern California on 7th of November 2000;

- The plane reached the altitude of 19.5km by 09:30 local time and the dose recorded at that moment is about 5.5 µGy/hr,
- At 10:30 plane is descended to altitude 14km at this level radiation dose is about four µGy/hr,
- The Plane continued to descend at reached the 11km at this level radiation dose is about 2.5 µGy/hr,
- Nearly 11:30 plane climbed to altitude 19.5km dose rate is increased back to 5.5 µGy/hr (Uchihori et al., 2003).

Research show that high altitude flights require specialized shielding which can deem the radiation dose at the acceptable rate for the personnel as well as the electronic equipment on board. The plot of the flight can be seen from the figure below (Figure 1.4);

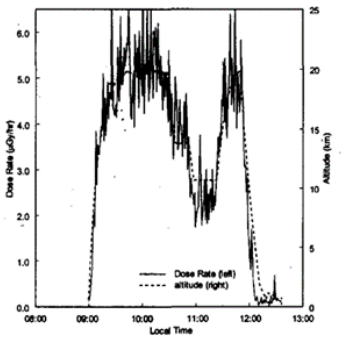

Figure 1.4 : Dose rate and altitude as functions of time for ER-2 Sortie No: 01-123 on 7th November 2000 (Uchihori et al., 2003).

Commercial Concorde planes are equipped with early warning systems which guide the pilot to lower its altitude in case of the radiation dose limits are passed. In such event merely the pilot lowers the altitude of the plane to meet the safety demands of the people and electronics on board (Lim, 2002). Unfortunately, such reaction is not possible for reconnaissance flights as it will be violations of airspace of the subjected country. Onboard equipment and personnel have to be shielded sufficiently to withstand any possible radiation dose increase situation including solar flare and solar wax activities.

1.1.3 Cloaking requirements for LEO satellites

Ground-based stations like the Russian Federation's Okno electrooptical complex (Figure 1.5) searches and later on tracks down space objects at an altitude between 2,000 to 40,000km. The detectors in the complex are calibrated to detect the sunlight reflecting from the space objects bigger than 20cm in diameter. After it collects coordinates and photometric information, the system sends the data to command and control infrastructure ("Okno ELINT complex in Tajikistan is becoming Russian," 2006; "ЗВЕЗДНЫЕ ВОЙНЫ НАЧИНАЮТСЯ В ПРЕДГОРЬЯХ ПАМИРА," 2014; "Россия прорубила новое «Окно» в космос," 2006).

Thus any satellite made from transparent or semi-transparent material traveling below the 2000km is immune to such detection while have to face the harsh environment of low earth orbit and other material problems that comes with transparency.

Figure 1.5 : 1109th Independent Electrooptical Node ("Okno" electrooptical complex), Nurek ("Okno ELINT complex in Tajikistan is becoming Russian," 2006).

1.1.4 Material properties for LEO's

A suitable structure is necessary to define a spacecraft without the structure a spacecraft is just a pile of circuit boards, wires and propulsion pipework (Harland & Lorenz, 2005). Structural design properties of the LEO satellites and HALE's requires a design review involves a multidisciplinary approach. The design parameters must be determined for each part as well as assessing the overall design parameters such as (alignment, thermal requirements, the field of view, screening, connections and accessibility (Figure 1.6) (Fortescue, Stark, & Swinerd, 2003).

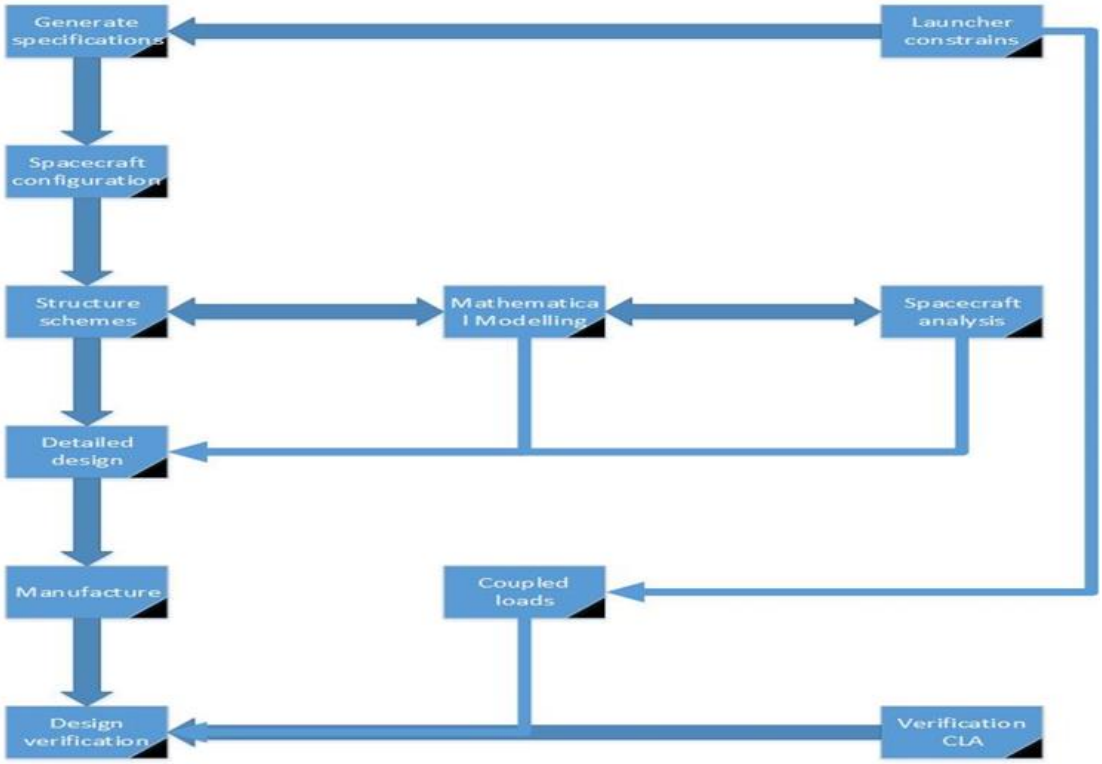

Figure 1.6 : Structural design progress (Fortescue et al., 2003).

LEO satellites are not subject to harsh radiation degradation as they are below the radiation belts (excluding ~ 90-degree inclination) but they are under the intense influence of atmospheric drag and atomic oxygen (AO) which requires better structural integrity and strong corrosion resistance. LEO satellites will be subject to;

- Decreasing density of natural atmosphere
- Orbital debris
- Atmospheric plasma
- AO corrosion

- Exposure to charged particles around the South Atlantic Anomaly
- Ultraviolet radiation
- Thermal cycle (6000 cycles per year) (Patel, 2005)

Thus structural materials for LEO satellites will have to withstand such detrimental effects. It is well known that solar arrays or spacecraft surfaces that are in the LEO can face solar array arc due to arc plume which brings the requirement for sufficient shielding to achieve successful operation (Kleiman, 2006).

The most commonly used polymeric material is Mylar which is a transparent material which can undergo thickness of 0.00025in. Sometimes Mylar is coated with very shallow layers of Aluminium to get reflectance. Another choice is Kapton which have higher strength and the ability to withstand temperature compared to Mylar. Both of the materials are useless for low orbit applications as they undergo significant degradation by the Atomic Oxygen (Griffin & French, 2004).

1.1.5 Material properties for HAP's

As the Wind patterns for the atmosphere evaluated (Figure 1.7) it is crucial an high altitude airplane to operate at an altitude range between 18km to 22km. To accomplish successful flying at this altitude requires a fast airspeed and very high value of lift coefficient as the air at this level is thinner than the altitudes below (Jenkinson & Marchman, 2003).

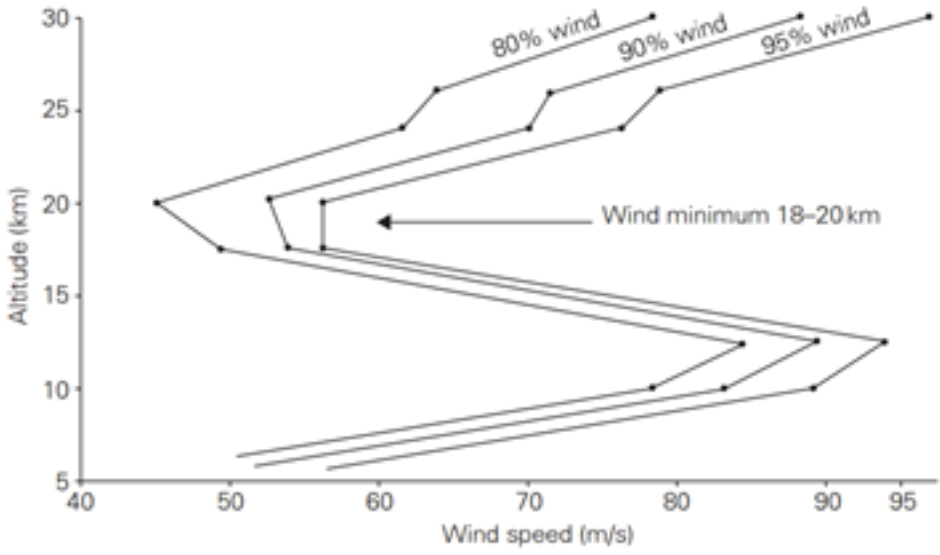

Figure 1.7 : Wind Speeds versus the altitude (Jenkinson & Marchman, 2003).

Uninhabited aerial surveillance vehicle (UAV) operate between 18km to 22km with a speed of 220 m/s; it expected to have 1800N/m2 (183.5 kg/sqm) loading occur at the wings (Figure 1.8) (Jenkinson & Marchman, 2003). Wing loading versus altitude can be seen from the diagram below;

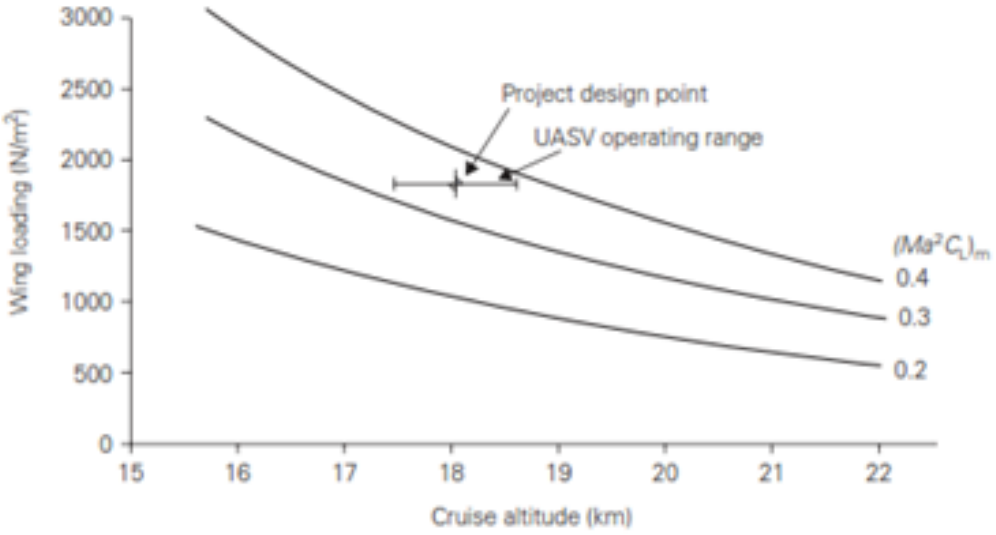

Figure 1.8 : High altitude airplane wing loading (Jenkinson & Marchman, 2003).

HAP systems will be subject to;

- Linear acceleration
- Structural transmitted vibration
- Shock
- Acoustic Loads
- Internal Pressure
- Thermal Stress (Griffin & French, 2004).

Thus structural materials for HAP systems will have to withstand such detrimental effects.

1.1.6 Self-Healing materials

With a materials scientist perspective “self-healing” means recovery of the material to the state of initial properties after a damage and/or change occurred by an environmental factor or internal pre-deposited factor such as internal stress (Fedrizzi,

Fürbeth, Montemor, European Federation of Corrosion., & Institute of Materials Minerals and Mining., 2011). There are some other synonym words in the literature to cover self-healing materials such as;

- Self-Repairing
- Autonomic-Healing
- Autonomic-Repairing

In most of the cases, the self-healing of the material requires external stimuli thus such materials are divided into two main groups;

- Autonomic (without any intervention);
- Non-autonomic (needs human intervention/external triggering)(S. K. Ghosh, 2009; Zheng & McCarthy, 2012).

Conventionally the damaged materials are repaired by patching, gluing or welding, which requires external intervention; the self-healing materials aim to minimize this intervention requirement with an ultimate aim to achieve zero intervention. Autonomous self-healing materials give zero intervention; such materials will extend the working life and the reliability of the whole systems while reducing the overall cost of maintenance. Self-healing materials take the attention of intuitions such as US Air Force and European Space Agency (Wu, Meure, & Solomon, 2008; Y. Yang & Urban, 2013).

1.1.6.1 Healing mechanisms

Self-Healing materials can recover from a damaged state to the point of original state by using the components inherently available to them; there are two primary classes of self-healing;

Intrinsic self-healing systems

Extrinsic self-healing systems

Intrinsic self-healing materials heal the damage by the properties of the material or material components such as heating the thermoplastic above the Tg which will increase the mobility of the molecules or manage the reversible crosslinking to perform desired reactions. *Extrinsic self-healing systems* are based on the incorporation of foreign materials to the system, which will interact with each other in case of crack

formation; such systems are usually formed from a liquid healing agent and a solid catalyst (Neuser, Michaud, & White, 2012). Self-healing should occur spontaneously, can be triggered by internal or external stimuli but the healed location must exhibit full or near properties of the virgin material. For getting best healing efficiency probable damage characteristics and the working conditions of the material should be well determined (Geckeler & Nishide, 2009).

During last decade, a variety of self-healing materials have been invented, which uses different components and compositions. Even the components and the compositions they mainly use common repairing mechanisms, these self-healing mechanisms can be divided based on the chemical reactions which are listed in Figure 1.9 below (Williams, Dreyer, & Bielawski, 2008).

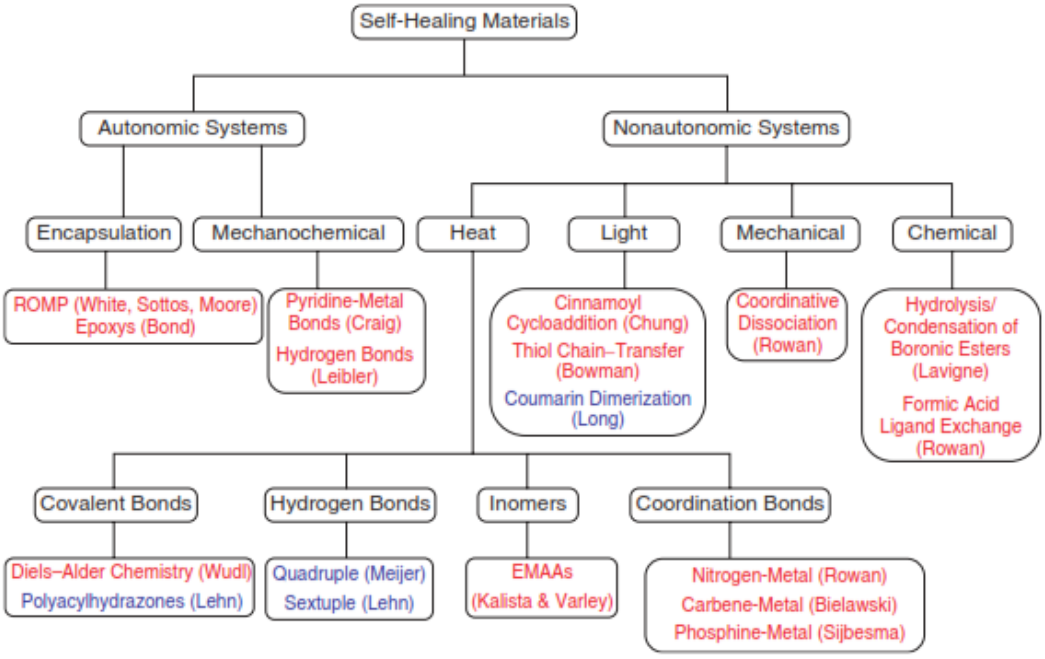

Figure 1.9 : Organization of self-healing materials based on their chemistry. The specific chemistry employed is noted and is accompanied by a representative list of associated principal investigators in parentheses. Red represents current or emerging materials, and blue represents possible materials. Note: ROMP is an acronym for ring-opening metathesis polymerization, and EMAAs are poly(ethylene-co-methacrylic acid) ionomers(Williams et al., 2008).

1.1.6.2 Release of healing agent

As a healing mechanism with a curing agent, some self-healing materials are loaded with microcapsules or networks of micropipes, which are loaded with active agents such as monomers, dyes, catalysts and hardeners as an example dicyclopentadiene

monomer encapsulated into microcapsules introduced into the epoxy matrix. In the event of crack formation, these reservoirs rupture as seen in Figure 1.10 below which induces the release of healing agent and movement through the material with capillary effect. As the healing agent meets with predisposed catalysts inside the solidification starts which gradually fills the cracked area, the whole process is induced by the crack formation as seen from the Figure 1.10 (S. K. Ghosh, 2009; Syrett, Becer, & Haddleton, 2010; White et al., 2001).

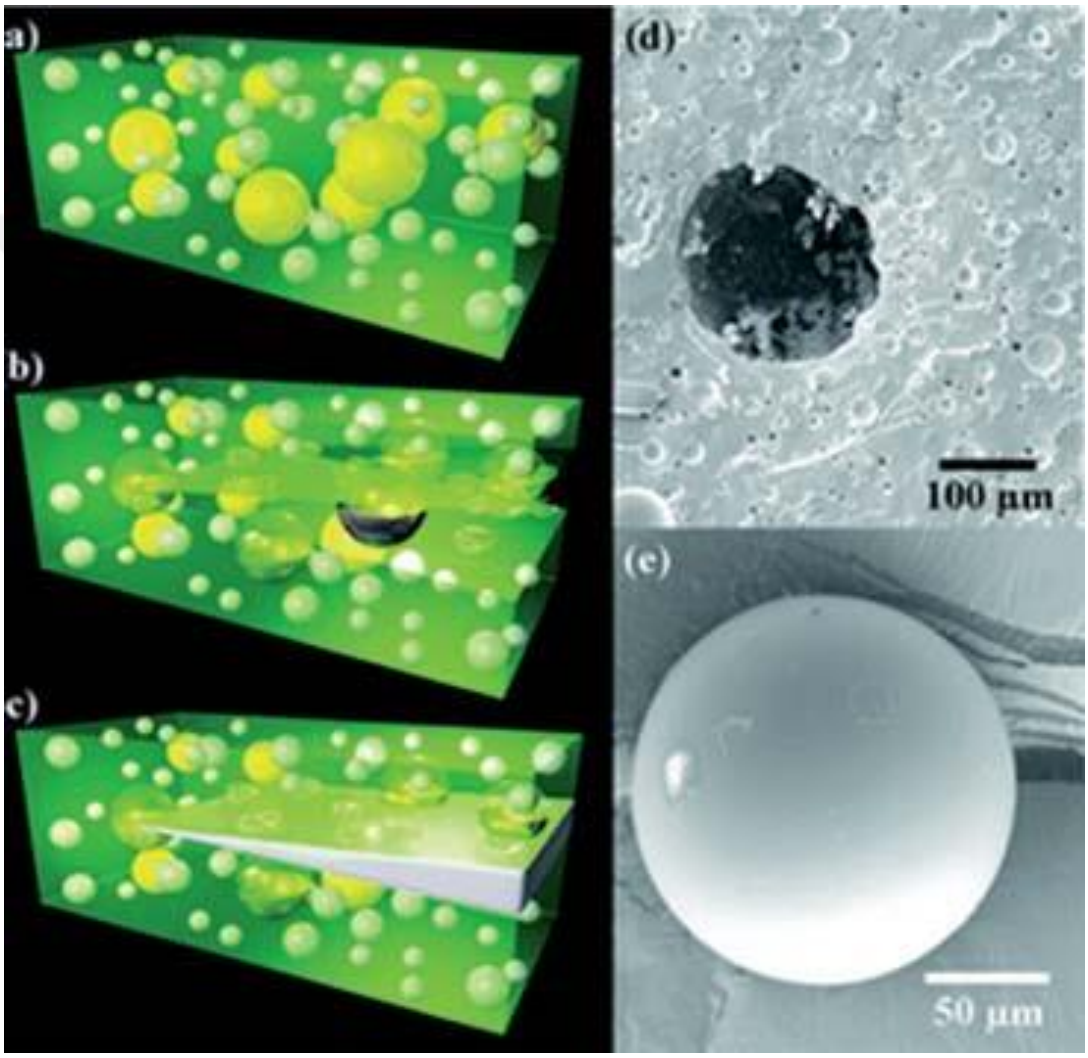

Figure 1.10 : Schematic of the self-healing process: (a) self-healing composite; (b) crack propagating into the matrix; (c) a crack healed by polymerized PDMS. SEM images of (d) the fracture surface, and (e)a representative microcapsule, (Syrett et al., 2010).

In the manufacturing process, the healing agent and the catalysts have to be disposed inside the material; the crack formation should trigger the process. The process should follow as described above for sufficient healing of the crack there need to be enough, and right healing agent and catalyst must have been disposed inside the material

(Vriezema et al., 2005; Ming Qiu Zhang & Rong, 2011a). For encapsulation of healing agent and or catalyst methods and triggering mechanisms are listed in Table 1.1 below.

Table 1.1 : Encapsulation systems and indicative triggers (Hughes, Cole, Muster, & Varley, 2010).

System	H_2O	pH	CL^-	Light	Temp	Mech.	Chem.
Direct incorporation	X	X					
Sol-Gel	X	X	X				X
Layered Compounds	X	X	X				X
Hierarchical	X	X	X				X
Hard polymer				X	X	X	
Polyelectrolyte		X	X		X	X	X
Micelle	X	X			X		X
Pickering particles		X				X	X

There are two primary mediums used for storing healing agent inside the material;

- Healing agent loaded pipelines
- Healing agent loaded microcapsules

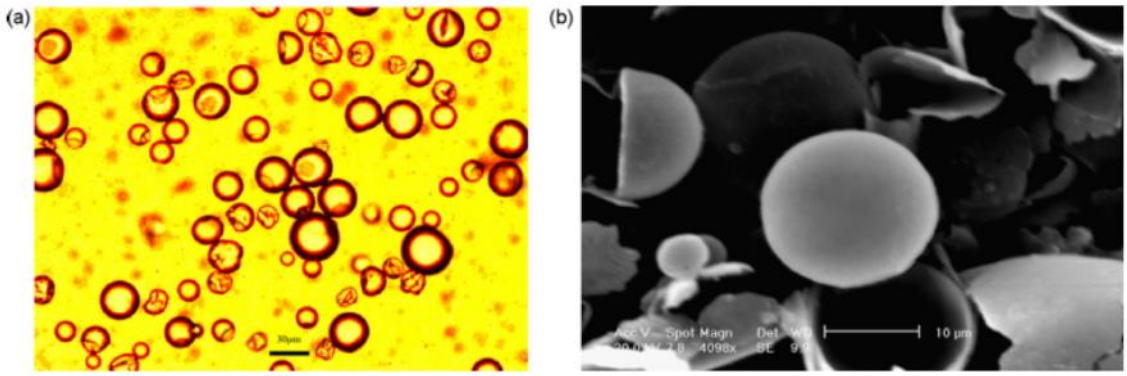

Figure 1.11 : Images of the microcapsules, obtained by (a) optical microscopy and (b) ESEM. They were prepared at an agitation speed of 1000rpm with a reaction time of 3h (Ming Qiu Zhang & Rong, 2011b).

As the crack formation induces the healing agent delivery there is no further manual intervention required as seen indistinct self-healing, the process works very well in different cases and environments although there is drawback due to depletion of healing agents and catalysts the process can be repeated locally for limited times (Figure 1.11). As a better biomimetic solution, the healing agent can be deposited inside networks of micropipes, which are interconnected to each other and a central

reservoir. Such microvascular networks are more efficient in delivering one or more healing agent to desired locations Figure 1.12 (Hager, Greil, Leyens, van der Zwaag, & Schubert, 2010; Ming Qiu Zhang & Rong, 2011a; M. Q. Zhang & Rong, 2012).

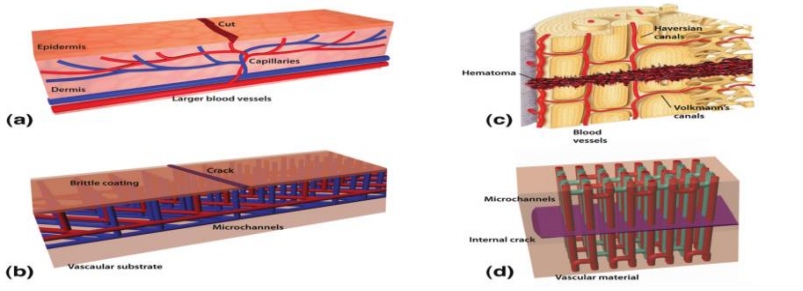

Figure 1.12 : Schematics of surface damage being healed in a) the epidermal layer via the vascularized dermis (Reprinted with permission. b) a brittle coating material via an interpenetrating vascular network within a substrate Schematics of internal damage being healed (c) in cortical bone within a synthetic vascular material(Hamilton, Sottos, & White, 2010).

Microvascular networks self-healing mechanism is inspired by the healing mechanism of the human skin. A minor cut to the skin triggers the healing mechanism. First, there is blood flow from the underlying dermal layer, afterward formation of coating material at and below the cut area as seen from the Figure 1.13 below. Microvascular networks mimic the same method and also for maximising the efficiency, the pipes locations are engineered to be located at probable crack formation locations and give the best flowability to healing agent(s)n(Hamilton et al., 2010). The healing system can be further developed by addition of pumps, valves and internal reservoirs (B. Ghosh & Urban, 2009; Toohey, Sottos, Lewis, Moore, & White, 2007).

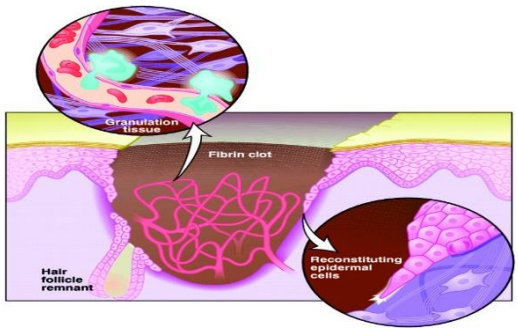

Figure 1.13 : Cartoon to illustrate the main phases in the healing of a skin wound. The tearing is temporarily plugged with a fibrin clot, which is soon infiltrated by inflammatory cells. Later, a dense capillary network and a temporary granulation tissue form. An epidermal layer is reconstituted from the edges of the wound and the remnants of the primary cute, hair-like follicles, by the migration of epidermal cells and by the production of collagen (Amendola & Meneghetti, 2009).

1.1.6.3 Controlled living polymerization

Foundation of living anionic polymerization followed by controlled/living polymerization made a considerable impact both on polymer and materials science. Because, it has opened new frontiers and capabilities in polymer science such as preparation of precisely defined molecular and nanostructures with a very well defined polymer (Müller & Matyjaszewski, 2010).

The main characteristics of the living polymerization are the quick initiation of the reactive chain ends as seen in the chain termination and the chain transfer in the polymer chain growing process. This gives living polymerization specialty of growing macromolecular species as there is monomers common living polymerization techniques are as listed in Table 1.2 below (Geckeler & Nishide, 2009).

Table 1.2 : Common living polymerization techniques for the preparation of block copolymers(Geckeler & Nishide, 2009).

Polymerization Technique	Monomers available
Anionic	Styrenes, vinyl pyridines, methacrylates, acrylates, butadiene, isoprene, N - carboxy anhydrides (amino acids), ethylene oxide, lactones, hexamethylcyclotrisiloxane, 1,3 - cyclohexadiene, isocyanates
Cationic ring - opening	Epoxides, siloxanes, tetrahydrofuran
Group transfer	Methacrylates, acrylates, nitriles, esters, butadienes, isoprenes
Ring - opening metathesis	Norbornenes
Stable free radical	Styrene, methacrylates, acrylates, Acrylamides, dienes, acrylonitrile
Atom transfer radical	Styrenes, methacrylates, acrylates, acrylonitriles
Reversible addition – fragmentation chain transfer	Methacrylates, styrene, acrylates

For thermoplastic polymers living polymerization at room temperature is an efficient way as there is no external intervention is needed, the build-up chemical bonds from the cracked planes induces self-healing without any external stimuli or catalyst. Most important of all the impact tests done up to now show that the material can withhold self-healing capacity for years, also such systems shows self-healing capacity against the radiation damage induced by ionizing radiation, UV, and electromagnetic radiation. Self-healing against radiation is done by recombination of free radicals induced by radiation damage and the macromolecular radicals on the chain ends as seen in Figure 1.14 (Ming Qiu Zhang & Rong, 2011a).

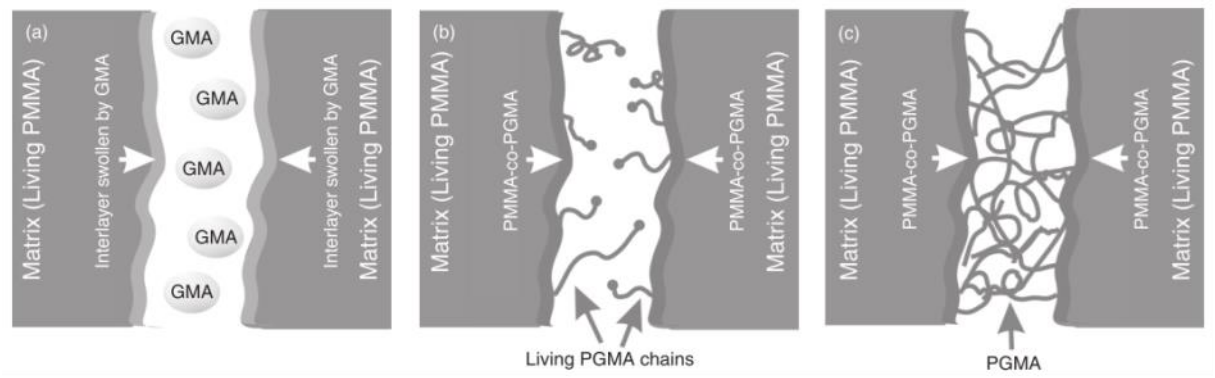

Figure 1.14 : Schematic drawing of crack repair by living copolymerization of GMA from the cracked surfaces of living PMMA matrix. (a) Diffusion of released GMA monomers into living PMMA matrix, leading to swollen interlayer at the cracked surface. (b) Growth of living poly(glycidyl methacrylate) (PGMA) chains from a copolymer of PGMA and PMMA (i.e.PMMA-co-PGMA). (c) Crack filled with PMMA-co-PGMA (Ming Qiu Zhang & Rong, 2011a).

Newly proposed nanoparticle-induced processes use high-quality nanoparticles with diluted organometallic precursors which causes sweeping particle surfaces with alkane-based ligands such as amines, n-alkyl thiols or phosphine oxides, such dispersion operations causes the particles to form clusters or aggregate at specific regions which undermines the proprieties of the composite. Leaving conventional ligands (in favor of new ones, which provide better interaction with polymer host) is one of the tested ways for the uniform dispersion of the nanoparticles, which leads to polymerization start from the surface of the nanoparticle and grow through the mixture. Polymerization methods such as controlled free-radical polymerization and ring-opening metathesis polymerization have proven themselves as viable options for uniform dispersion of the nanoparticles (Balazs, Emrick, & Russell, 2006).

Another way of living polymerization self-healing is dispersing the glycidyl methacrylate (GMA) monomer containing microspheres inside a living polymer poly-(methyl methacrylate) (PMMA) matrix when the microcapsules rupture by a crack the GMA is released into the living polymer PMMA matrix. The GMA acts as an initiator, so without requiring an external catalyst the polymerization starts and heals the cracked area (Syrett et al., 2010).

1.1.6.4 Reversible cross-links

While reversible cross-linked materials show, the capacity of self-healing there is always a requirement of an external stimulus, which can be photo, thermal or chemical activation to start reversibility. Although reversible-crosslinking materials show the

self-healing capacity their healing capacity is not autonomous(B. Ghosh & Urban, 2009). Formation of a crack inside a polymeric material requires the breaking of chemical bonds, for a crack to propagate inside the polymer this chain breakage must continue towards the crack propagation route. Thus an efficient self-healing mechanism by reversible cross-links involves the formation of new bonds as seen in the Figure 1.15 below, as this healing mechanism is in molecular scale it offers the capacity to s repeated healing of the material (Habault, Zhang, & Zhao, 2013; Ming Qiu Zhang & Rong, 2011a).

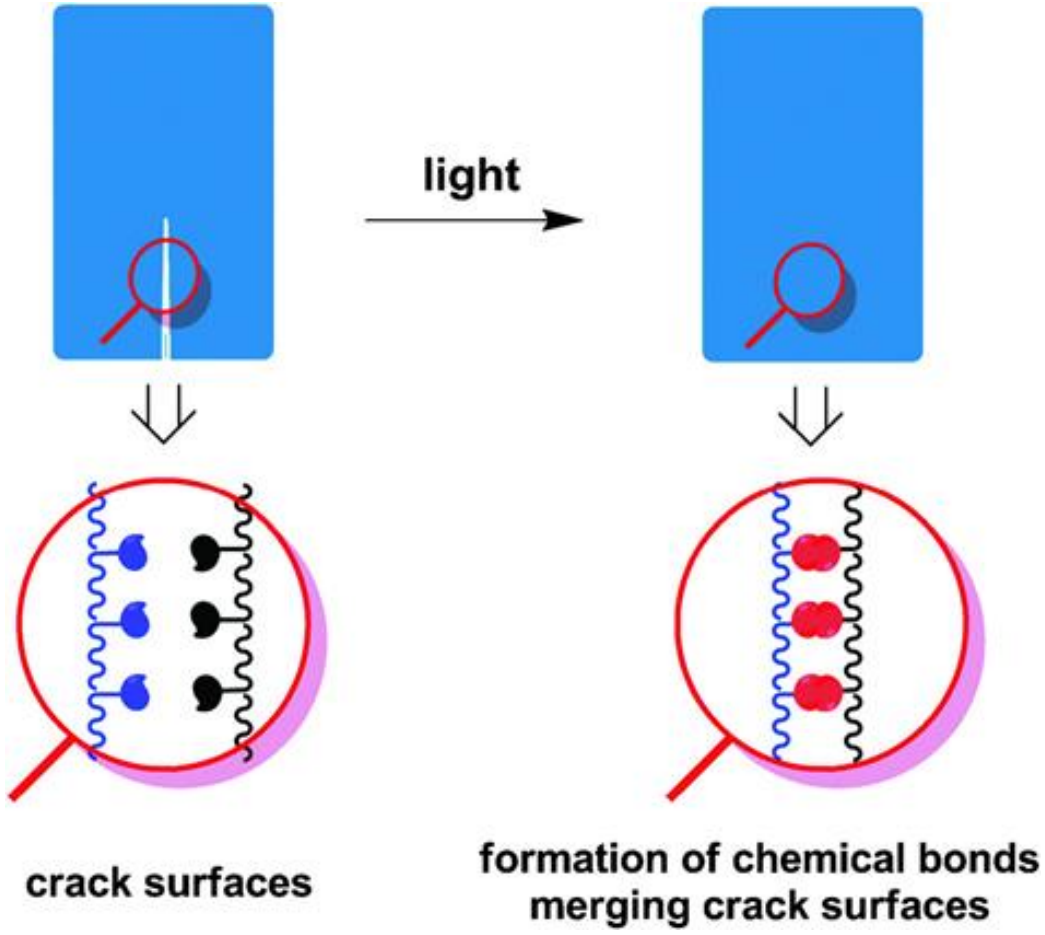

Figure 1.15 : Schematic illustration of light-triggered self-healing of a crack, requiring formation of new chemical bonds and fusion of crack surfaces(Habault et al., 2013).

To achieve a mechanical and electrical self-healing, inorganic components and polymer matrix should have a perfect compatibility, which will lead to uniform dispersion of the inorganic materials towards the polymer matrix that prevents electrical percolation. Better compatibility may induce movement of the inorganic

component inside polymer matrix that will increase the uniformity of the dispersion thus the electrical conductivity.

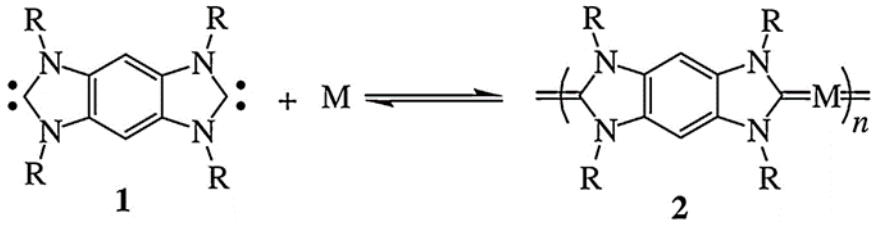

Figure 1.16 : Self-healing organometallic polymer and the dynamic covalent chemistry in the polymer (Benight, Wang, Tok, & Bao, 2013).

As an example, the reversible bonds between the transition metals and the N-heterocyclic carbenes (NHCs) prepare electrically conductive self-healing polymer networks with dynamic structures by cross-linked conjugated cores as seen Figure 1.16 above. When a micron-sized crack occurs on the cross-linked film the resistivity at the localized area increases, the damage is mostly healed by the heating of the specimen inside a DMSO vapor at an ambient temperature of 150°C (Benight et al., 2013).

Chain cleavage of cyclobutane (PFCB) under stress is represented by the Figure 1.17. As a result of the cleavage trifluorovinyl esters (TFVE)'s form and those trifluorovinyl esters (TFVE)'s reform by the cycloreversion, this step by step cleavage characteristics makes crosslinking a viable self-healing mechanism for the trifluorovinyl esters Figure 1.17 (TFVE) (Y. Yang & Urban, 2013).

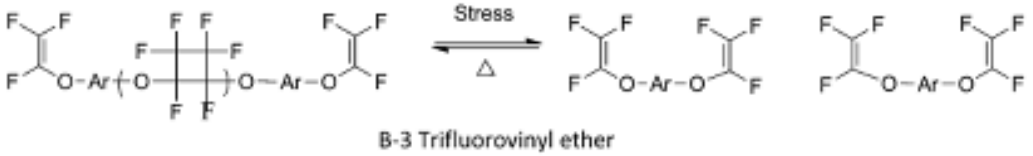

Figure 1.17 : Mechanically induced chain cleavage in perfluoro-cyclobutane (Y. Yang & Urban, 2013)

Four-membered ring opening by the wavelength of 254nm and ring closure by the wavelength 366nm of the anthracene derivatives [4 +4] is schematically shown in the Figure 1.18 below, which offers a reversible polymerization for the anthracene derivatives.

Self-Healing by light is possible if the crack is on the surface. If the crack is deep inside the material, the sample should be transparent for the used wavelength of the radiation to achieve self-healing. To ensure successful process application,

monochromatic radiation at required wavelength should be at disposal. Monochromatic radiation can selectively reactivate groups inside the heterogeneous networks. As the radiation was applied to damaged area; the local temperature change due to radiation exposure (Habault et al., 2013; Y. Yang & Urban, 2013).

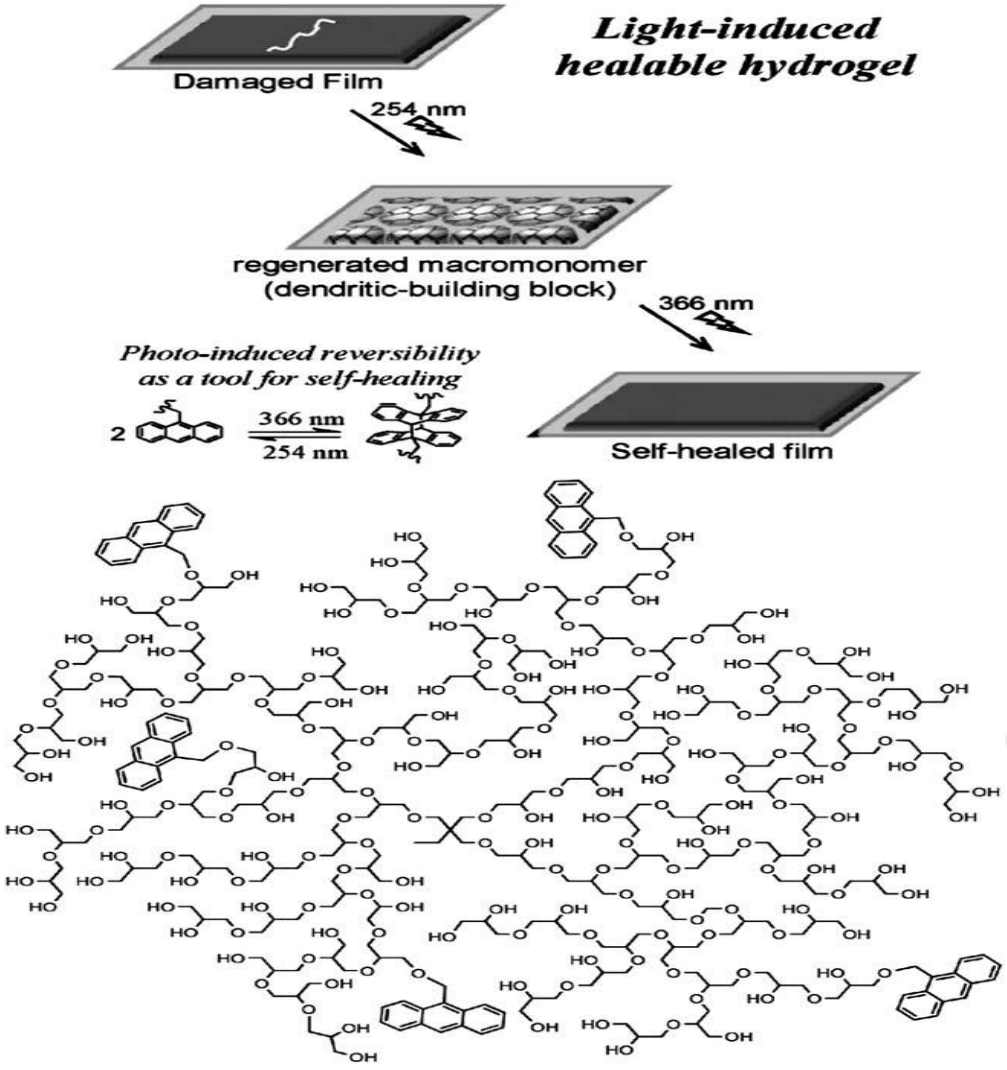

Figure 1.18 : Photo-induced self-healing hydrogels based on the cycloaddition reaction between two anthracene groups using an anthracene-containing hyperbranched polyglycerol(Liu & Chuo, 2013).

Multi-furan and multi-maleimide can synthesize highly cross-linked polymers via Diels-Alder (DA) reaction when such polymer is heated above 120°, C the intermonomer links break down until the material cooled back to room temperature, which will induce recombination of linkages between monomers. This process is reversible and can be used to heal fractured parts as seen Figure 19 below (Ming Qiu Zhang & Rong, 2011a).

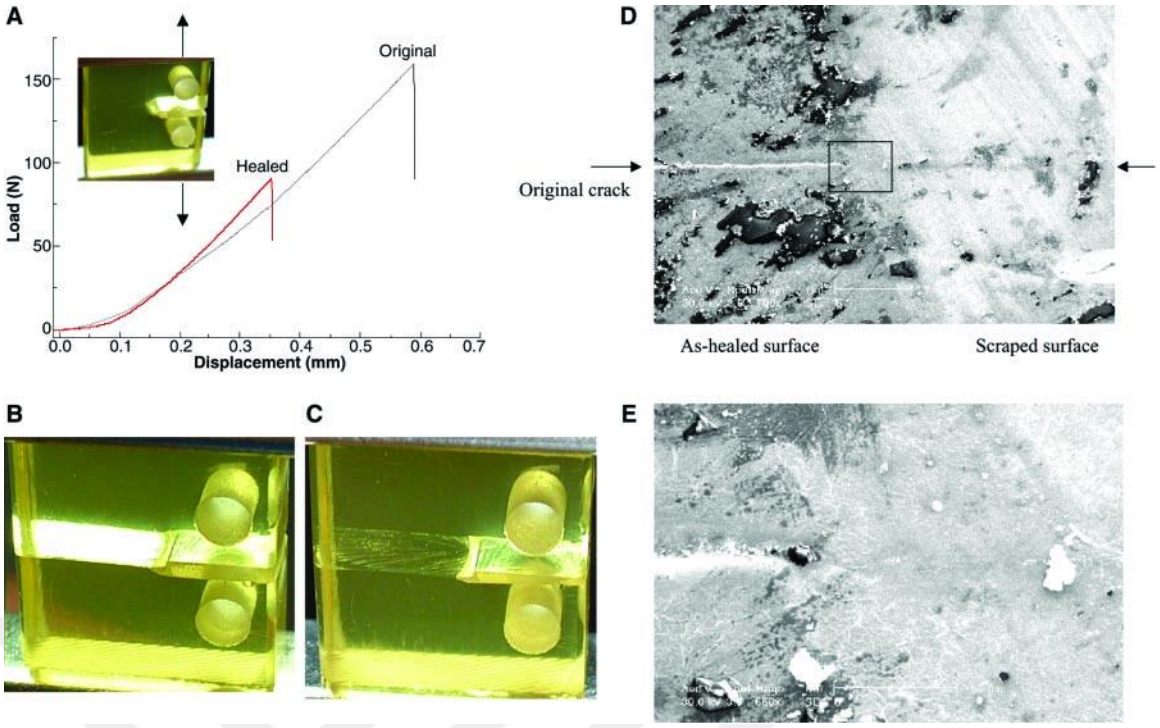

Figure 1.19 : Mending efficiency of polymer 3. (A) Mending efficiency, (B) Broken specimen (C) After thermal treatment. (D) SEM image of the surface of a healed sample, (E) Boxed area in (D)(Chen et al., 2002).

1.1.6.5 Self-Healing by heating the material over Tg

Molecular diffusion is the driving factor of self-healing mechanism by heating the material above its glass transition (Tg) temperature. Autonomous self-healing can be achieved by low Tg materials which give molecular chains the capacity to access the free volume easily and have higher mobility. When two pieces of the same polymer put in contact and heated above glass transition temperature, the interface slowly disappears, and mechanical performance increases with time which can take minutes (in Figure 1.20) days or even years to complete healing (Urban, 2012). There are five stages of self-healing of crack induced damage:

- Surface rearrangement
- Surface approaching
- Wetting
- Diffusion
- Randomization

Lin et al. have treated PMMA with methanol from 40° to 60°C and observed with a given time it is possible to achieve complete recovery of material up to the point of virgin material tensile strength (Wu et al., 2008; M. Q. Zhang & Rong, 2012). Self-healing by heating above Tg applies to many thermoset materials including but not limited to epoxy, PMMA, polyamides, polyethylene, polyketones, polystyrene (Billiet, Hillewaere, Teixeira, & Du Prez, 2013).

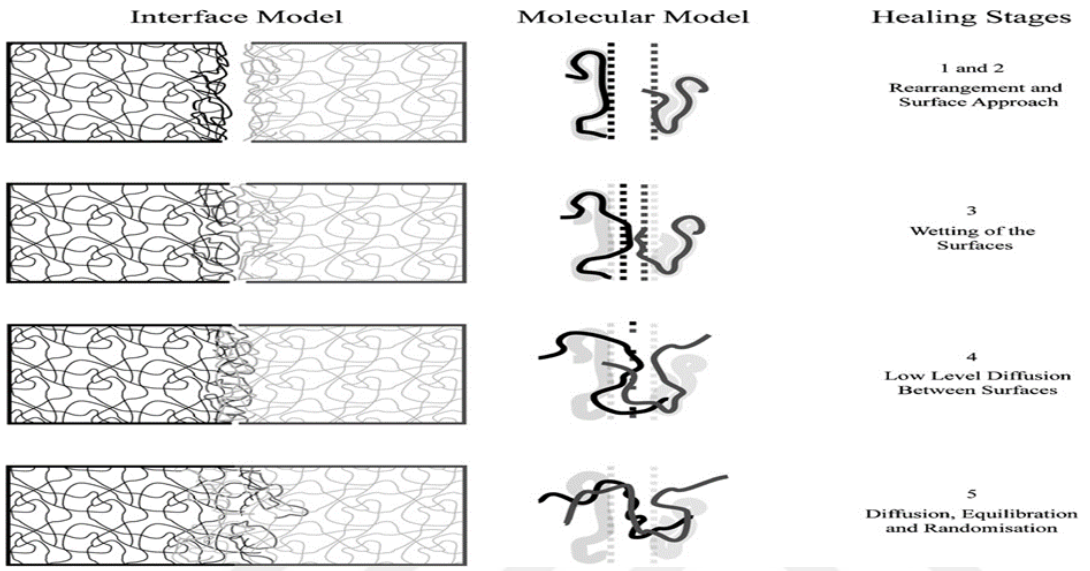

Figure 1.20 : Mechanisms involved in self-healing via molecular interdiffusion (Wu et al., 2008).

Although self-Healing of monomers is based on same principles, the process is slightly different from other forms of self-healing. The local melting of ionomer with the energy deposited by high impact induces self-healing of the material. The healing process is induced by the thermal reversibility of the ionic interaction as represented in the Figure 1.21 below (Syrett et al., 2010).

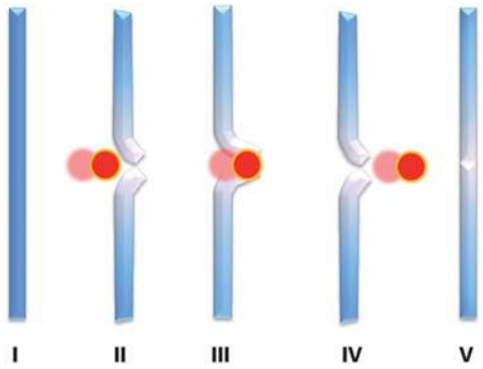

Figure 1.21 : Friction causes melt. Elastically rebounds. The polymer is still molten, able to reformat the damage site (Syrett et al., 2010).

Self-Healing by heating can be achieved with the heterogeneous thermoplastic copolymer systems, the heterogeneous system of hard polystyrene (PS) as a structural handler and soft polyacrylate amide (PA-A) pendent groups with multiple H-bonding sites provides self-healing through heating above the glass transition temperature. Copolymer heated hydrophobic and hydrophilic reactions paves the way for phase separation's which gives the self-healing characteristics as seen the Figure 1.22 below (Y. Yang & Urban, 2013). Superhydrophobic properties have been achieved by incorporating colloidal particles inside a highly fluorinated crystalline fusible wax. Colloidal particles are removed from the surface by scratching after the damaged blend melted it is seen that most of the colloidal particles reorganized near surface area due to the tendency of wax to crystallize near the surface (Ionov & Synytska, 2012).

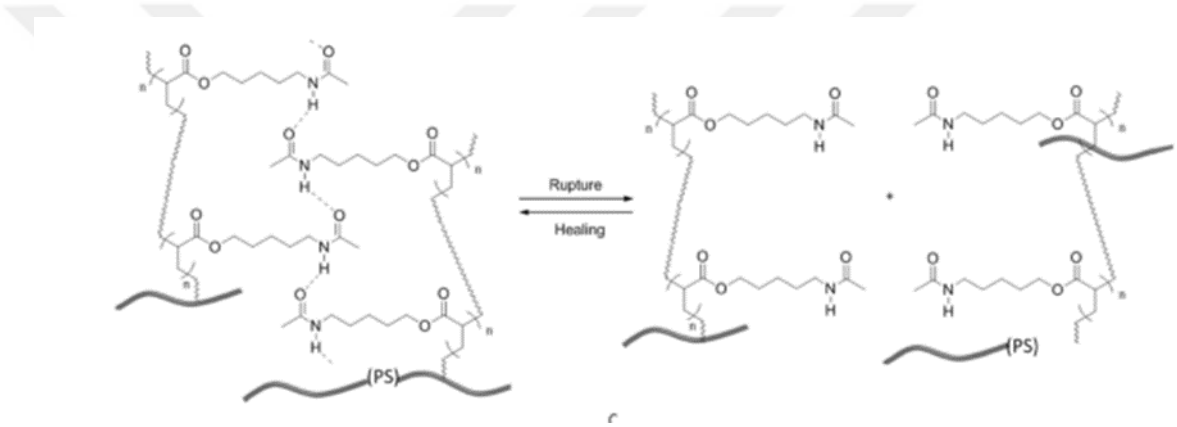

Figure 1.22 : Copolymers are combining hard polystyrene (PS) backbones with soft polyacrylate amide (PA-A) pendant groups carrying multiple H-bonding sites(Y. Yang & Urban, 2013).

Also in another approach utilizing selective microwave absorption of the graphene layers, an area is locally heated, and temperature over Tg self-healing mechanism is induced. For the visible spectrum of light silver nanoparticles which have visible light surface plasma adsorption bands have provided local heating in the presence of visible light which leads to local temperature increase thus self-healing (Y. Yang & Urban, 2013).

Supramolecule polymers and polymerlike are soft materials which have relatively low Tg. This nature of such materials gives a unique advantage over covalent bonding. These materials remodeled reversibly within a short period either high free volume fluidic characteristics or low free volume solid-like characteristics, which gives material different elastic and plastic properties (Y. Yang & Urban, 2013).

1.1.6.6 Nanomaterial self-healing

Self-healing for coating materials is different from the bulk materials; coating self-healing mechanisms require much more delicate containers. To meet dimensional requirements, the many different approaches are tried,

Nanocomposites are solid materials, which have repetition distance in the scale of nanometers for the different phases. Most typically such materials are made of an inorganic solid containing an organic component, as a more complex option material can have three or more organic/inorganic combination while one of the components is in nanoscale (Ajayan, Schadler, & Braun, 2006; Koo, 2006).

Incorporation of nanoparticles into polymer matrix nanocomposites have opened new capabilities to build new materials that have superior optical, mechanical and electrical properties while providing an option of flexible if desired. The best examples of such cases are the variation in the nanoparticle size and coating providing scientists new self-healing materials matching better durability requirements and auto-corralling rods for the photovoltaic industry. There is enormous demand for developing production techniques, equipment and processes which will carry the microscopic beneficial effects of the nanoparticles through the material (Balazs et al., 2006).

Polymer nanocomposites (PNs) are made from polymeric materials (e.g., elastomers, thermosets, or thermoplastics) exhibit significant improvements including mechanical properties, thermal stability, gas barrier properties, fire retardancy and many more (Koo, 2006). The biggest overwhelming problem of the self-healing polymer nanocomposites is finding a natural controllable and cost-effective process, which provide the dispersion of nanoparticles within the polymer matrix. Nanoparticles inside the polymer matrix tend to form domains, and aggregate specific areas which provide the adverse effect as the matrix material away from the domains do not have the beneficial effects of the nanoparticles (Balazs et al., 2006).

Nanoparticles inside polymer nanocomposites have a unique capacity to segregate to crack surface, and the movement of nanoparticles inside polymeric fluid induces seal the cracked area, such reaction by the attraction between the crack surface and the nanoparticle. Even computational studies on such healing mechanism predict %75 to%100 recovery for the mechanical properties; such healing mechanism have not demonstrated yet (B. Ghosh & Urban, 2009).

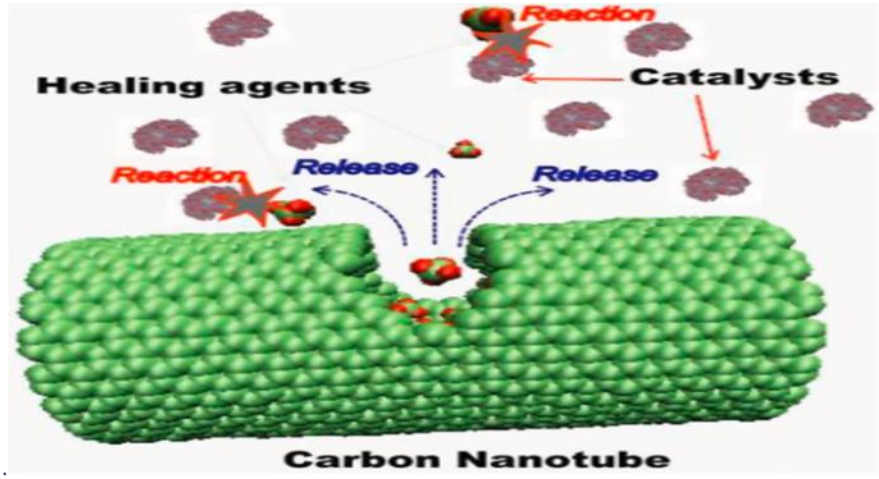

Figure 1.23 : Molecular model of carbon nanotube and organic molecules for the self-healing system (Lanzara, Yoon, Liu, Peng, & Lee, 2009)

Another approach involves carbon nanotubes; CNT (carbon nanotubes) are filled with healing agent molecules and dispersed inside the matrix material, catalysts are located the either covered outer surface of the CNTs or mixed to the matrix material. The healing mechanism can be triggered even by a crack at the nanoscale. First, the CNTs wall stops the crack. Then when the CNTs break reservoir opens and healing agent and the catalyst heals the cracked area or on its outer wall forms a superstructure, which in both cases stop the crack and heals the damage Figure 1.23 (Lanzara et al., 2009).

Computational simulations so far showed a clear relation between the crack propagation near the surface and the melt induced “depletion attraction” of the nanoparticles, which drives the nanoparticles towards the crack region, such action provides a path for the autonomic recovery path for homopolymers. Such path has been demonstrated in a poly (methyl methacrylate) matrix which have PEGylated CdSe nanoparticles and in contact with a brittle silicon layer. Heating the materials in junction with each other above the glass transition temperature of the PMMA matrix composite, caused cracks at the SiO_x which is later filled by the nanoparticles at the PMMA matrix nanocomposites as shown in the fluorescence optical micrograph Figure 1.24 below. For smaller nanoparticles, it is seen that polymer takes the place of the nanoparticles without a significant entropic penalty. There is another example of such case CdSe is dispersed inside polystyrene(PS) matrix. Although the underlying mechanism has not been identified it has been observed that nanoparticles tend to segregate to the tip of the crack, which leads to a significant change in the crazing

characteristics of the nanocomposites and almost doubling the strain to failure ratio (Balazs et al., 2006; Y. Yang & Urban, 2013).

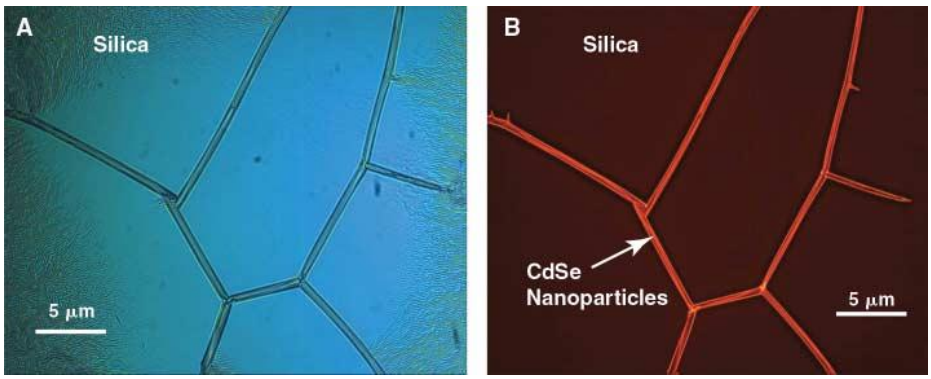

Figure 1.24 : (A) A reflection optical micrograph of a thin film of a mixture of 6-nm PEGylated CdSe nanoparticles particles in poly(methyl methacrylate) that was spin-coated onto a silicon wafer. A 0.1-mm layer of silicon oxide was evaporated onto the nanoparticle composite, and the trilayer was heated to 160°C for 4 hours. The difference in the thermal expansion coefficients of silicon oxide and the PMMA composite produced the cracks observed. (B) The same film viewed with a fluorescence microscope, in which the segregation of the CdSe nanoparticles to the cracks is highlighted by the fluorescence of the nanoparticle(Balazs et al., 2006).

1.1.6.7 Shape memory assisted self-healing

For retaining self-healing by shape memory a temporary shape is given to a shape memory polymers (SMP) above the T_{tr} (either T_g or T_m), after the shape is retained the polymer is cooled down to $T<T_{tr}$ temperatures. During this step chain, relaxation has to prevent with physical or chemical crosslinking, by confining the stress arises by the deformation, which will be the driving force of the shape memory effect. When the stress preserved adequately when the material is heated back to $T>T_{tr}$ the polymer takes back of its original or permanent form. The released stress energy induces change because of the chain mobility. Chen et al. introduced nanocomposite with single-walled carbon nanotubes into the Nafion matrix, which has the capacity of embedding at least three irregular shapes, which has a range of thermal expansion characteristics. It is demonstrated that single-walled carbon nanotube (0.5%wt) dispersed Nafion matrix nanocomposite have the capacity of retaining different shapes by the different wavelength radiation which has given this material self-healing capability by the photothermal effect. As seen on the Figure 1.25 808nm NIR radiation material retained 2D wave-like form, by increasing the temperature another irregular shape was derived from the irregular shape of the lower temperature Figure 1.25 (Habault et al., 2013).

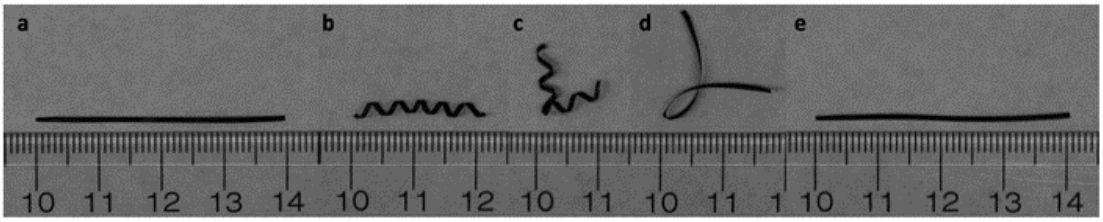

Figure 1.25 : Pictures showing the photocontrol of the shape memory behavior of Nafion containing dispersed CNT (0.5 wt%): (a) permanent shape; (b) first temporary shape (coiling) obtained using 808 nm NIR light exposure (6mWmm^{-2}, T = 70–75 1C) followed by cooling; (c) second temporary shape (bending at the center of the coil) obtained by localized 808 nm NIR light exposure (25 mW mm^{-2}, T = 140–150 1C) followed by cooling; (d) uncoiling in an oven at 75 1C while preserving the bending; and (e) unbending to the permanent shape via 808 nm NIR light (T = 140–150 1C). (Habault et al., 2013).

1.1.6.8 Electrohydrodynamics

For achieving self-healing by electrohydrodynamics, colloidal particles are suspended between the walls of the double-walled metallic cylinder, which has a metallic layer followed by a ceramic layer coating. When the damage occurs on the double walled metallic cylinders ceramic layer current density locally increases which induces agglomeration of the colloidal particles to the damaged area by the EHD (electrohydrodynamics) flow Figure 1.26 (S. K. Ghosh, 2009).

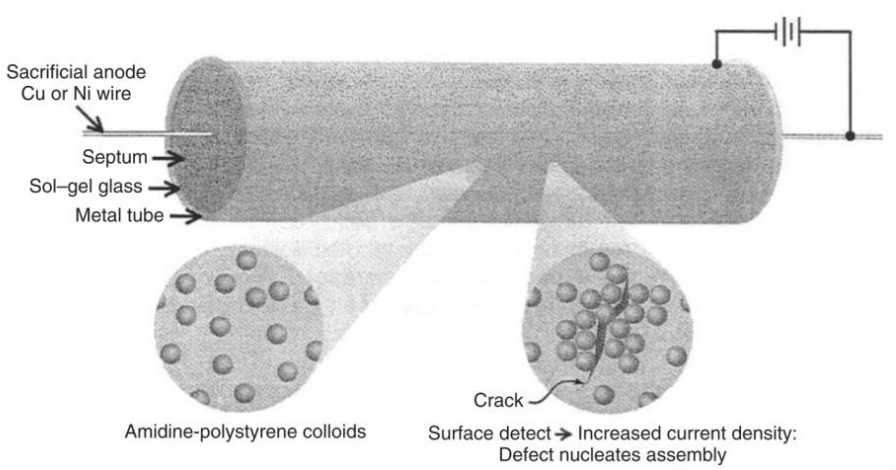

Figure 1.26 : Schematic showing electrohydrodynamics aggregation of particles(S. K. Ghosh, 2009).

1.1.6.9 Electrically conductive and resistance heating self-healing polymers

Such mechanism is not currently available for industrial applications. The healing mechanism is based on the heating of the polymer as the links between conducting polymers breaks by nanocracks. This nanocrack increases the temperature locally,

which triggers recombination of severed bonds in molecular scale. Under the presence of a solvent, razor blade damaged multi topis N-heterocyclic carbenes (NHCs) show smoothing after polymer was resistance heated to 200°C for 25 minutes. The process could be applied to carbon fibers which have not presented to the literature yet Figure 1.27 (Syrett et al., 2010).

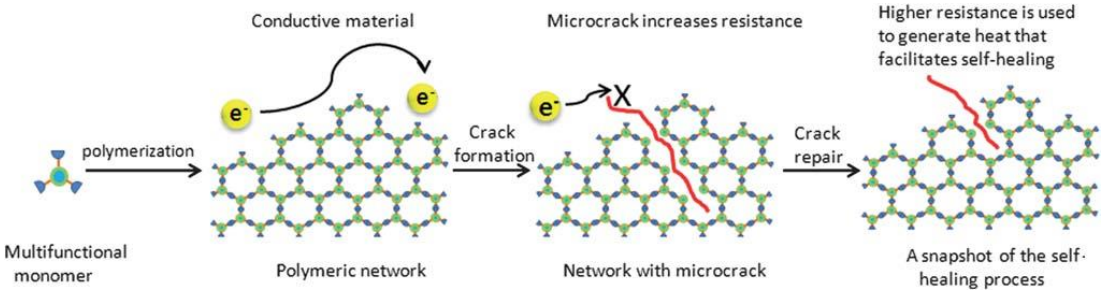

Figure 1.27 : The concept of an electrically conductive, self-healing material. Electrical resistance increases upon formation of a microcrack, as the total number of electron percolation pathway decrease. As the microcrack is the source of the resistance increases, the generation of heat as localized at the fracture point (Syrett et al., 2010).

1.1.6.10 Layer by layer approach

Deposition of organic and inorganic compounds Layer-by-Layer (LbL) on a surface of material changes the interfacial area's properties dramatically, which may lead to change in the overall properties. The mobility of materials induces Self-healing by LbL at multilayers, which can respond external stimuli. The availability of unbound mobile chains within the LbL layers is the critical factor of self-healing in this approach. LbL assembly structures can use to develop extrinsic self-healing materials Figure 1.28.

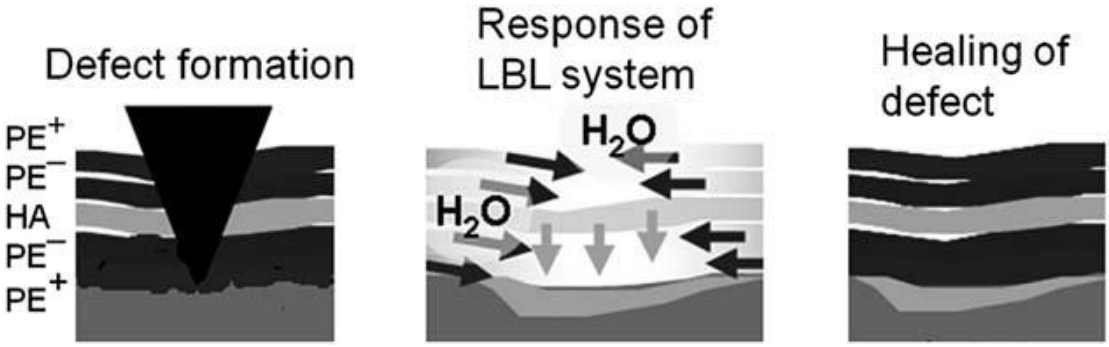

Figure 1.28 : Schematic illustration of the self-healing behavior of LbL films (positively charged polyelectrolytes, PE+, negatively charged polyelectrolytes, PE and healing agent, HA) stimulated by water penetration into the multilayers. The healing agent released from the multilayers and healed surface defects. Finally, the multilayers restore film integrity (Skorb & Andreeva, 2013).

For industrial and biomedical applications, there are the varieties of LbL proposals. Under physiological conditions, it is possible to release of DNA from LbL films. Also, polyelectrolyte multilayers can self-heal, the mobility induced by environmental factors such as pH, temperature, ionic strength, light. LbL self-healing method is used in developing self-healing superhydrophobic surfaces as can be seen from Figure 1.29 below (Skorb & Andreeva, 2013; X. Wang, Liu, Zheng, & Sun, 2011).

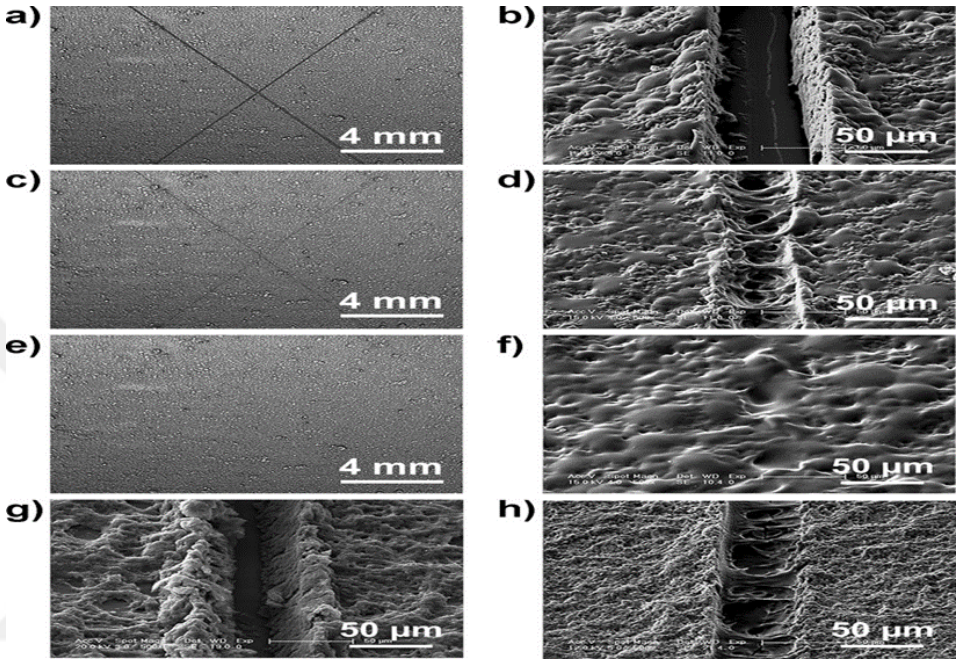

Figure 1.29 : Visual observation of (bPEI10.5/PAA3)*30 and (bPEI6.5/ PAA3)*300 coatings with cuts 50 mm wide after different times of immersion in water. a–f) The (bPEI10.5/PAA3)*30 coating immersed in water for 0 s (a,b), 10 s (c,d), and 5 min (e,f). g,h) The (bPEI6.5/ PAA3)*300 coating immersed in water for 0 s (g) and 24 h (h(X. Wang et al., 2011)).

Atomistic diffusion and rearrangement are different at the surface and the internal part of the materials. Near the surface area in nanometre scales, the boundary diffusion increases with respect to central locations (Y. B. Wang et al., 2011). As an example to such approach Polyallylamine hydrochloride (PAH) is used to create a rough surface, poly(acrylic acid) (PAA) multilayers and suffocated poly(ether ether ketone) (SPEEK) bounded by covalent bonds to hydrophobic 1H,1H,2H,2H-perfluorooctyl triethoxysilane (POTS).

Hydrophobic Rearrangement of polyelectrolyte chains induce the POTS molecules with covalent attachments to move to the surface as the damage occur PAH-SPEEK/PAA multilayers swell in a humid environment,. PAH-SPEEK/PAA multilayers are healed by diffused fluoroalkyl chains (Skorb & Andreeva, 2013).

1.1.6.11 Mechanical properties of self-healing polymeric materials

There is a need for correlating the morphology of the self-healing materials with the mechanical performance; such correlation requires better understating of the flexible chains and the stable nanoscopic interactions and their effect on the material as a whole (Balazs et al., 2006). Main aspects affecting performance of self-healing materials are;

- Healing agent/catalyst depletion
- Stability of the healing agent in microcapsules
- Process survivability of Microcapsule shells
- Release of healing agent from capsule
- Bonding of capsule/matrix interface
- Viscosity and volatility of healing agent
- Diffusion characteristics of healing agent
- Distribution characteristics of healing agent/catalyst

All of the concerns above have a direct or indirect effect on mechanical properties of in self-healing virgin or healed material (Brochu, Craig, & Reichert, 2011).

1.1.6.12 Damage propagation and recovery mechanisms of the self-healing materials

Polymers and composites are commonly used in aircrafts, ships, cars, construction industries and defense as structural materials, many techniques are used to repair detectable damages although these methods are applicable for visible deformations while being ineffective against microcracks (Wu et al., 2008). Self-healing materials possess unique characteristics, which solves the most profound problem in structural materials, which are hidden damage and microcracks.

Self-healing materials increase the service life of structural materials by healing microcracks, which are precursors to structural failure. Preventing microcracks also decreases degradation by the environmental factors such as swelling by moisture or stress corrosion cracking (White et al., 2001).

The most common damage possibilities for self-healing polymeric materials are

- Delamination,
- Impact/indentation surface cracking,
- Fiber debonding,
- Fiber rupture and pullout,
- Transverse and shear cracking,
- Puncture,
- Deepcutincoating,
- Corrosion in protected metal,
- Crazing,
- Scratch,
- Ablation,
- Microcracking, and
- Opening crack.

Depending on the characteristics of polymer matrix, amount and rate of loading damage mode changes as can be seen from Figure 1.30 below (Blaiszik et al., 2010);

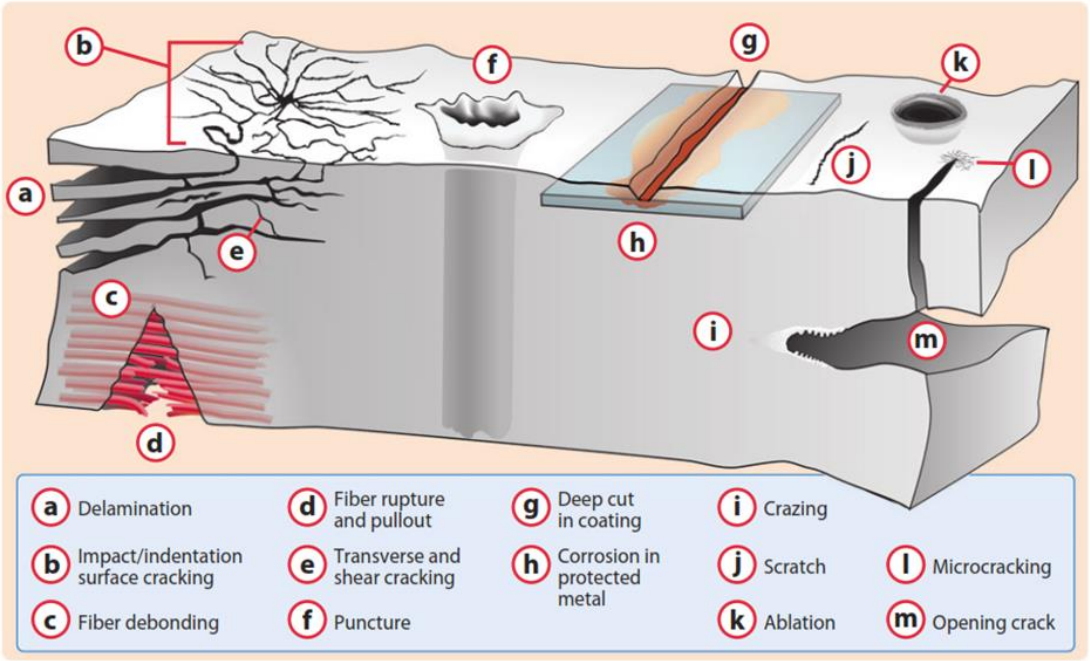

Figure 1.30 : Damage modes in self-healing polymeric materials (Blaiszik et al., 2010).

When microcrack forms inside a self-healing material, which have microcapsules loaded with healing agent microcapsule and the surrounding matrix are under a far-field tensile loading σ_∞ , which is perpendicular to the crack plane. The stiffness of the microcapsule determines the stress state of the crack tip as well as the matrix material covering microcapsule as can be seen from Figure 1.31 below. If the microcapsule is stiffer than the matrix material the stress field near the crack tip has asymmetry, which can be interpreted as, the crack will deflect away from the microcapsule, which is an event highly undesirable. If microcapsule is compatible with crack will be attracted to the microcapsule, which will cause the crack move towards to the microcapsule, followed by rupture of the crack and release of healing agent finalized by the healing of damaged area (White et al., 2001).

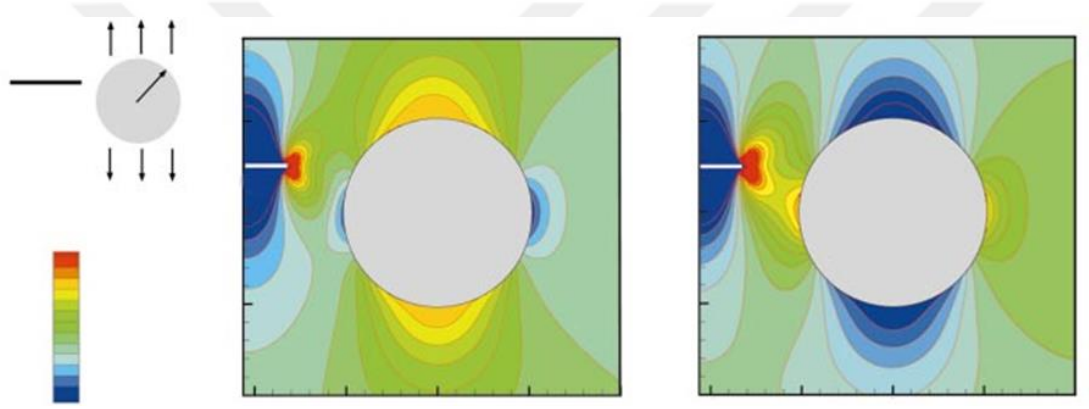

Figure 1.31 : Stress state in the near of a planar crack. (White et al., 2001).

1.1.7 Mechanical properties

Many of the characteristics of the self-healing materials can be evaluated by mechanical tests (Table 1.3). Most common mechanical tests performed for determination of self- healing characteristics of materials are; impact test, flexural test and compression test.

1.1.7.1 Impact test

The impact tests are used to determine the impact properties of materials. Plat plate specimens are prepared by molding or cutting from the larger component. The specimen is fixed from both edges and a vertically falling metal piece impacted to the center. The impact performance of the material is the amount of the energy it absorbs during tests. The absorbed energy is the accumulation of deformation and damage

energy. This method is used to determine the energy required to break the material. This method is widely used for polymers and polymer composites (Swallowe, 1999).

1.1.7.2 Flexural test

The material's ability to withstand perpendicular and longitudinal forces are called flexural strength. The flexural load has two components; compressive and tensile stress. Stress and strain at outside surface of the test bar determine the flexural properties of materials.

There are two basic flexural test methods; four-point bending and three-point bending. For 3 point bending flat specimens pun on two support legs. From the middle of these legs, a third leg applies a load from the middle. This method is used for quality control and determination of the specification of materials. Four point bending test has the same principle, but there are two loading legs instead of one. The distance between the loading and support legs are kept the same. Also, the distance between the load legs is kept as the 1/3 of the support span (Kutz, 2002).

1.1.7.3 Compression test

Composite materials compressive characteristics are widely studied. Voids, stress concentrations, and inhomogeneous effects the compressive behavior of the materials. There are three types of methods for compressive tests;

- Type I the specimen is short and unsupported,
- Type II the specimen is long and supported,
- Type III the specimen is straight sided and loaded to a honeycomb core.

As general the specimen pun in the middle of the two loading legs. These legs apply load the specimen until critical failure occurs. Compression test is widely used for composites and polymers (O'Brien, Fibers, & Composites, 1991).

Table 1.3 : Mechanical test done to determine self-healing capacity of the materials (adopted and recreated from resources (Wu et al., 2008; Ming Qiu Zhang & Rong, 2011a)

Matrix	Healing Type	Healing Method	Test Medhod			Ref.
			Impact Test	Bending Test	Compression Test	
Thermoplastic	Molecular	Photo-induced healing		✦		(Chung, Roh, Cho, & Kim, 2004)
Thermoplastic	Encapsulated (GMA) Glycidyl methacrylate	Living Polymerization	✦			(H. P. Wang, Yuan, Rong, & Zhang, 2010)
Thermoplastic	Bulk	DA reaction		✦		(Y. Zhang, Broekhuis, & Picchioni, 2009)
Thermoset	Structural	Thermoplastic additives	✦			(Hayes, Zhang, Branthwaite, & Jones, 2007)
Thermoset	Bulk	Postcuring of residual functional groups	✦			(Hsieh, Yang, & Lee, 2001)
Thermoset	Hollow tubes containing healant	Curing of healant	✦	✦		(Trask, Williams, & Bond, 2007)
Thermoset	DCPD stored in 3D microvascular networks	Ring-opening metathesis polymerization		✦		(Toohey et al., 2007)
Thermoset	Encapsulated epoxy monomer	Cationic polymerization	✦			(Xiao, Yuan, Rong, & Zhang, 2009)
Thermoset	Bulk	DA reaction		✦		(Park et al., 2010)
Thermoset	Bulk	DA reaction			✦	(Murphy et al., 2008)
Thermoset composites	Structural	Thermoplastic additives		✦		(Zako & Takano, 1999)

1.1.8 Healing efficiency

Healing of the self-healing materials can be accepted as recovery on the fracture toughness, tensile strength, molecular weight, conductivity and surface smoothness of the damaged specimen, as self-healing have such broad range of definitions it is difficult to measure and compare the self-healing efficiency (Wu et al., 2008). The extent of healing must be determined separately for each of the mechanical properties. Healing efficiency can be explained by Equation 1.1. (Blaiszik et al., 2010; Herbst, Dohler, Michael, & Binder, 2013);

$$Healing\ efficiency\ = \frac{Mechanical\ value}{mechanical\ value_{pristine}} \tag{1.1}$$

Self-healing materials show some characteristics for self-healing;

- Intrinsic self-healing has the recovery at molecular scale but can recover small damages
- Vascular systems can heal more significant damages while little or nonresponsive to small damages
- Microencapsulation shows performance in between intrinsic and vascular systems (Blaiszik et al., 2010).

Healing efficiency comparison can be seen from Figure 1.32 below;

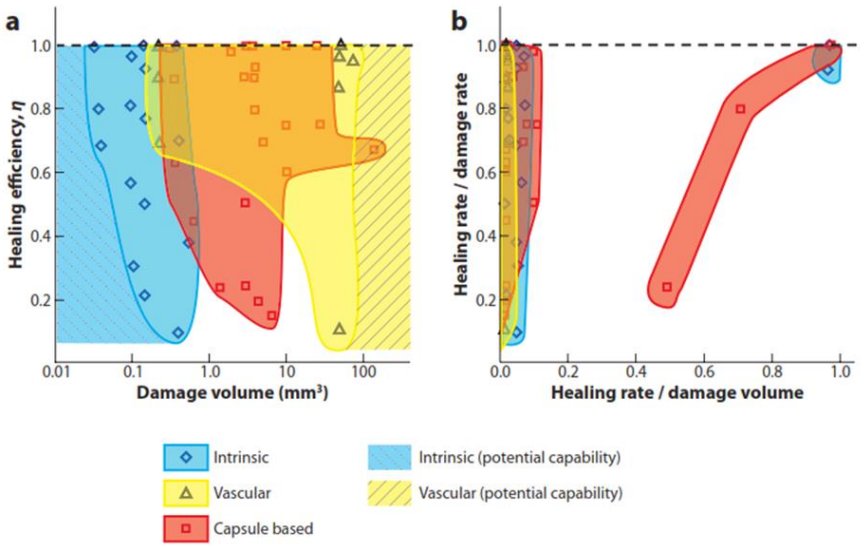

Figure 1.32 : Performance maps for self-healing materials (Blaiszik et al., 2010).

As there is, no recovery time is given to different type self-healing materials impact test is the best solution to evaluate different types of self-healing materials. The tests are done as follows; first, the specimens are prepared, and impact test is applied the values are recorded regarding joule. Broken pieces are put together and time is given to self-healing material for recover impact test is repeated and the value in terms of a joule is compared with virgin or other materials which might have different breaking and healing cycles. Such approach prevents the effect of dynamic recovery that might affect the values in a simple tension test. Also, impact test calculations are more reliable than toughness calculations. Measuring self-healing capacity with toughness is inherently unreliable as the loading rate is wholly neglected while the time is a dominant factor for some self-healing materials.

1.1.9 Radiation shielding properties

1.1.9.1 Linear and mass attenuation

Radiation is stopped by the collisions inside the material. Radiation absorption characteristics of material should be determined for designing shielding materials. For shielding materials, the attenuation of gamma rays follows the Equation 1.2. The proportionality of passing photons explained by the (linear or mass) attenuation coefficient (μ) (Equation1.2) (Was, 2007).

$$I = I_0 e^{-\mu x} \tag{1.2}$$

I = transmitted radiation intensity

I_0 = initial radiation intensity

μ = linear attenuation coefficient

x = the travel distance of radiation

The tests are conducted as follows; the samples were placed between a collimated radiation source and detector. The radiation passing through the material and reaching to the certified detector was calculated by the attached computer. The connection of the system was performed by using multi-channel analyser and the application of software. Hence linear attenuation of radiation by increasing thickness (cm) was

studied. Mass attenuation thickness (cm^2/g) is calculated by multiplying the linear attenuation values with a density of the material (Choppin, Liljenzin, Rydberg, & Ekberg, 2013).

1.1.9.2 Half-value layer

Half-value layer (HVL) is the thickness requirement of the material to stop half of the incoming radiation. Half-value layer is also called as half-value thickness.; calculated by equation 1.3. HVL is very practical in terms comparing two materials radiation shielding capacity.

$$HVL = \frac{0{,}693}{\mu} \tag{1.3}$$

Theoretical and experimental; linear and mass attenuation coefficients data was used to determine the half value thickness (Was, 2007).

1.2 Hypothesis

The mass reduction by decreasing the amount of shielding from the space radiation lower the launch costs. With current metal and polymer shielding, even the vehicle survives a hostile environment it carries its damage during its service life. The material shows a significant decrease in its capabilities to perform its duties with cumulative radiation damage.

A metal shielding material will fail even below tolerable radiation amounts. In this thesis, our advanced materials multiphase self-healing capacity will give it to recover to its original state, as close as possible and with time get ready for next incident. Also living polymer matrix gives the capability to build the material various shape sizes and end uses for addressing different radiation shielding of aeronautics industry.

PMMA nanocomposite material consisting of GMA healing agent microspheres (MK) can be used against the ionizing radiation such as gamma, beta, alpha, and neutrons. Hence it can be used as a multi-scale self-healing nanocomposite shielding material for aerospace applications.

2. METHODOLOGY

2.1 Nanocomposite Synthesis

2.1.1 Materials

Nanocomposites are defined as materials has one self-repetitive component less than 100 nm, or whose structure is at the nanoscale. The mechanical and physical properties of the matrix materials can be significantly modified by mixing the inorganic particles nanoparticles. The main reasons for the development of polymer nanocomposites are that the material has multi-functional properties (Koo, 2006).

Halloysite clay nanotubes (HNTs) are a naturally occurring aluminosilicate nanotubes. The two-layered halloysite tubes resemble kaoline chemically. Halloysite clay nanotubes (HNTs) are ~ 15 x 1000 nm in size compared to multiwalled carbon nanotubes (Outside diameter × Length, 6-9 nm × 5000 nm). HNTs are hollow nanotubes. HNTs can provide good integration when a matrix is added to a structure. HNTs are nanoparticles that can be mixed well with polymers without any surface modification (Abdullayev & Lvov, 2013).

Montmorillonite clay nanoplates can be homogeneously distributed in the polymer structure. Thus, the homogeneous distribution of the clay nanoplates in the polymer improves the mechanical strength of the polymers (Yeh et al., 2002). The nano-sheet-like montmorillonite nanoparticles are the preferred nanoclusters for polymer applications and can readily conform to the polymer structure. Montmorillonite clay nanoplates (MMT) can be homogeneously distributed in the PMMA matrix. MMT improves the mechanical properties of the polymer (Qu, Guan, Liu, She, & Zhang, 2005). Montmorillonite nanoclay consists of nano-plates stacked in multi-layered stacks of ~ ten μm in size with metal cations on the surface. Montmorillonite nanoclay is nanoclusters that are compatible with the molten polymer structure and can increase the temperature at which the polymer begins to bend (Yeh et al., 2002).

Although the nanoparticle form of Colemanite (CMT) is not currently available, previous reports stating attractive radiation shielding characteristics of CMT motivated

the study to reinforce PMMA with CMT for potential applications against hazardous radiation. Additionally, production of advanced material for critical applications by utilizing low-cost CMT is another attractive point of this work. Colemanite (CMT) (Ca2B6O11·5H2O) is the most important of 200 different boron minerals. CMT accumulates 70% of all Turkey boron reserves which is the largest in the world (Celik, Depci, & Kılıc, 2014; Gönen, Nyankson, & Gupta, 2016; Kalay, Yilmaz, & Çulha, 2013). CMT theoretically has 50.8% B_2O_3 and a specific weight of 2.52g/cm2 with monoclinal structure. CMT dissolves in acid, has a greenish grey color (Sallı Bideci, 2016). CMT is used in the production of glass and high-tech ceramics (Uysal, Mutlu, & Erdemoğlu, 2016).

Demir et al. studied the gamma attenuation coefficients of CMT ore (Demir, 2010). Okuno has proposed a neutron shielding material by mixing CMT with epoxy resin (Okuno, 2005). Several different concretes reinforced with CMT have been proposed for neutron radiation environments (Derun & Kipcak, 2012; T. Korkut et al., 2012; Turgay Korkut et al., 2010; Malkapur et al., 2017; Mesbahi, Alizadeh, Seyed-Oskoee, & Azarpeyvand, 2013).

In this study, PMMA, PMMA/MK, PMMA/MK/HNTs, PMMA/MK/MMT and PMMA/MK/CMT polymer structures were produced by using Atom Transfer Radical Polymerization (ATRP) technique. In PMMA, the clay nanotube, clay nanoplate and colemanite particles were homogeneously dispersed. The production parameters of the polymer nanocomposite were determined experimentally. To survive the dispersion problem in PMMA nanocomposites restricted to maximum MK 1% wt. and nano-clay 5% wt.

Figure 2.1 : Chemicals used in production of nanocomposites

The chemicals used in production of nanocomposites are; Tetra-n-butyl ammonium bromide($C_{16}H_{36}BrN$), Copper(I) bromide 99.999% trace metals basis (CuBr), Methyl methacrylate, 99%, stab. ($CH_2=C(CH_3)COOCH_3$) , N, N, N′,N″,N″-Pentamethyldiethylenetriamine ($[(CH_3)_2NCH_2CH_2]_2NCH_3$), Ethyl α-Bromoisobutyrate ($(CH_3)_2CBrCOOC_2H_5$) EBIB (% 98), Formaldehyde solution; ACS reagent, 37 wt. % in H_2O, contains 10-15% Methanol as a stabilizer (to prevent polymerization).

Melamine 99%; 2,4,6-Triamino-1,3,5-triazine, sym-Triaminotriazine. Sodium dodecylbenzenesulfonate technical grade Dodecylbenzenesulfonic acid sodium salt. PVA Mw 85,000-124,000, 99+% hydrolyzed, 1-Octanol ACS reagent, ≥ 99% Alcohol C8, Capryl alcohol, Octyl alcohol, Halloysite clay nanotubes (HNTs) and montmorillonite clay nanoplates (MMT) are obtained from Sigma Aldrich. Purified Colemanite ($Ca_2B_6(OH)_{10}\cdot 8H_2O$) were obtained from mine Bursa Kestelek (Turkey). The characteristics of the CMT is given in the reference (Bulutcu, Ertekin, & Celikoyan, 2008).

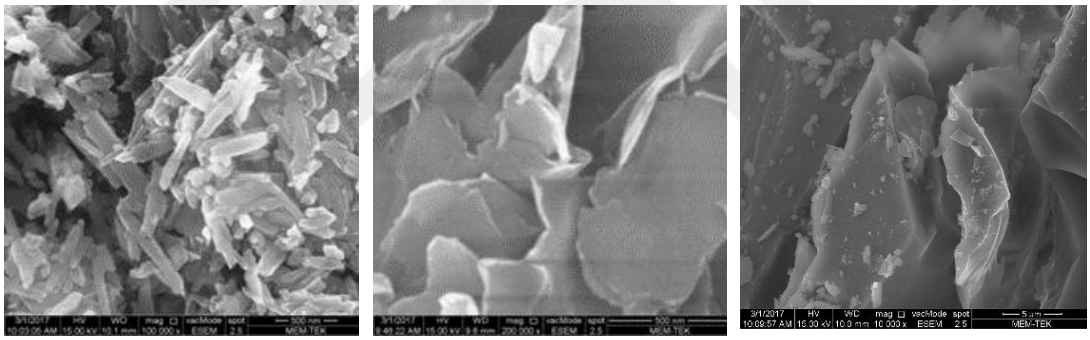

(a) (b) (c)

Figure 2.2 : SEM images of a) HNTs, b) MMT and c) CMT.

Halloysite clay nanotube (HNTs) dimensions (diameter × length) are 30-70 nm × 1-3 μm (Figure 2.2-a). Montmorillonite (MMT) based clay nanoplates, 35-45 wt. % dimethyl dialkyl (C14-C18) amine. The montmorillonite-based clay nanoplate particle size used in this study is ≤ 20 μm (Figure 2.2-b). The CMT was grinded to an average particle size between 5μm to 10μm (Figure 2.2-c).

2.1.2 Production of Glycidyl Methacrylate (GMA) loaded microcapsules (MK)

Encapsulation is a process; trapping active core by the wall inside a material. Wall can be synthetic polymers or natural polymers. Melamine Formaldehyde (MF) has been chosen as the shell resin. MF resin shell is a brittle material which can break and set

healing agent free easily. MF resin has excellent thermal and water resistance. Glycidyl Methacrylate (GMA) loaded microcapsules has several practical advantages such as; high boiling point (189 °C) and low water solubility.

For encapsulation of GMA;

- 0.06 mol and 0.2 mol melamine and formaldehyde were respectively included in a 20 ml three-neck flask with deionized water,
- Two wt % NaOH solution was added to solution up to PH was 8.5 − 9.0,
- Solution was mechanically stirred (Figure 2.3)

Figure 2.3 : MK production setup.

- The temperature was increased to 65 − 70 °C,
- After 30 min Prepolymer of melamine and formaldehyde were obtained,
- Sodium Dodecyl Benzenesulfonate (SDBS) was utilized as emulsifier,

- 26.2 ml GMA, Poly(vinyl alcohol) (PVA) aqueous solution and 100 ml Sodium Dodecyl Benzenesulfonate were supplemented in prepolymer solution,
- pH of solution was lowered to ~ 4.0,
- Mixture was stirred for 30 min to get a stable emulsifiable solution,
- PVA was performed to protect the colloids,
- High-speed mechanical stirring was continued for 6 hours.

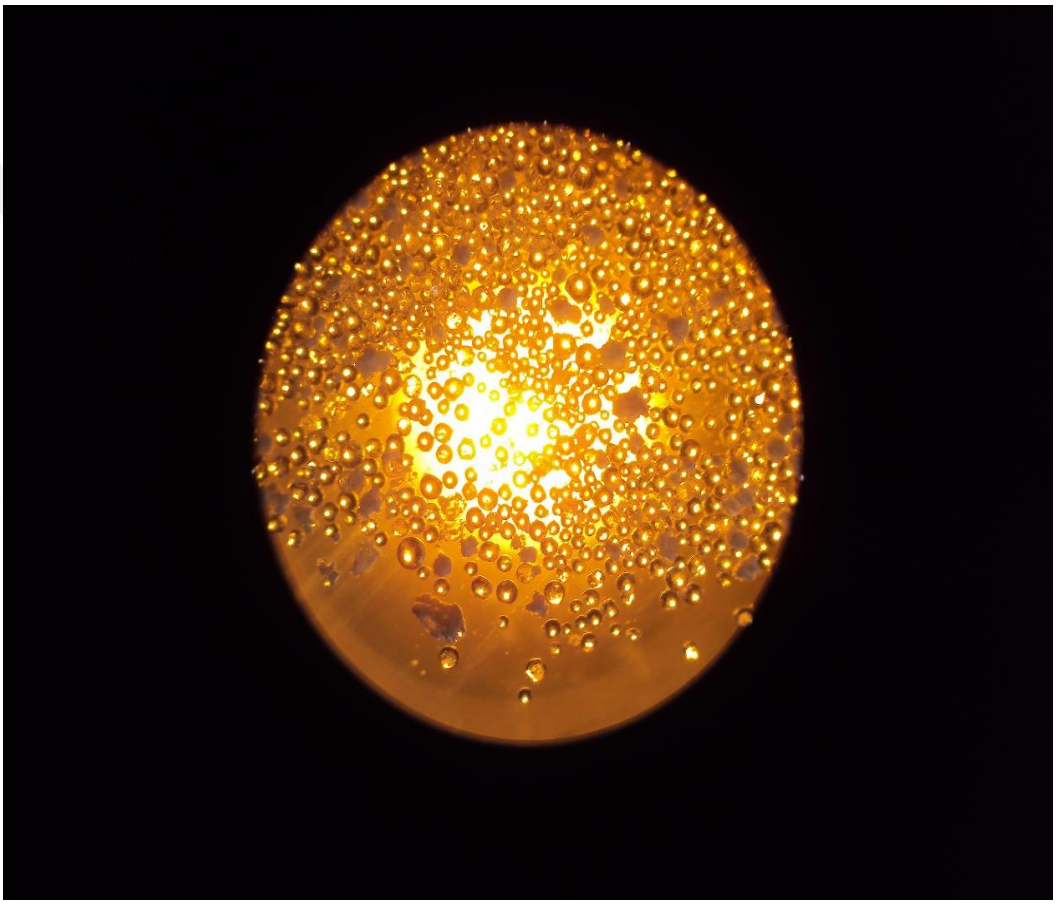

Figure 2.4 : Glycidyl Methacrylate (GMA) loaded microcapsules (MK).

Resultant solution water washed and then dried at room temperature. Thus the Glycidyl Methacrylate (GMA) loaded microcapsules (MK) was produced (Figure 2.4).

2.1.3 Nanocomposite synthesis.

38,4 mmol Tetra-n-butyl ammonium bromide (Bu_4NBr 12,372g) and 4,8 mmol Copper(I) bromide (CuBr 0,684g) measured inside a glove bag filled with argon. After

the weight measurements had been finished, the reaction tube was sealed with silicon septum (Figure 2.5).

Figure 2.5 : Weight measurements were finished, and the reaction tube was sealed.

Before pouring the Methyl Methacrylate (MMA), the porous ceramic fitted glass pipe was used to create argon bubbles inside the MMA. An extra pure argon purge was continued for 30 minutes inside a 500-mL beaker.

Figure 2.6 : An extra pure argon purge for 30 minutes.

After MMA is degassed, 280ml MMA was measured, and the 20ml syringe was prepared (300ml total). The tube was opened inside a glove bag filled with argon, MMA inside the syringe has first applied followed by the remaining MMA.

4,8 mmol PMDETA ($C_9H_{23}N_3$ 0,828g) was added to the mixture, and the mixture was degassed (Figure 2.6). Later 4,8 mmol EBiB (0,936g,) was added, and the tube was sealed with silicon septum and Parafilm at 25°C.

Figure 2.7 : The solution was stirred using a magnetic stirrer.

The resulting solution was stirred using a magnetic stirrer for 4 – 6 hours at 25°C with 600 rpm (Figure 2.7). Stirring was done to ensure homogeneity of the solution. PMMA samples were filled with 3,12gr (% 1wt.) MK. After MK, 3,12gr (% 1wt.), 9,36gr (% 3wt.) and 15,6gr (% 5wt.); HNTs, MMT, and CMT was added to the partially

polymerized mixture inside a glove bag under argon atmosphere. The partially polymerized solution of the nanocomposite was homogenized by an Interlab brand rotating shaker.

Figure 2.8 : Moulds were placed inside vacuum desiccators inside a glove bag and sealed with polymer industrial polypropylene.

A few hours later, the viscosity of the solution increases and mobility of the fillers were stopped. The mostly polymerized mixture was poured into glass molds inside a glove bag under argon atmosphere. Moulds were placed inside vacuum desiccators inside a glove bag and sealed with polymer industrial polypropylene film. 24 hours later cured samples are removed from the desiccators (Figure 2.8).

(a) (b) (c)

Figure 2.9 : Samples a) taken out from the mold, b) cut, c) polished.

It should be noted that melt mixing became more difficult with the addition of filler higher than 5 wt. % as the result of agglomeration. Melt mixing period has been extended by adding filler after shorter times from the initiation of polymerization to achieve; homogeneous distribution of the filler in the structure of the composites, filler addition has been made after six hours of initiation of polymerization for 1wt. % and

2 wt.% composites while after 5 hours for 5 wt. % composites. Later samples were cut and polished (Figure 2.9).

2.2 Structural characterization

X-Ray Diffraction analyses for all the samples were carried out using Panalytical PW3040. XRD patterns of PMMA, PMMA/MK, PMMA/MK/HNTs, PMMA/MK/MMT and PMMA/MK/CMT composite samples are presented in Figure 3.1-4. X-ray diffraction (XRD) carried out by Cu α (λ=1.54Å) radiation.

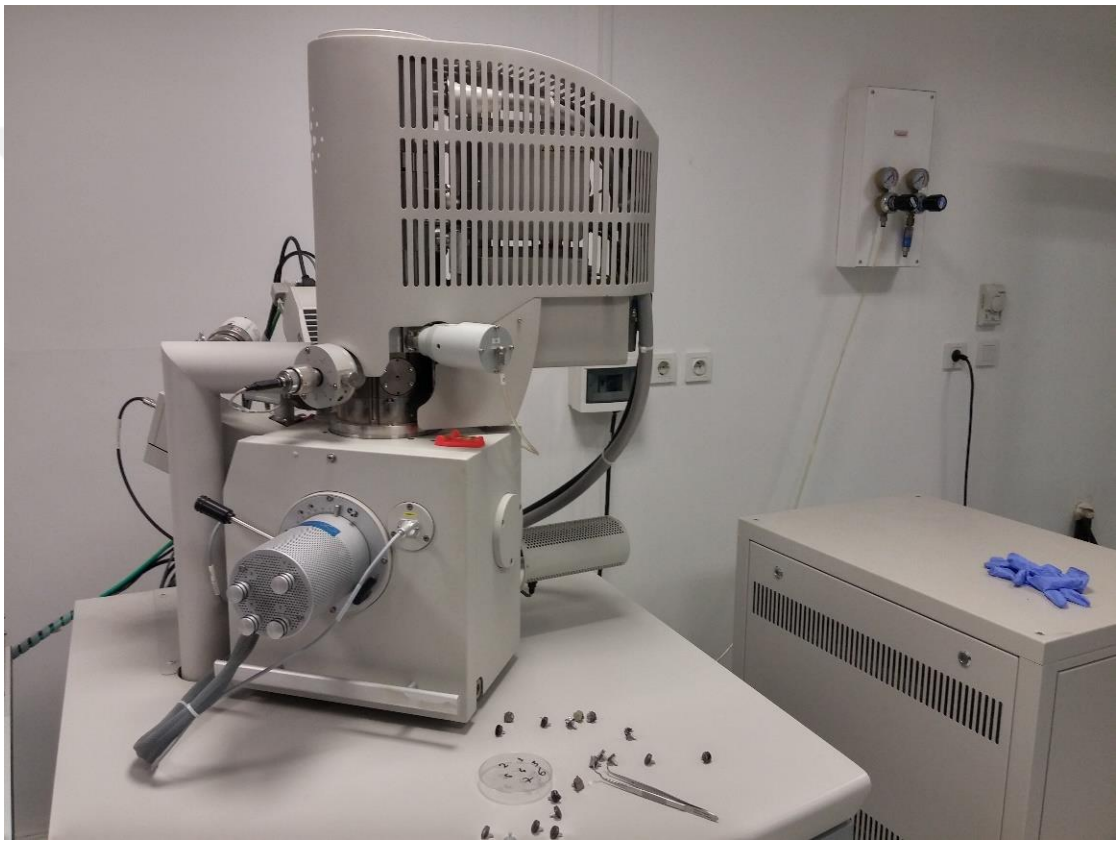

Figure 2.10 : Field-Emission Environmental Scanning Electron Microscope.

Field-Emission Environmental Scanning Electron Microscope (FESEM) was used to evaluate the micrographs of PMMA, PMMA/MK, PMMA/MK/HNTs, PMMA/MK/MMT and PMMA/MK/CMT composite samples (Figure 2.10).

Figure 2.11 : Gold Plating of samples

The samples were gold coated to prevent surface charging before SEM images were captured (Figure 2.11). The thermal stability analysis was made by the TA Instruments DSC SDT Q600 Thermogravimetric Analyzer. 3-5 mg samples were heated from 25°C to 100°C with 5°C/min increase, at 100°C kept isothermal for 5 min and from 100°C to 600°C 20°C/min increase under 100 ml/min nitrogen flow.

Fourier transform infrared spectroscopy (FTIR) analyses made by PerkinElmer Spectrum One FTIR Spectrometer. FTIR spectra were measured in the transmittance mode. Band assignments obtained from the literature (Budak & Gönen, 2014; Cetin, Unal, & Erol, 2012; Elashmawi & Hakeem, 2008; Frost, Xi, Scholz, Belotti, & Cândido Filho, 2013; Namouchi et al., 2009; Ramesh, Leen, Kumutha, & Arof, 2007). 3D surface image and 2D and surface roughness of PMMA, 5wt.% MK PMMA/MK, 1wt.% MK, 5wt.% HNTs, PMMA/MK/HNTs, 1wt.% MK, 5wt.% MMT, PMMA/MK/MMT and 1wt.% MK, 5wt.% CMT, PMMA/MK/CMT composites were investigated using the Zygo NewView 8000 optical profilometer (Figure 3.12 a-l).

2.3 Mechanical properties characterization

To investigate the mechanical properties of PMMA, PMMA/MK, PMMA/MK/HNTs, PMMA/MK/MMT nanocomposites and PMMA/MK/CMT composite, Shore D hardness test, Izod impact test without a notch, 3-point bending test, and compression test were applied. The change in Shore D hardness of the prepared nanocomposite specimens is given in Figure 3.14.

The change in Shore D hardness of the nanocomposite samples according to the type and proportion of the reinforcing component was investigated. Based on the type and ratio of the reinforced component of the micro and nanocomposite structures produced, the change of the notched Izod impact resistance was determined. Izod impact tests were carried out according to the general principles of the ASTM D256 standard, and the samples were also tested without indentation to reveal possible indentation effects of the reinforcing components in the composite structure.

Figure 2.12 : 50 J-capacity Zwick impact test device

In experiments where a 50 J-capacity Zwick impact test device is used, the impact resistance measured per unit area is calculated by dividing the measured impact resistance by the cross-sectional area of the samples (Figure 2.12). The variation of the bending strength depending on the type and ratio of the micro and nanocomposite structures, reinforcing component produced was investigated.

Figure 2.13 : Shimadzu electromagnetic testing machine.

Bending strength was determined by 3-point bending test (Figure 2.13). The change in compressive strength is determined depending on the type and ratio of reinforcing component and micro and nanocomposite structures produced. The compression test was carried out on cylindrical specimens by applying an axial compression load along the height and after the maximum compression load value was reached the test was terminated. The compressive strength was determined by dividing the maximum compressive load values by the cross-sectional area calculated from the initial diameter

of the sample. According to the type of PMMA nano-composite component; the change in flexural strength after self-repair was examined comparatively.

2.4 Application of radiation transmission technique

The behavior of the PMMA/MK, PMMA/MK/MMT nanocomposites and PMMA/MK/CMT composite samples under radiation conditions (Cs-137 radioisotope) has been done by utilizing gamma spectrometer containing a detector (Canberra Bicron Model: 802-2X2) and connected to a 1024-channel Multi-Channel Analyzer for counting the gamma-ray intensity coming from the source (I_0 initial radiation intensity) (Figure 2.14).

Figure 2.14 : Radiation transmission set-up

The diameter of the Cs-137 radioisotope is 6 mm. The properties of the used Cs - 137 radioisotopes are; specific gamma constant, $K\gamma$ = 3.8 x 10-1 mR/hr/mCi ; half-life, $T_{1/2}$ = 30.17 years ; energy of the emitted photons, $E\gamma$ = 0.662 MeV; activity A = 8.06 microCi.

The hole of the collimator for gamma rays was 7 mm for Cs-137 and 10 mm for Pu-Be. A distance of 200 mm for Cs-137 and 400 mm for Pu-Be was maintained between

the radiation source and the detector during the measurements. The distance between the radiation source and the sample was 100 mm for Cs-137 and 140 mm for Pu-Be. The samples were placed between the detector and the gamma source (Figure 2.15). The intensity was counted 25 min for each sample (I, transmitted radiation intensity). All measurements were repeated at five times at the same experimental conditions. MyCurve Fit program was used to make the curve fit the data better.

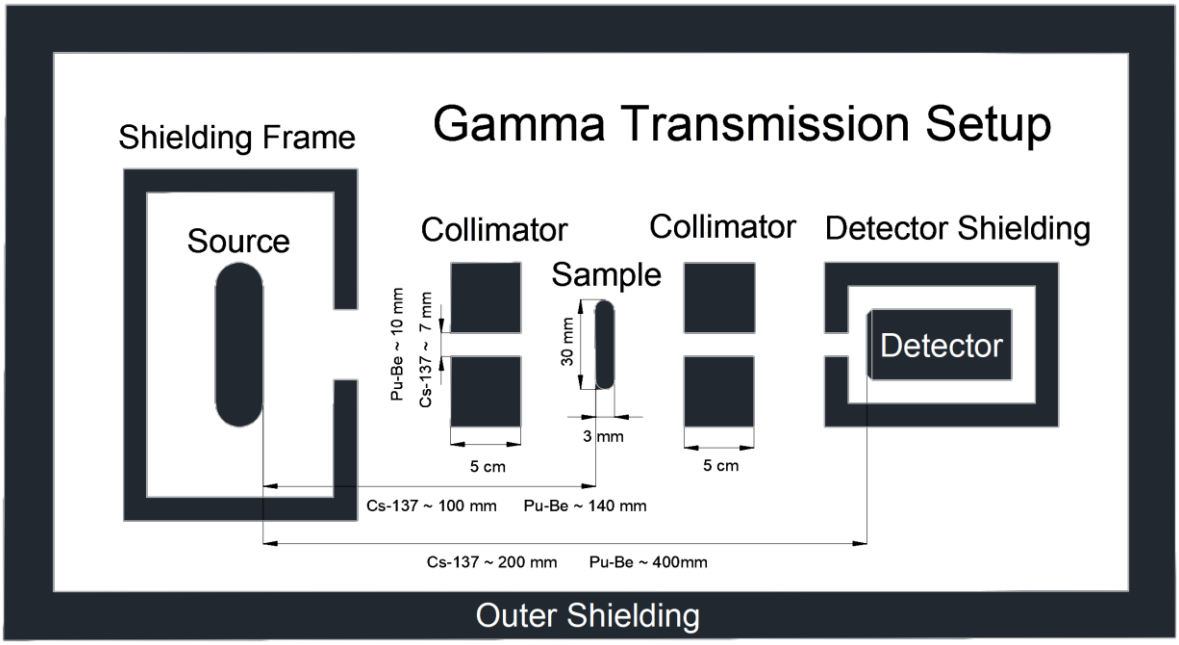

Figure 2.15 : Schematic diagram of radiation set up.

Neutron transmission tests were made by using a certified PuBe Neutron Howitzer (Pu-239) produced by Nuclear Chicago Corporation. PuBe neutron source has 5 MeV average neutron energy with 5 Ci activity. Neutron Howitzer (NH-3) generates neutron flux of 10^6 n/cm^2. He-3 detector was used for counting the neutrons. The distance between source and samples were 14 cm. Incoming neutrons were collimated to a narrow beam with a collimator which has 10 mm hole. First, the initial intensity was measured (I_0) then the reduction in intensity observed with increasing thickness (I). Background radiation levels were reduced. Thermal neutron transmission values were calculated from the generated data for PMMA/MK, PMMA/MK/MMT nanocomposites and PMMA/MK/CMT composite samples.

3. RESULTS

PMMA, PMMA/MK, PMMA/MK/HNTs, PMMA/MK/MMT nanocomposites and PMMA/MK/CMT composite samples were successfully produced. Reinforcement of PMMA had improved the radiation shielding properties. The physical properties of PMMA, PMMA/MK, PMMA/MK/HNTs, PMMA/MK/MMT nanocomposites and PMMA/MK/CMT composite samples were studied by X-ray powder diffraction (XRD) and Field-Emission Environmental Scanning Electron Microscope (FESEM), Fourier Transform Infrared Spectroscopy (FTIR), Thermal Gravimetric Analysis and 3D-2D Optical Profilometry. Radiation shielding capacity was experimentally assessed by Gamma and Neutron attenuation tests. Space readiness of the selected samples was tested by Japan Aerospace Exploration Agency (JAXA). Selected samples were handed over to JAXA team after ground tests were completed.

3.1 Structural Characterization Results

3.1.1 X-Ray diffraction analyses

XRD patterns of the PMMA and the composites are presented in Figure 3.4. The broad and weak peaks of PMMA at 15° and 30° (H. P. Zhang et al., 2007) indicate that PMMA had an amorphous structure (H. P. Zhang et al., 2007). Addition of Colemanite caused the appearance of sharp diffraction peaks of CMT at 15°, 28°, 31° and 51° (Tabanli, Bilir, & Eryurek, 2017).

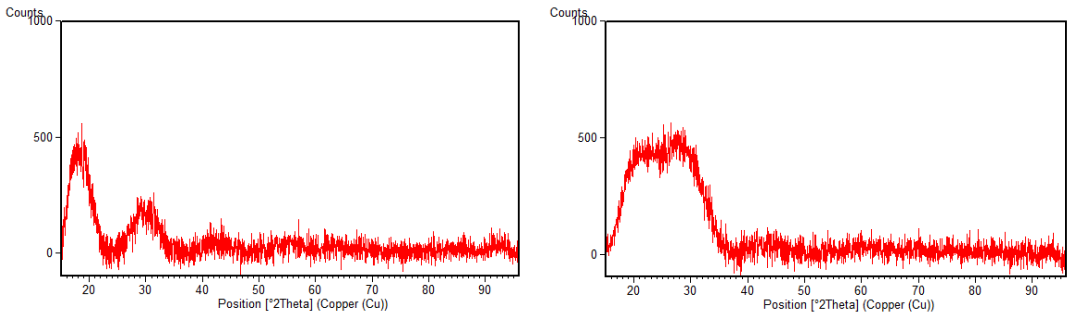

(a) (b)

Figure 3.1 : XRD pattern of a) PMMA and b) 5 wt.% MK PMMA/MK composite.

Addition of MK, HNTs, and MMT made new peaks to appear. PMMA, PMMA/MK, PMMA/MK/HNTs, PMMA/MK/MMT nanocomposites are amorphous.XRD Pattern of PMMA and 1 wt.% PMMA/MK shows characteristics of amorphous structure (Figure 3.1 a-b).

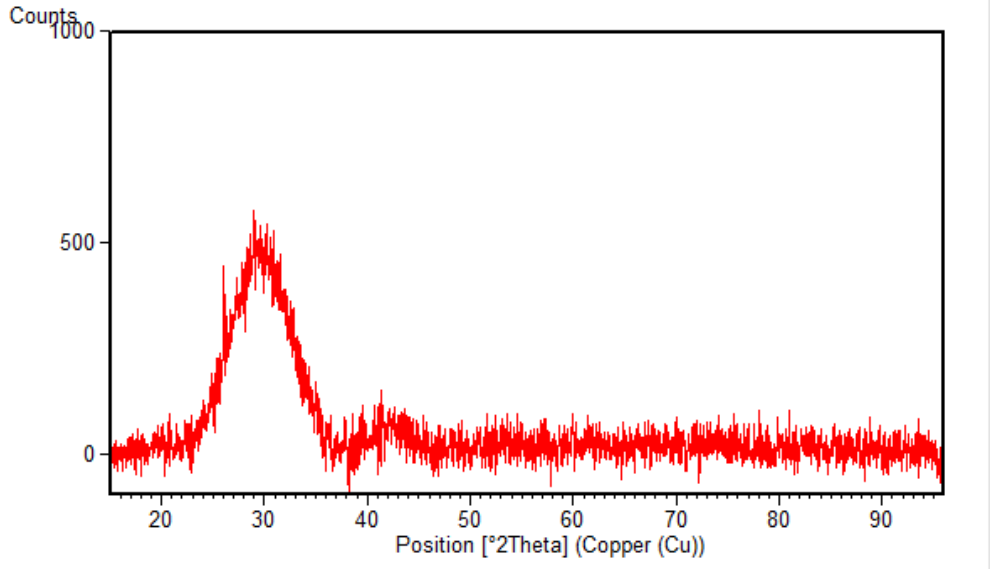

Figure 3.2 : XRD pattern of 1wt.% MK, 5wt.% HNTs, PMMA/MK/HNTs composite.

XRD Pattern of 1wt.% MK, 5wt.% HNTs, PMMA/MK/HNTs composite shows characteristics of amorphous structure (Figure 3.2).

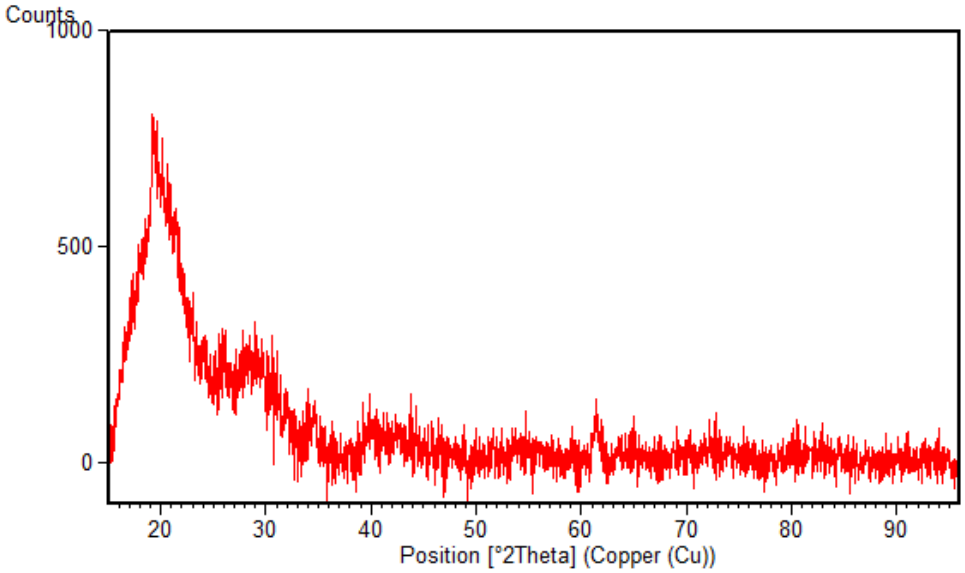

Figure 3.3 : XRD pattern of 1wt.% MK, 5wt.% MMT, PMMA/MK/MMT composite.

XRD Pattern of 1wt.% MK, 5wt.% MMT, PMMA/MK/MMT composite shows characteristics of amorphous structure (Figure 3.3).

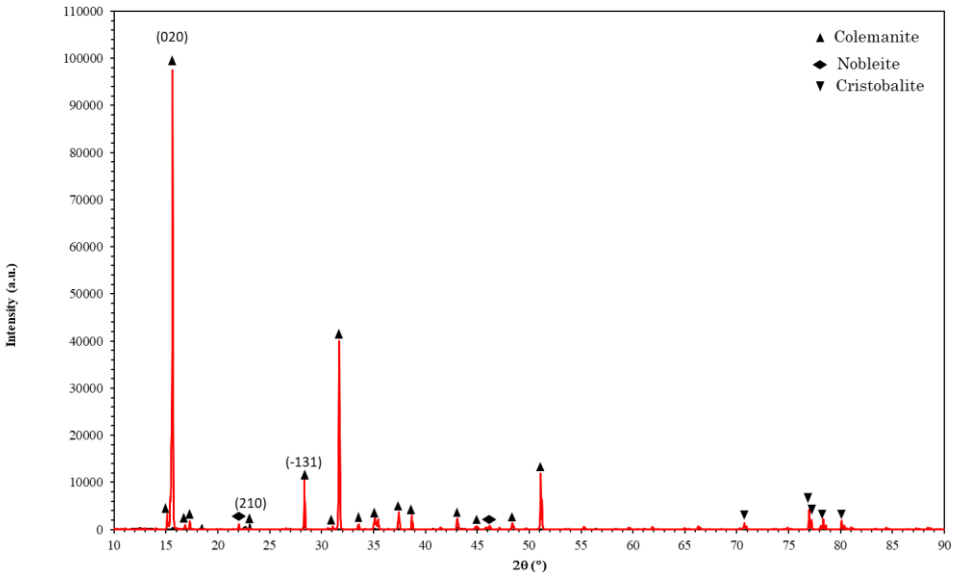

Figure 3.4 : XRD pattern of 1wt.% MK, 5wt.% CMT, PMMA/MK/CMT composite.

XRD Pattern of 1wt.% MK, 5wt.% MMT, PMMA/MK/MMT composite shows characteristic peaks of CMT with some boron mineral Nobleite and Cristobalite impurities (Figure 3.14).

3.1.2 Scanning electron microscope analyses

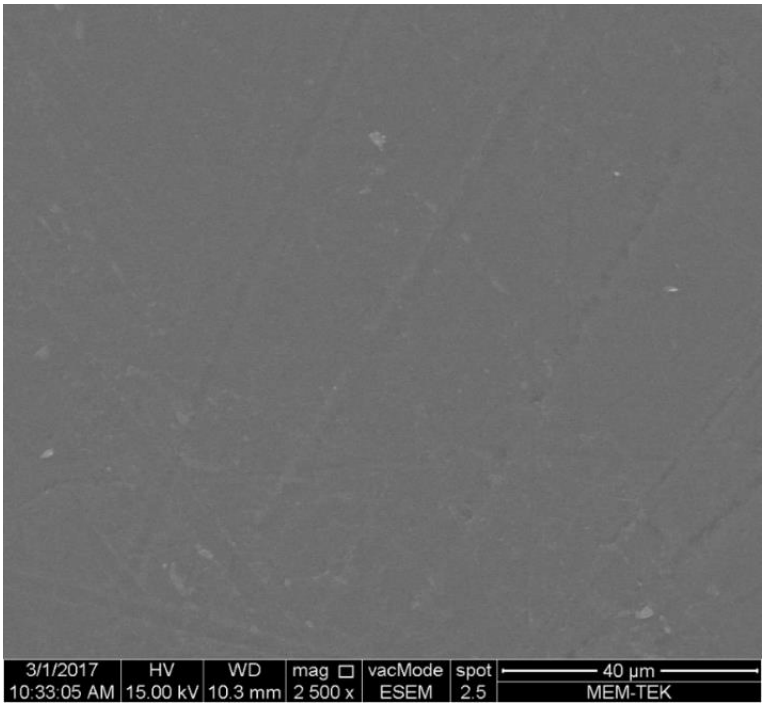

Figure 3.5 : SEM images of PMMA.

Scanning electron image of PMMA showed pure, smooth surface morphology of PMMA (Figure 3.5).

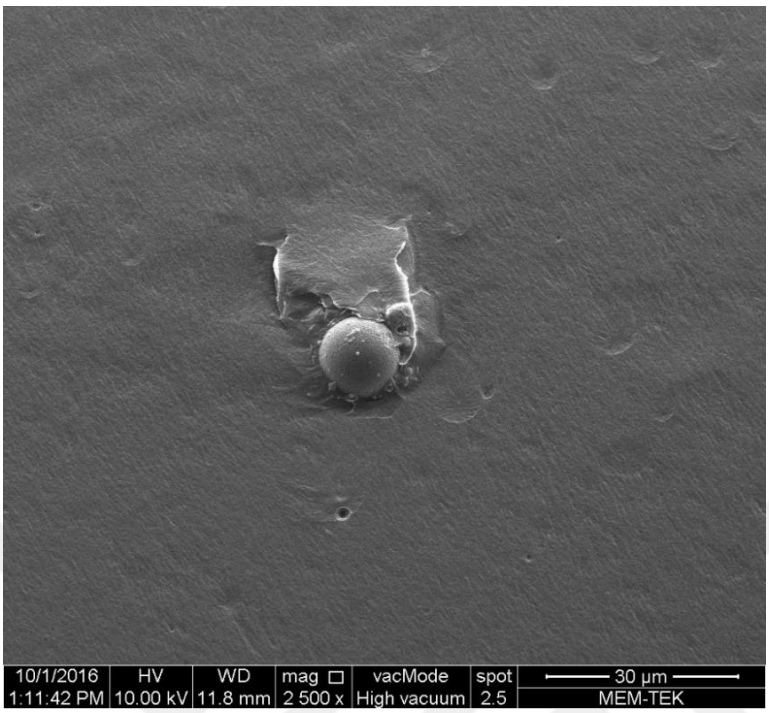

Figure 3.6 : SEM image of 1wt.% MK, 5wt.% MK PMMA/MK composite.

Scanning electron image of 5wt.% MK PMMA/MK composite showed pure, smooth surface morphology of PMMA. The microspheres well integrated to matrix PMMA, there is no visible voids or defects at the interfacial area (Figure 3.6).

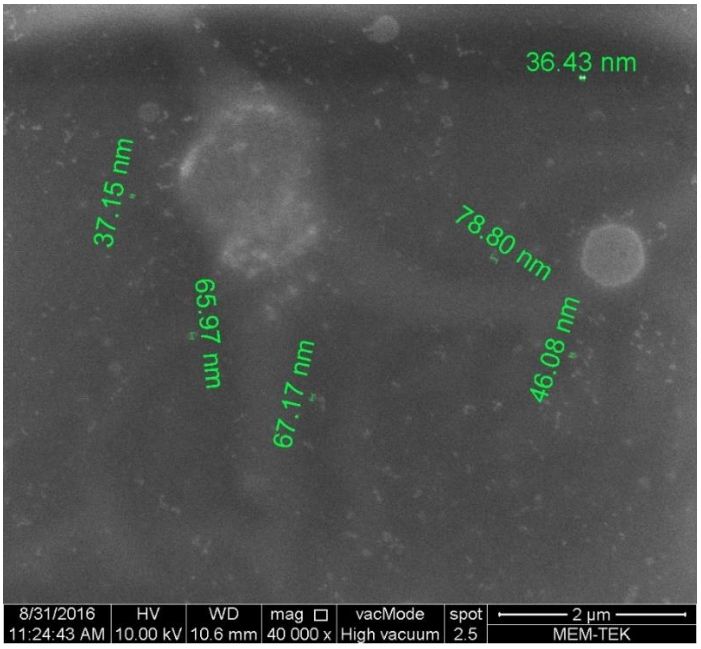

Figure 3.7 : SEM images of 1wt.% MK, 5wt.% HNTs, PMMA/MK/HNTs composite.

SEM images of 1wt.% MK, 5wt.% HNTs, PMMA/MK/HNTs indicate well distribution of HNTs inside PMMA Matrix (Figure 3.7).

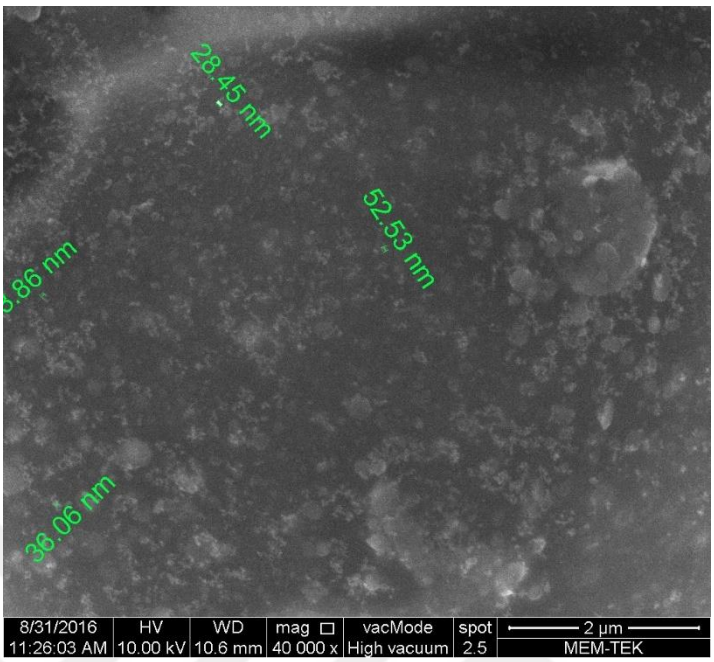

Figure 3.8 : SEM images of 1wt.% MK, 5wt.% MMT, PMMA/MK/MMT composite.

SEM images of 1wt.% MK, 5wt.% MMT, PMMA/MK/MMT composite indicate reasonable distribution of MMT inside PMMA matrix (Figure 3.8).

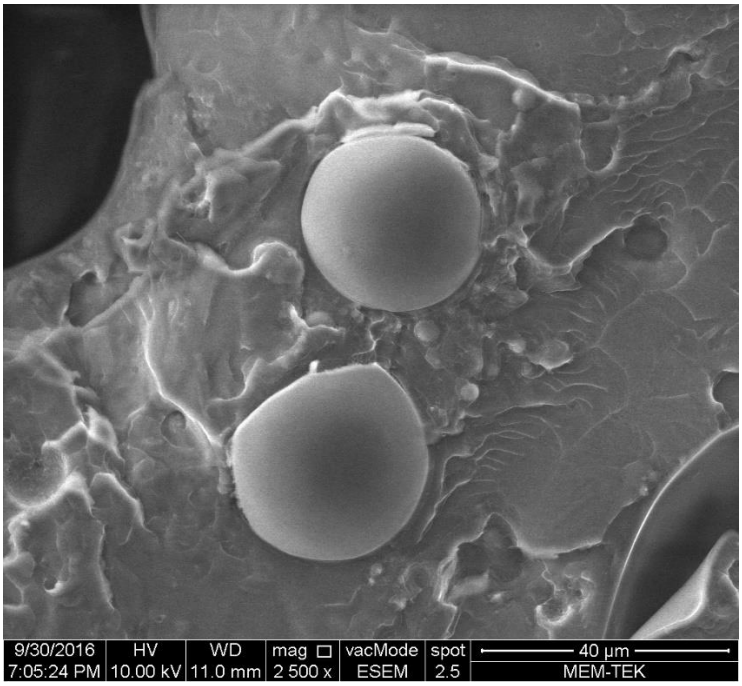

Figure 3.9 : SEM images of of 1wt.% MK, 5wt.% CMT, PMMA/MK/CMT composite.

SEM images of 1wt.% MK, 5wt.% CMT, PMMA/MK/CMT composite shows the excellent integration of MK to composite. From images, it can be seen that CMT have tendency form clusters around MKs (Figure 3.9).

3.1.3 Thermal stability analysis

The effect of the CMT wt. Percentage increase in thermal degradation of PMMA is presented in Figure 3.10. The decomposition starts at ~220°C, and CMT and HNTs addition to PMMA shifted the degradation curves to higher temperatures which are an indication of improvement of thermal stability. Addition of MK and MMT shifted the degradation curves to lower temperatures which are an indication of a decrease in thermal stability.

Figure 3.10 shows TGA thermograms of PMMA, PMMA/MK, PMMA/MK/HNTs, PMMA/MK/MMT nanocomposites and PMMA/MK/CMT composite samples. All samples had the double step degradation behavior.

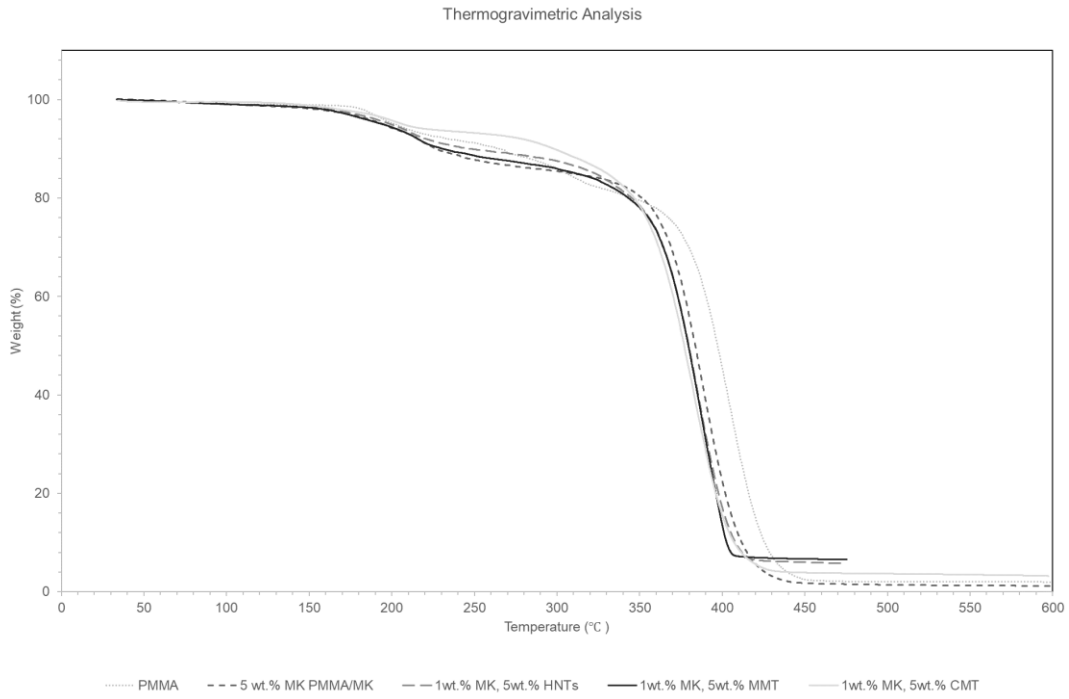

Figure 3.10 : Thermal stability analysis of PMMA, 5wt.% MK PMMA/MK, 1wt.% MK, 5wt.% HNTs, PMMA/MK/HNTs, 1wt.% MK, 5wt.% MMT, PMMA/MK/MMT and 1wt.% MK, 5wt.% CMT, PMMA/MK/CMT.

3.1.4 Fourier transform infrared spectroscopy analysis

FTIR spectra of PMMA, a composite containing PMMA, 5wt.% MK PMMA/MK, 1wt.% MK, 5wt.% HNTs, PMMA/MK/HNTs, 1wt.% MK, 5wt.% MMT,

PMMA/MK/MMT and 1wt.% MK, 5wt.% CMT, PMMA/MK/CMT are presented (Figure 3.11 a-e).

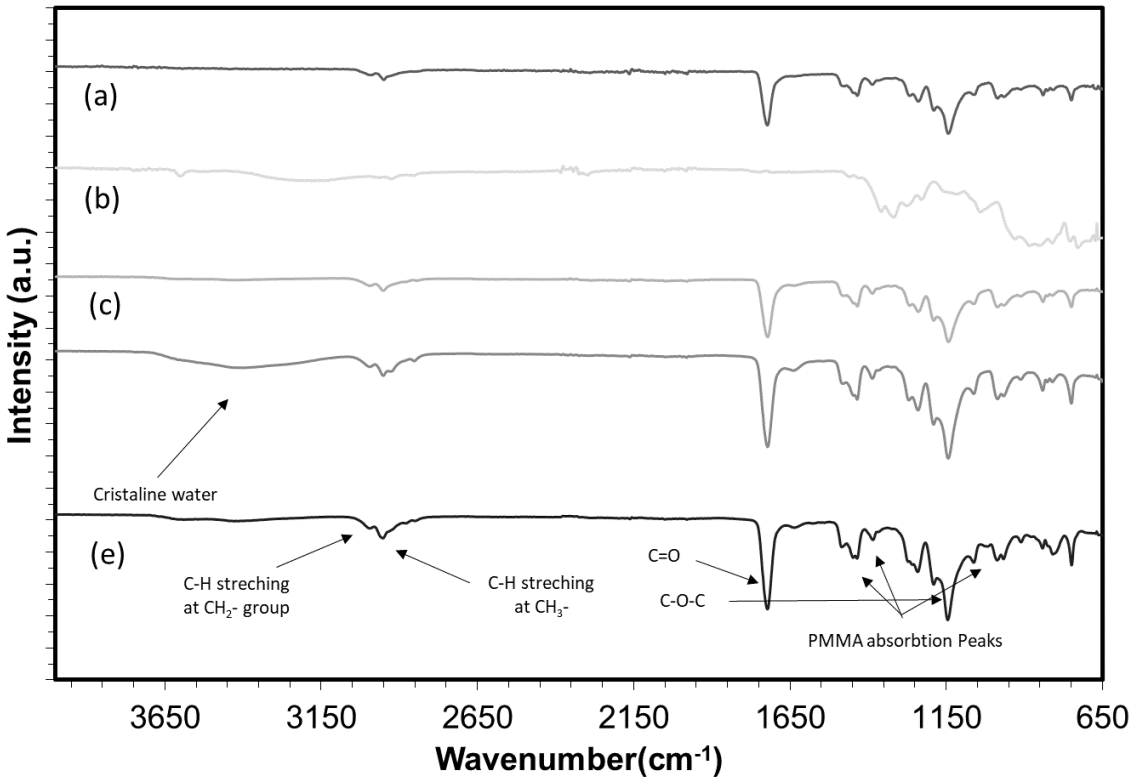

Figure 3.11 : Fourier transform infrared spectroscopy (FTIR) analyses of a) PMMA, b)MK 1% wt., MMT 5 % wt. PMMA/MK/CMT, c) MK 1% wt., HNTs 5 % wt. PMMA/MK/HNTs, d) MK 1% wt., MMT 5 % wt. PMMA/MK/MMT and e) MK 5 % wt. PMMA/MK,

Chemical reactions between PMMA and MK, HNTs, MMT, and CMT were explored with Fourier-transform infrared spectroscopy (FTIR). The region from 3950 to 650 cm^{-1} was investigated. FTIR patterns of the PMMA and composites are presented in Figure 3.11.

Band assignments were listed in Table 3.1 (Budak & Gönen, 2014; Cetin et al., 2012; Elashmawi & Hakeem, 2008; Frost et al., 2013; Namouchi et al., 2009; Ramesh et al., 2007).

Table 3.1 : PMMA and PMMA/CMT composites, the band assignments

Description of vibrations	**Wavenumbers (cm^{-1})**	**Ref.**
Stretching vibration of CMT OH units	3600	(Frost et al., 2013)
C–H bond stretching vibrations of the $–CH_3$ groups	2951	(Ramesh et al., 2007)
C=O stretching	1725	(Namouchi et al., 2009)
Bending asymmetric (CH_2)	1480	(Elashmawi & Hakeem, 2008)
Asymmetric bending vibration C–CH_3 stretching	1440	(Namouchi et al., 2009)
B-O stretching vibrations	1363	(Cetin et al., 2012)
C-O stretching vibrations of ester groups	1190	(Namouchi et al., 2009)
	1140	
Bending (CH_3-O)	987	(Elashmawi & Hakeem, 2008)
Wide peak of CMT	between 812 - 987	(Elashmawi & Hakeem, 2008)
B-O-H twisting	812	(Cetin et al., 2012)
Wagging deformation (-CH_3)	752	(Elashmawi & Hakeem, 2008)

FTIR Peaks of PMMA and composites had no shift in the absorption bands indicating no additional compound has been formed in the composites (H. P. Zhang et al., 2007).

3.1.5 Surface morphology analysis

The surface roughness of the PMMA matrix structure was determined as the Ra value, and the roughness was determined to be 0.086 micrometers. To determine the effect of nanotube and nanoparticle clay nanoparticles on surface morphology, the surface roughness of the polymer composite with 3D and 2D surface images was investigated (Figure 3.12 a-l).

3D Surface Morphology	2D Surface Morphology	(Ra)µm
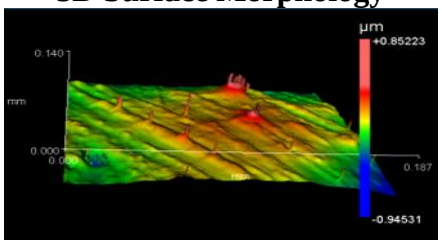	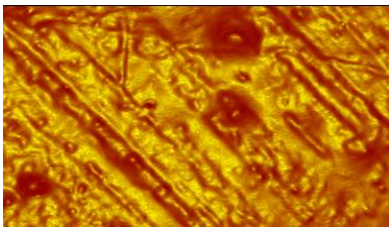	0.086
(a)	(b)	
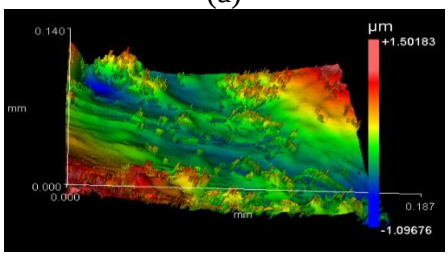	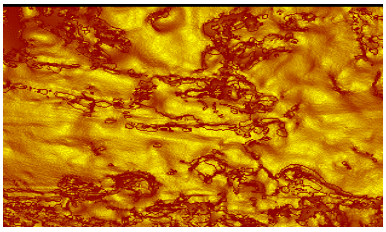	0.131
(c)	(d)	
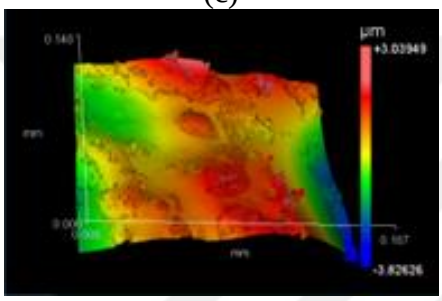	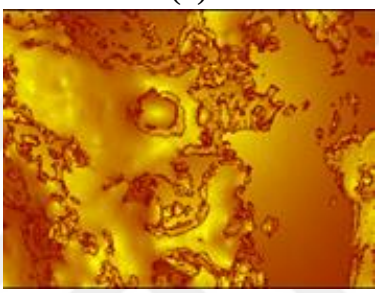	0.601
(e)	(f)	
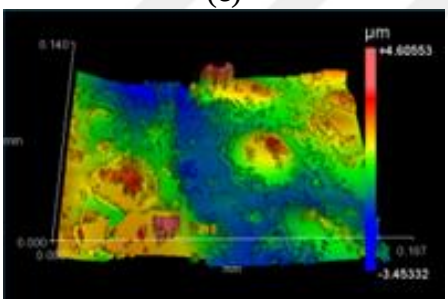	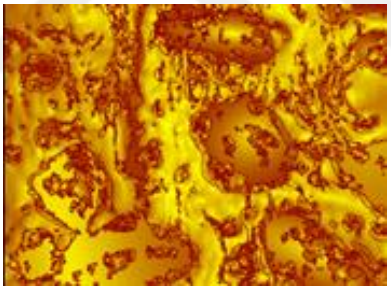	0.619
(g)	(h)	
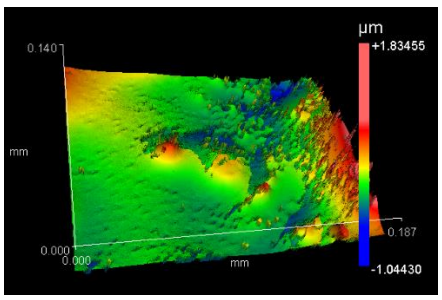	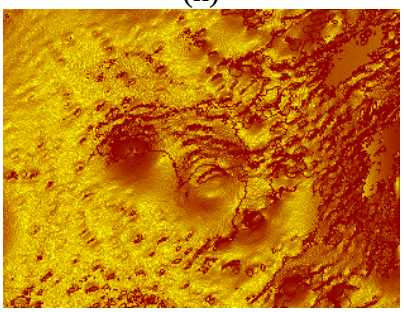	0.171
(k)	(l)	

Figure 3.12 : 3D Optical profilometry images of a) PMMA, c)MK 1% wt., CMT 5 % wt. PMMA/MK/CMT, e) MK 1% wt., HNTs 5 % wt. PMMA/MK/HNTs, g) MK 1% wt., MMT 5 % wt. PMMA/MK/MMT and k) MK 5 % wt. PMMA/MK and 2D Optical profilometry images of b) PMMA, d)MK 1% wt., CMT 5 % wt. PMMA/MK/CMT, f) MK 1% wt., HNTs 5 % wt. PMMA/MK/HNTs, h) MK 1% wt., MMT 5 % wt. PMMA/MK/MMT and l) MK 5 % wt. PMMA/MK.

In the case of MMT nanoplates and HNTs nanotubes reinforcement at the highest (5 Wt.%) concentrations, the change in surface roughness was determined. When the three-dimensional image and roughness of the PMMA/MK/HNTs and PMMA/MK/MMT nanocomposites are compared, it has been found that the nanocomposite surface forms a somewhat coarse surface when MMT is added in general. Surface images show MK and CMT do not make significant changes in surface roughness.

3.2 Mechanical Test Results

3.2.1 Hardness test results

The hardness of the original PMMA sample is 64 ± 2 Shore D (Figure 3.13). The reinforcing components incorporated into the PMMA have increased the rigidity of the PMMA. This rate of increase ranges from 1.5 to 17% depending on the reinforcing component and the ratio in the composite.

The stiffness of the composite containing only 0.5% MMT is about 3% lower than the original PMMA. On the other hand, in each composite group, the hardness increases consistently when the proportion of the reinforcing component increases. However, in each composite group, the hardness contribution of the proportion of the components is at a different level. In composites using Nano clay (HNTs group), hardness increase was observed compared to the original sample.

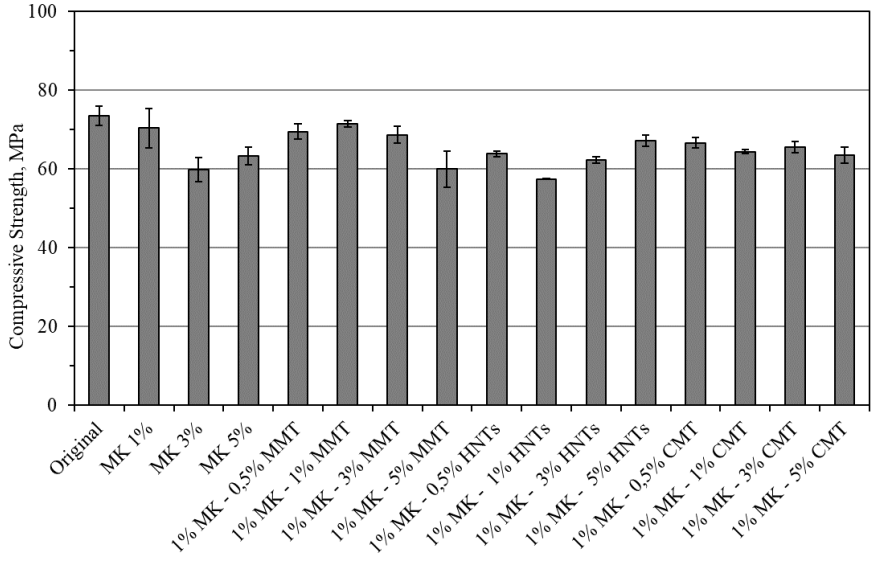

Figure 3.13 : Shore D hardness results of Pure PMMA and PMMA with nano and micro size reinforcements.

Hardness increase rate was slower with reinforcing component ratio, and it was 3-10% according to the original sample depending on the ratio of HNTs used. Composites in which the modified nanoclusters are used (MMT group) are the composite group which increases the hardness in the lowest ratio (1.5-5%) compared to the original sample.

3.2.2 Impact test results

In all of the samples, the fracture occurred on a linear plane from the point of impact, and no distortion was observed in the samples. When the impact resistance of the samples is examined, it is seen that the original PMMA sample has the lowest impact resistance (~ 1.5 J/cm^2) in all the samples, and the impact resistance of the composite structures increases 1.5 - 4 times compared to the original PMMA sample (Figure 3.14).

The highest impact resistance value (~ 9 J/cm^2), MK 1% wt., HNTs 5% wt. composite containing PMMA/MK/HNTs was obtained. In each composite batch, there is no significant change in impact resistance depending on the change in the ratio of reinforcing component. However, it has been determined that the impact resistance of the samples using nano-clay (HNTs) as a reinforcing component show a more stable behavior. When the results of the impact test are evaluated together with the results of the hardness test given in Figure 3.14, it is seen that composite structures produced by incorporation of micro and nanoparticles as reinforcing component in PMMA increase

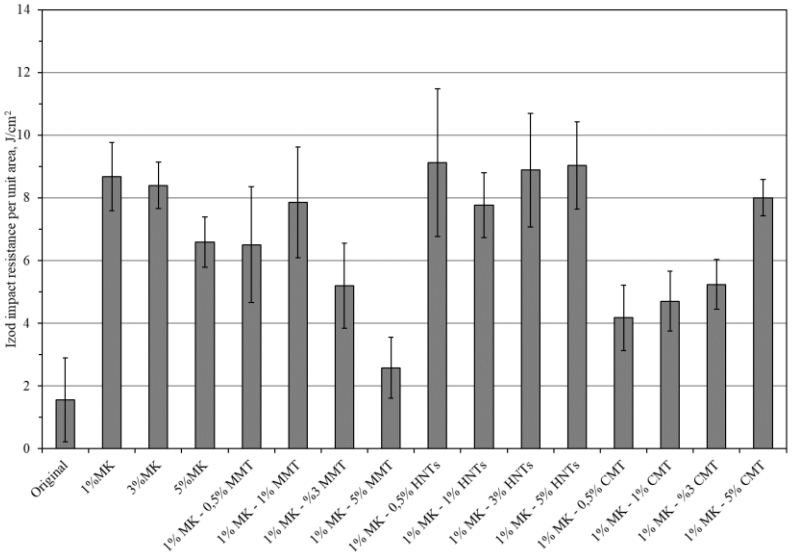

Figure 3.14 : Impact test results of Pure PMMA and PMMA with nano and micro size reinforcements.

PMMA hardness and impact resistance together. When the composite structures are evaluated in themselves, the hardness and impact characteristics are obtained at the optimum level due to the fact that the nano-clay samples (HNTs group) used as the reinforcing component exhibit comparable hardness values to the other groups and the impact resistance change is more stable depending on the component ratio sample group.

3.2.3 Bending test results

The highest bending strength in the samples examined was obtained at the original PMMA sample. The bending strength of the composite materials produced with the components incorporated in the PMMA is lower than that of the unmodified PMMA. When an evaluation is made based on the composition of the composite component, the highest flexural strength in the composites is obtained in the sample containing 0.5% CMT. However, the flexural strength at higher CMT ratios is reduced. It has been determined that the overall tendency of composites is to obtain better bending strength values at relatively low component ratios (Figure 3.15).

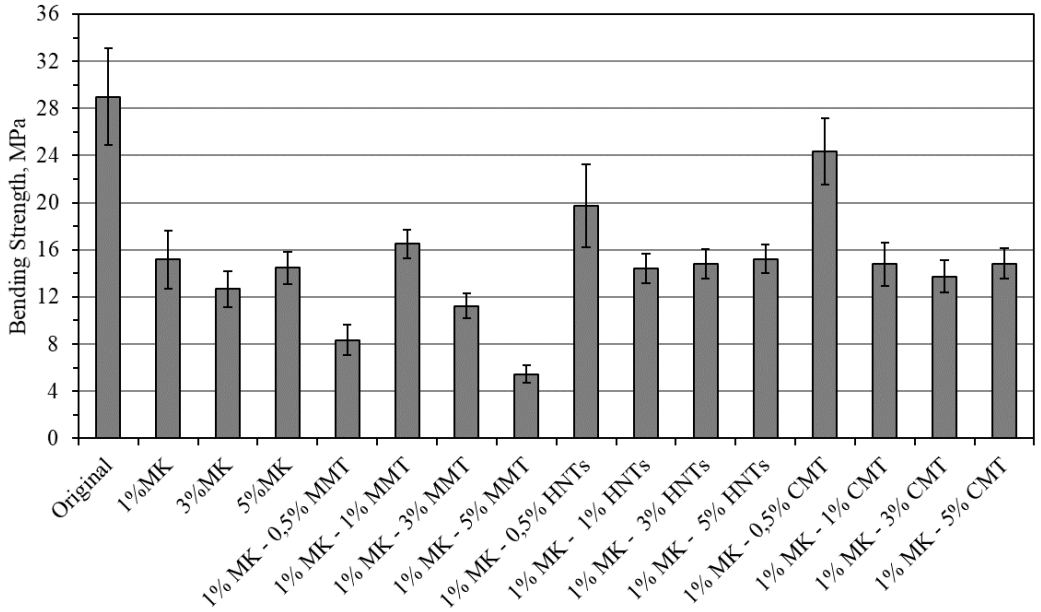

Figure 3.15 : Bending test results of Pure PMMA and PMMA with nano and micro size reinforcements.

3.2.4 Compression test results

As can be seen from Figure 3.16, the highest compressive strength was obtained at the PMMA sample without the additive. In composite materials containing different types

and proportions, compressive strength decreases by 3-20%. When an evaluation is made according to the component type, it is understood that there is no significant group with higher compressive strength than the others, and it is understood that the components of different types and proportions affect the compression strength of the composite similarly.

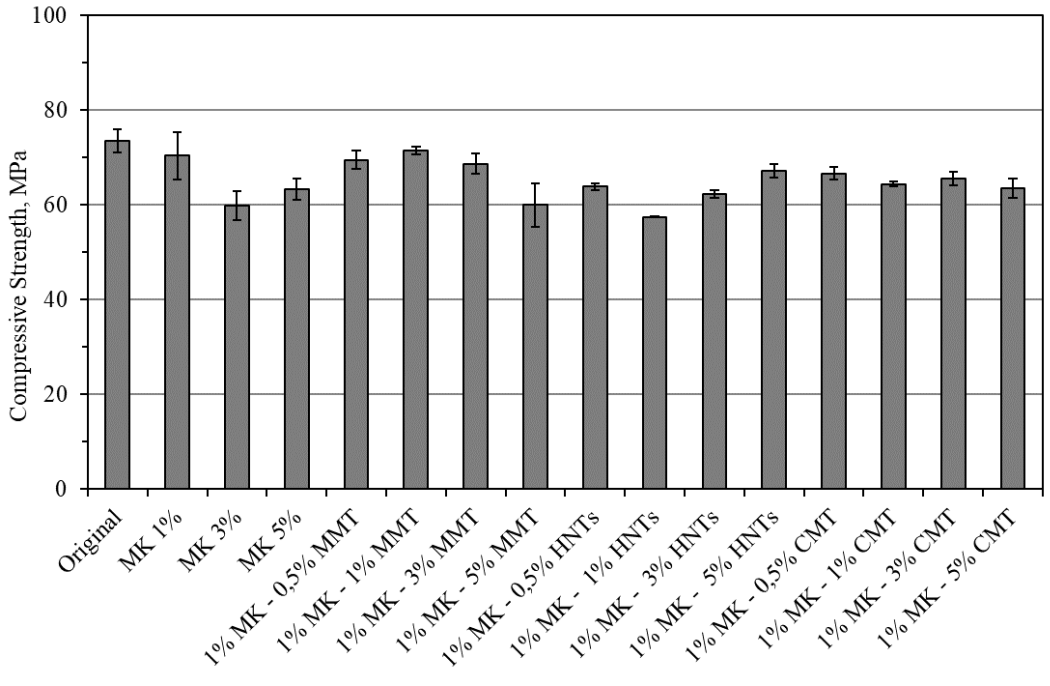

Figure 3.16 : Compression test results of Pure PMMA and PMMA with nano and micro size reinforcements.

3.2.5 Evaluation of self-healing capacity

After the self-healing process, the bending strength of the PMMA composite component was compared with the conventional one (Figure 3.17-18). Thanks to the GMA reinforcement, after the self-healing process has been achieved, the change in the flexural strength of microspheres and nanoclusters reinforced PMMA has been evaluated as comparable. For this purpose, the 3-point bending test was re-applied under the same conditions to investigate the bending strength of the microsphere and nanoclay reinforced PMMA polymers after the self-repair process was achieved. The highest bending stiffness in the specimens examined was determined in PMMA polymer with up to 5% HNTs (Figure 3.18). MMT reinforced PMMA structures were found to be close to each other at all reinforcement ratios (Figure 3.18).

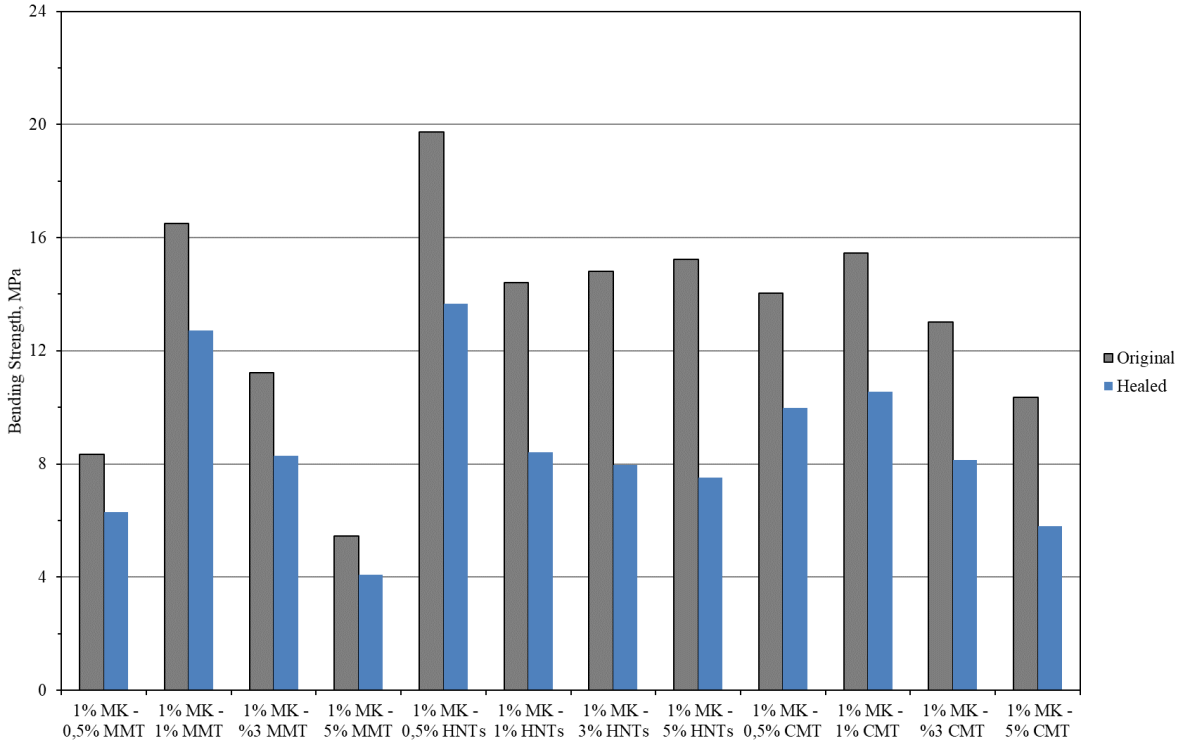

Figure 3.17 : Bending test results of Pure PMMA and PMMA with nano and micro size reinforcements.

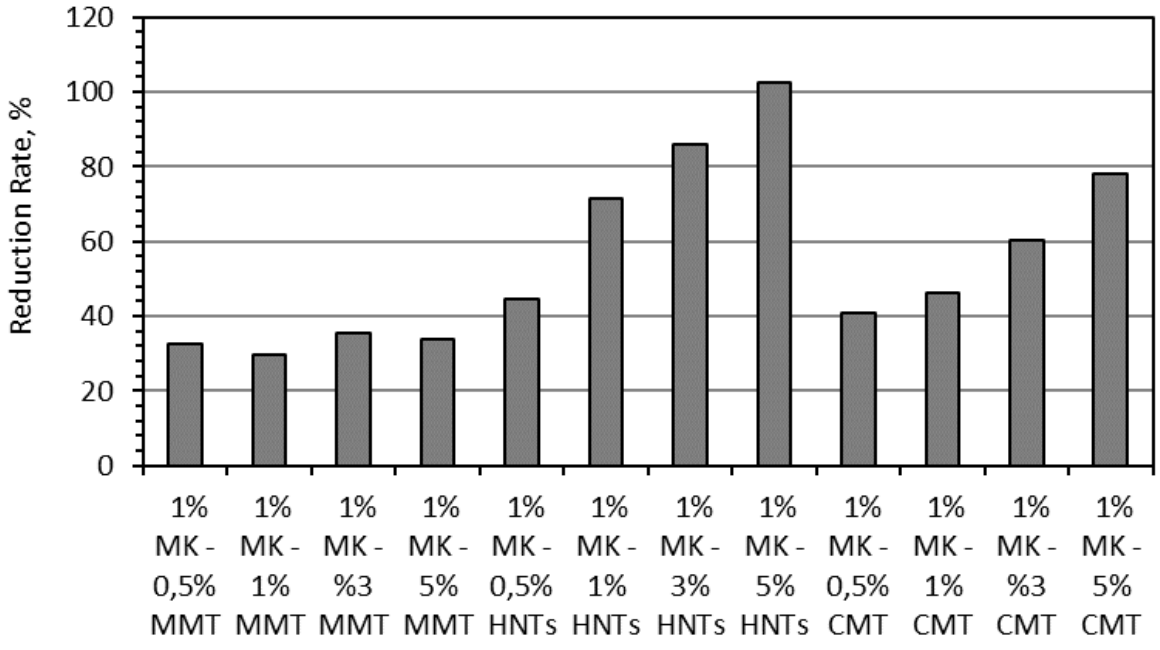

Figure 3.18 : Reduction in flexural strength of PMMA and PMMA reinforced with micro-sphere nanoclay and CMT.

3.3 The applications of ionizing radiation

According to the mechanical test results of PMMA/MK/MMT nanocomposite was chosen as a multi-scale self-healing nanocomposite shielding material for aerospace applications and the radiation tests were applied. Further, the purified CMT was used to improve neutron absorption performance of the living polymer as an advanced study. Therefore, the radiation tests were applied to PMMA/MK/CMT composites.

3.3.1 Gamma transmission studies

As a general tendency, the increase in the filler content in PMMA caused an increment in μ value which indicates the development of the gamma radiation shielding performance.

Table 3.2 : Gamma attenuation coefficients of samples for Cs-137 radioisotope.

Material	Linear Attenuation Coefficient μ (cm^{-1})		Mass Attenuation Coefficient μ (cm^2/g)	
	Theoretical	Experimental	Theoretical	Experimental
PMMA/MK (MK 1% wt.)	0.98	0.98	0.082	0.083
PMMA/MK/MMT (MK 1% wt., MMT 5 % wt.)	0.103	0.102	0.082	0.081
PMMA/MK/CMT (MK 1% wt., CMT 5 % wt.)	0.103	0.102	0.082	0.081

In this respect addition of 5 wt. %, MMT and 5 wt. %, CMT into PMMA/MK caused an increase in μ value from 0.098 to 0.102 which corresponds to ~4% enhancement in shielding performance of PMMA.

3.3.2 Neutron transmission studies

Neutron radiation shielding properties of PMMA/MK composites improved dramatically with the increasing filler percentage (Table 3.5). With increasing filler the neutron shielding capacity increases.

Table 3.3 : Pu–Be neutron source total macroscopic cross-sections ($\sum_T$) (cm^{-1}).

Material	Total macroscopic cross-section $\sum_T$ (cm^{-1})	Mean free path $1/\sum_T$ (cm)
PMMA/MK (MK 1% wt.)	0,1076	9,293680297
PMMA/MK/MMT (MK 1% wt., MMT 5 % wt.)	0,1081	9250954995
PMMA/MK/CMT (MK 1% wt., CMT 5 % wt.)	0,1128	8,866427273

The maximum decrease in neutron intensity was determined as % 4,83 for 5 wt. % MK 1% wt., MMT 5 % wt in PMMA/MK/CMT. The shielding capacity was increased by boron content and a hydrogen concentration of PMMA/CMT. The hydrogen concentration of PMMA/CMT thermalized incoming neutrons. Boron absorbed the incoming thermal and thermalized epithermal neutrons. MMT also showed some improvement in neutron shielding properties.

3.3.3 Evaluation of radiation recovery

After the radiation recovery process, the compressive strength of the PMMA composite component was compared with the conventional one (Figure 3.19 a-c). Thanks to the living polymer matrix, rapid the radiation recovery have been achieved.

(a) (b) (c)

Figure 3.19 : Co-60 Gamma radiation irradiated samples a)60kGy b)30kGy c)120kGy

The change in the compressive strength of microspheres and filler reinforced PMMA has been evaluated as comparable. For this purpose, samples were irradiated with a Co-60 radioisotope. 30kGy, 60kGy, and 120kGy radiation doses were applied to samples.

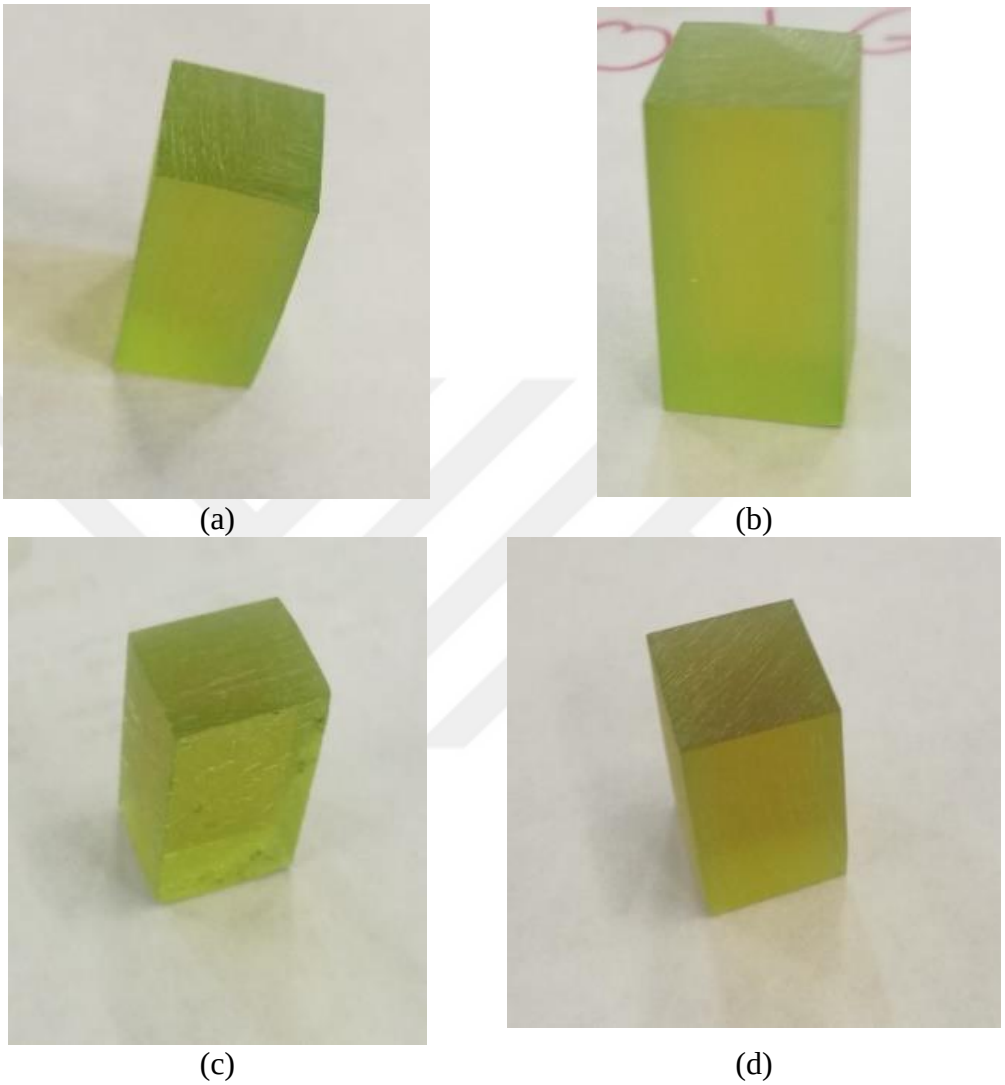

(a) (b)

(c) (d)

Figure 3.20 : Irradiated samples after 2 days a)not irradiated b) 30kGy c)60kGy and d)120 kGy irradiated samples

Compression test was re-applied to irradiated samples under the same conditions to investigate the compressive strength of the microsphere and nanoclay reinforced PMMA polymers after the radiation recovery was achieved.

Table 3.4 : Radiation recovery of PMMA/MK, MK 1% wt., MMT 5 % wt. PMMA/MK/MMT and MK 1% wt., MMT 5 % wt. PMMA/MK/CMT

Material	Radiation Dose	Compressive Strength MPa	Compressive Strength MPa after 2-day recovery
PMMA/MK (MK 1% wt.)	0 kGy	70.4	-
PMMA/MK/MMT (MK 1% wt., MMT 5 % wt.)		67	-
PMMA/MK/CMT (MK 1% wt., CMT 5 % wt.)		63.54	-
PMMA/MK (MK 1% wt.)	30kGy	147	108
PMMA/MK/MMT (MK 1% wt., MMT 5 % wt.)		145	105
PMMA/MK/CMT (MK 1% wt., CMT 5 % wt.)		140	100
PMMA/MK (MK 1% wt.)	60 kGy	160	115
PMMA/MK/MMT (MK 1% wt., MMT 5 % wt.)		159	110
PMMA/MK/CMT (MK 1% wt., CMT 5 % wt.)		153	111
PMMA/MK (MK 1% wt.)	120 kGy	204	125
PMMA/MK/MMT (MK 1% wt., MMT 5 % wt.)		201	121
PMMA/MK/CMT (MK 1% wt., CMT 5 % wt.)		195	117

When an evaluation is made according to the component type, it is understood that the components of different types and proportions affect the radiation recovery of the nanocomposites similarly.

3.3.4 Space compliance studies

As a spin-off of the Ph.D. studies; 4 samples have been prepared for the space compliance studies (Figure 3.21).

Figure 3.21 : JAXA production studies.

Space compliance and space environment tests were made with the corporation of Japan Aerospace Exploration Agency (JAXA). Successfully 4 distinct samples were prepared and handed over to JAXA team for the settlement to ExHAM at Kibo Japanese Experiment Module (Figure 3.22).

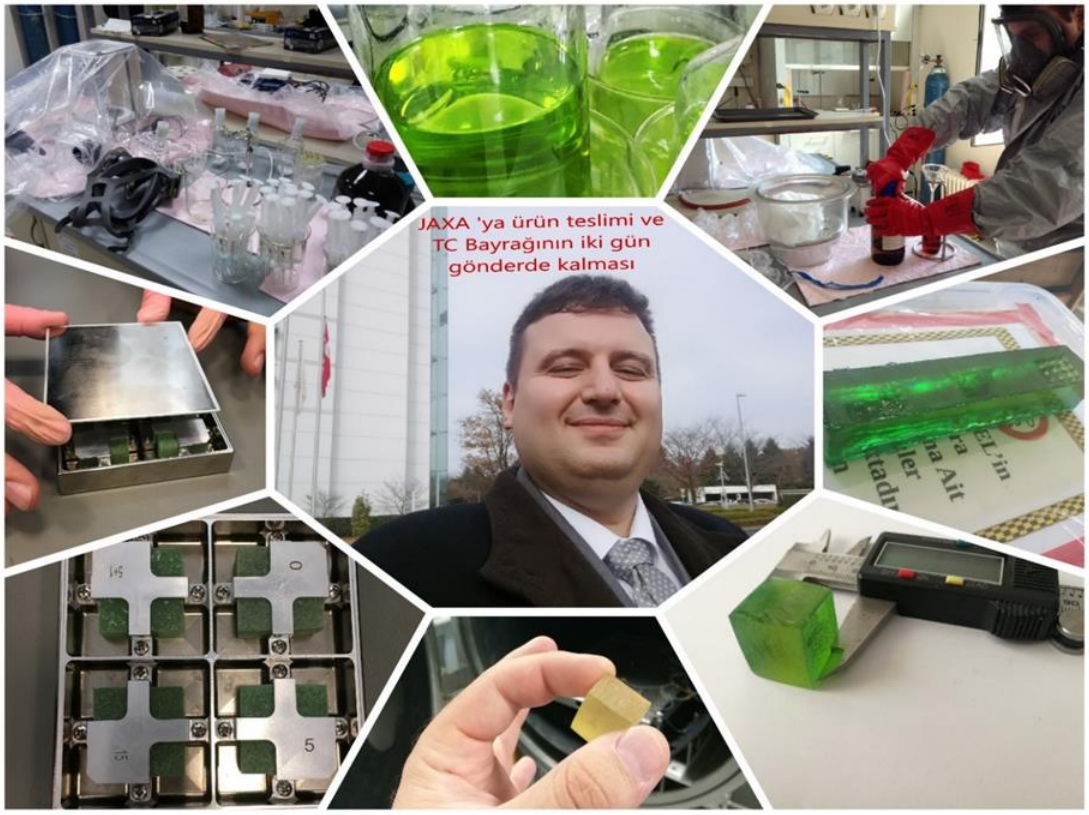

Figure 3.22 : Four samples prepared for the JAXA.

Space compliance tests and the matrix is the property of the Japan Aerospace Exploration Agency (JAXA) and subject to export control. Thus space compliance tests are not defined within the scope of this thesis (Figure 3.23).

Figure 3.23 : Fit-check of prepared samples at JAXA.

4. DISCUSSIONS

XRD pattern of PMMA, PMMA/MK, PMMA/MK/HNTs, and PMMA/MK/MMT nanocomposites shows the characteristics of amorph structure (Figure 3.1–4) (Tabanli et al., 2017). The XRD pattern of filler shows that a significant phase was CMT (Ref Code: 98-001-1737) (Figures 3.1-4) (Celik et al., 2014). In the PMMA/MK/CMT composite, peaks corresponding to both CMT and PMMA were found in this study. The XRD pattern of 1wt.% MK, 5wt.% CMT, and PMMA/MK/CMT peaks (Figures 3.1-4) corresponding to CMT prevailed, which indicates that the fillers did not dissolve in the polymer matrix (Baskaran, Selvasekarapandian, Kuwata, Kawamura, & Hattori, 2006). FTIR spectra gave the absorption lines for PMMA, PMMA/MK, PMMA/MK/HNTs, PMMA/MK/MMT, and PMMA/MK/CMT (Figure 3.11) (Huth et al., 2012). These were not the broadened and shifted stretching bands. This indicates that fillers just interacted physically with the PMMA. No chemical reaction occurred among PMMA, MK, HNTs, MMT, and CMT (Ramesh & Ang, 2010). It is conceivable that the CMT particles encapsulated by the PMMA molecules and the interactions between them were physical (Yunhua Yang & Dan, 2003). FTIR analyses show that PMMA/MK, PMMA/MK/HNTs, PMMA/MK/MMT, and PMMA/MK/CMT nanocomposites had been synthesized successfully. The broad peak between 812 to 987 cm-1 was attributed to CMT. SEM images of the 5wt.% MK PMMA/MK indicates well-integrated MK at the PMMA matrix (Figure 3.6). SEM images show that HNTs had needle-like structures and were well-dispersed inside the polymer matrix (Figure 3.7). The SEM images of the MMT nanoplates depict reasonable distribution of nanoplates across the PMMA matrix (Figure 3.8). The CMT has an excellent smooth and nonporous crystal structure (Figure 3.9). Ultrafine particles are not dominant; particles have prismatic shape with a short width and long length (Uysal et al., 2016). The SEM image of 1wt.% MK, 5wt.% CMT, PMMA/MK/CMT shows that CMT tends to form clusters around the MK.

Thermal degradation of the PMMA/CMT composites were determined by TGA measurements. The PMMA degrades in two steps, around 180°C and 350°C (Guzel, Sivrikaya, & Deveci, 2016). The MK and MMT have moved the degradation curves

to lower temperatures, which is an indication of loss of thermal stability. On the other hand, the addition of CMT and HNTs moved the degradation curves to higher temperatures. Moving the degradation curves to higher temperatures shows the improvement in the thermal stability. This result is a product of the thermal stability of HNTs and CMT. The PMMA degradation causes bimolecular reactions between newly formed confined radicals. Degradation goes on and causes the decrease in surface-free energy. According to Vyazovkin et al.'s theory, CMT platelets migrate gradually to the surface and form a barrier (Nikolaidis, Achilias, & Karayannidis, 2011). The HNTs and CMTs are well-known flame retardant additives for polymers (Wilkie & Morgan, 2010). There is a variety of studies on the CMT fire retardancy (Cavodeau, Viretto, Otazaghine, Lopez-Cuesta, & Delaite, 2017; Kaynak & Isitman, 2011; Waclawska, Stoch, Paulik, & Paulik, 1988). Thus, the addition of HNTs and CMT increased the thermo-stability and flame resistance of the nanocomposite.

The main factors determining the mechanical properties of polymer matrix composite materials reinforced with reinforcing components are; the type, size, and distribution of the component. Other factors affecting mechanical properties; uniform distribution of the matrix in the matrix (Orman & Altınten, 2017), and a robust interface with the matrix (B. Li & Zhong, 2011). If the bond strength of the interface is high, the load transfers the joint with the higher elastic modulus. Load transfer capacity can be increased by transferring the reinforcing component. The type and size of the component is an important factor, affecting the bond strength of the interface. The homogeneous distribution of the component in the matrix ensures that this effect is obtained throughout the entire composite. Although the hardness values of the examined composites do not show a significant change depending on the component type, the hardness increases with increasing component ratio. At the end of this, composite structures with higher hardness than the unmodified PMMA sample were obtained in the majority of the component type and ratio combinations investigated. The hardness value is measured in a tiny area where the nature of the hardness test is required. In this respect, it is not affected by (or only slightly affected by) possible structural defects such as porosity, and it can be a good indicator of the component-matrix interaction. This indicates that strong interface bonds are formed between the matrix and the component. The reinforcing effect of the component is provided in these

composites (Al-Saadi & Jihad, 2015; Aydoğan & Nazım, 2015; Bilgili, Salamcı, Abdurrahman, Rahmi, & Valov, 2016; L. Y. Zhang & Zhang, 2016).

The impact resistance values of the nanocomposites were found to be higher than that of PMMA with no additives. The impact resistance of polymer matrix composites depends on the component-matrix interface strength and the matrix-tocopherol effect of the component. The higher impact resistance values recorded in comparison to the unmodified PMMA indicate that the component-matrix interface resistance is high and the distribution of the components within the structure is homogeneous, which is similar to the results from the hardness test.

The bending strength values determined by the 3-point bending test of the composite specimens that were examined are lower than those of the unmodified PMMA. In bending tests, the specimen is supported on a horizontal plane while the thickness is forced to bend through the application of force to the longitudinal axis. At this time, when the specimen is subjected to concave bending, and therefore compression stresses at the part where the load is applied, cambered bending and tensile stresses are produced on the other surface. Therefore, the deformation of the sample during bending and the final fracture behavior are determined by tensile stresses. In composite structures under tensile stress, achieving better strength values is possible by transferring the load to the matrix via the reinforcing components and spreading it over a wider area. Therefore, bending strength is affected by structural defects such as porosity as well as the homogeneous distribution of reinforcing components and a good interface with the matrix. Obtained low bending strength in the tested composites shows that the composite charge transferability is not at the level of unadulterated PMMA. In this case, it is expected that the removal of porosity type imperfections in the structure will increase the bending strength, similar to the values of hardness and impact resistance.

As a measure of the strength of the material under load (load carrying capacity), compression and bending tests can be compared. Therefore, the factors determining the compression strength are the size and distribution of the porosity type defects, which are the decisive factors for the bending strength as well as the homogeneous distribution and the proper component-matrix interface strength, which are primarily necessary for providing the benefits expected from the composite materials. In this respect, it is expected that the defects mentioned above as a reason for low

bending strengths will similarly affect the compression strength similarly. However, although the compressive strength of the composites is reduced relative to the unmodified PMMA, the amount of this reduction is not as high as the flexural strength. This is attributed to the fact that the compression forces are influenced by the compressive stress (force) of the sample (instead of tensile strain) in the course of the compression test and the compressive forces force the structural defects such as porosity to close, resulting in some structural defects closing down and not significantly reducing the load carrying capacity of the composite.

It has been observed that there is no enhancing or reducing the effect of MMT in self-repair capacity. The highest flexural strength in nanoclay-reinforced composites is 1% wt of MK, 0.5 wt% of HNTs. PMMA / MK / HNTs. The flexural strength of HNTs is higher than 0.5%. With increasing HNTs, the decrease in bending strength after the self-repair is increasing. It is stated in the literature that hollow tubular HNTs nanotubes can be loaded with chemically active substances. It is also suggested that this hollow space in HNTs nanotubes with an internal cavity diameter of ~ 15-30 nm acts as an efficient container by loading chemical substances (Abdullayev & Lvov, 2013). In this study, HNTs were supplied as Sigma Aldrich with a void volume of 1.26–1.34 mL/g. Nanotubes with hollow spaces HNTs 30–70 nm × 1–3 μm (diameter x length) were added at later stages of polymerization, in other words, as the polymerization was partially completed. Thus, it was thought that some of the HNTs nanotubes remained empty, while the HNTs nanotubes were homogeneously dispersed using a rotary shaker and the viscosity of the mixture was high. The progress of the GMA liquid is leaving the microspheres during the damage with the effect of trapping the vacant HNTs in the interior and reducing the self-repairing capacity of the material. Therefore, the self-repair process of PMMA/MK composites has been found to be more efficient in montmorillonite clay nano-plates than in HNTs clay nanotubes.

It is not suitable to use high Z materials and metals in neutron environments to decrease the neutron energy in case high Z materials and metals increased the scattering of the neutrons. When metallic shielding materials are exposed to cosmic radiation such as high energy Fe ions, they generate secondary radiation (Buckey, 2006). Hence, it is not proper to use ground-level shielding materials for aeronautics and space applications. According to our results, it seems possible to propose the PMMA/MK/HNTs and PMMA/MK/CMT as a new radiation shielding material for

aeronautics and space applications. The possible applications for the novel shielding material include facilities such as biological shielding of nuclear submarines, high-altitude planes, satellites, space shuttles, medical cyclotrons, nuclear investigation centers, and linear accelerators.

5. CONCLUSIONS

In this study, surface-modified Montmorillonite (MMT) nanoplates and Halloysite (HNTs) clay nanotubes with a thickness of 15 nm in the polymer melt could be dispersed in a manner compatible with the polymer structure without agglomerating. Due to the presence of canals in the clay HNTs nanotubes, better integration of HNTs with the monomer present in the polymer melt can be achieved. It has been determined that HNTs are more readily dispersed in the polymer structure when the dispersion time (~ 1 hour) of the HNTs in the polymer structure and the dispersion time (~ 2-3 hours) of the MMT in the polymer structure are compared. The SEM studies have shown that HNTs and MMT are distributed more homogeneously in the matrix structure than in CMT. The surface images obtained show that the HNTs reinforcements have improved the processability of the material.

High flexural strengths in nanocyl-reinforced composites, MK 1% wt., HNTs 0,5% wt. PMMA / MK / HNTs and MK 1% wt., MMT 1% wt. PMMA/ MK/MMT. It has been found that, after self-repair, the rate of decrease in flexural strength remains at the same level in MMT-reinforced specimens; whereas in HNTs' reinforced specimens, the self-repair capacity decreases with an increasing reinforcement ratio. Considering the increase in impact strength by ~4 times and the change in bending strength test after self-repairing, the MK was 1% wt., MMT 1% wt. The PMMA/MK /MMT nano-composite was chosen as the best self-repairing material.

The changes in gamma attenuation properties of MK at 1% wt., MMT 5 % wt., PMMA/MK/MMT, and 1wt.% MK, 5wt.% CMT, and PMMA/MK/CMT for Cs-137 radioisotope were compared theoretically (WinXCOM) and experimentally studied. Neutron shielding capacity was experimentally studied with a neutron howitzer (^{239}Pu - Be). The incorporation of 1wt.% MK, 5wt.% CMT, PMMA/MK/CMT had increased the ^{239}Pu-Be neutron attenuation capacity by % 4,83. CMT includes both boron and hydrate; thus, it is effective against shielding both fast and thermal neutrons. MK 1% wt., MMT 5 % wt. PMMA/MK/MMT and MK 1% wt., CMT 5 % wt. PMMA/MK/CMT has improved Cs-137 attenuation capacity by ~4%. Thus, both MMT and CMT increased the radiation-shielding capacity of the PMMA. Further

studies are suggested for the purification and nano-sized production of CMT. Nano-sized CMT can be used for PMMA/MK/CMT nanocomposites.

Hence, it was possible to produce MK 1% wt. and MMT 1% wt. The PMMA/MK/MMT nano-composite was a multi-scale self-healing nanocomposite shielding material for aerospace applications.

MK 1% wt., MMT 1% wt. The PMMA/MK/MMT increases the impact strength by ~4 times. The loss in the bending strength test after self-repairing is the lowest for the MK 1% wt. and MMT 1% wt. The PMMA/MK/MMTThe possible applications for the novel PMMA/MK/MMT shielding material include facilities such as the biological shielding of nuclear submarines, high-altitude planes, satellites, space shuttles, medical cyclotrons, nuclear investigation centers, and linear accelerators.

REFERENCES

Abdullayev, E., & Lvov, Y. (2013). Halloysite clay nanotubes as a ceramic "skeleton" for functional biopolymer composites with sustained drug release. *Journal of Materials Chemistry B, 1*(23), 2894-2903.

Ajayan, P. M., Schadler, L. S., & Braun, P. V. (2006). *Nanocomposite science and technology*: John Wiley & Sons.

Al-Saadi, T. M., & Jihad, M. A. (2015). Preparation and Characterization of Graphene/PMMA Composite. *IJARSET, 2*, 902-909.

Amendola, V., & Meneghetti, M. (2009). Self-healing at the nanoscale. *Nanoscale, 1*(1), 74-88. doi:10.1039/b9nr00146h

Aragón-Zavala, A., Cuevas-Ruiz, J. L., & Delgado-Penín, J. A. (2008). *High-altitude platforms for wireless communications*. Chichester, U.K.: Wiley.

Aydoğan, B., & Nazım, U. (2015). Nanokil Ve Kabaran Alev Geciktirici İlavesinin Rijit Poliüretan Köpük Malzemelerin Isil Bozunma Ve Yanma Davranişlarina Etkilerinin İncelenmesi. *Gazi Üniversitesi Mühendislik-Mimarlık Fakültesi Dergisi, 30*(1).

Balazs, A. C., Emrick, T., & Russell, T. P. (2006). Nanoparticle polymer composites: where two small worlds meet. *Science*, *314*(5802), 1107-1110. doi:10.1126/science.1130557

Baskaran, R., Selvasekarapandian, S., Kuwata, N., Kawamura, J., & Hattori, T. (2006). Conductivity and thermal studies of blend polymer electrolytes based on PVAc–PMMA. *Solid State Ionics, 177*(26–32), 2679-2682. doi:http://doi.org/10.1016/j.ssi.2006.04.013

Benight, S. J., Wang, C., Tok, J. B. H., & Bao, Z. A. (2013). Stretchable and self-healing polymers and devices for electronic skin. *Progress in Polymer Science, 38*(12), 1961-1977. doi:10.1016/j.progpolymsci.2013.08.001

Bilgili, E. Z., Salamcı, E., Abdurrahman, A., Rahmi, Ü., & Valov, R. (2016). Elmas Nano Parçacik Takviyeli Krom Kaplanmiş Gözenekli Toz Metal Parçalarin Korozyon Davranişlarinin Araştirilmasi. *Gazi Üniversitesi Mühendislik-Mimarlık Fakültesi Dergisi, 31*(3).

Billiet, S., Hillewaere, X. K. D., Teixeira, R. F. A., & Du Prez, F. E. (2013). Chemistry of Crosslinking Processes for Self-Healing Polymers. *Macromolecular Rapid Communications*, *34*(4), 290-309. doi:10.1002/marc.201200689

Blaiszik, B. J., Kramer, S. L. B., Olugebefola, S. C., Moore, J. S., Sottos, N. R., & White, S. R. (2010). Self-Healing Polymers and Composites. In D. R. Clarke, M. Ruhle, & F. Zok (Eds.), *Annual Review of Materials Research, Vol 40* (Vol. 40, pp. 179-211). Palo Alto: Annual Reviews.

Brochu, A. B. W., Craig, S. L., & Reichert, W. M. (2011). Self-healing biomaterials. *Journal of Biomedical Materials Research Part A, 96A*(2), 492-506. doi:10.1002/jbm.a.32987

Buckey, J. C. (2006). *Space physiology*. Oxford ; New York: Oxford University Press.

Budak, A., & Gönen, M. (2014). Extraction of boric acid from colemanite mineral by supercritical carbon dioxide. *The Journal of Supercritical Fluids, 92*, 183-189. doi:http://doi.org/10.1016/j.supflu.2014.05.016

Bulutcu, A., Ertekin, C., & Celikoyan, M. K. (2008). Impurity control in the production of boric acid from colemanite in the presence of propionic acid. *Chemical Engineering and Processing: Process Intensification, 47*(12), 2270-2274.

Carter, A. B. (1986). Satellites and anti-satellites: The limits of the possible. *International Security*, 46-98.

Cavodeau, F., Viretto, A., Otazaghine, B., Lopez-Cuesta, J.-M., & Delaite, C. (2017). Influence of colemanite on the fire retardancy of ethylene-vinyl acetate and ethylene-methyl acrylate copolymers. *Polymer Degradation and Stability, 144*(Supplement C), 401-410. doi:https://doi.org/10.1016/j.polymdegradstab.2017.08.016

Celik, A. G., Depci, T., & Kılıc, A. M. (2014). New lightweight colemanite-added perlite brick and comparison of its physicomechanical properties with other commercial lightweight materials. *Construction and Building Materials, 62*, 59-66. doi:http://doi.org/10.1016/j.conbuildmat.2014.03.031

Cetin, B., Unal, H. I., & Erol, O. (2012). SYNTHESIS, CHARACTERIZATION, AND ELECTROKINETIC PROPERTIES OF POLYINDENE/COLEMANITE CONDUCTING COMPOSITE. *Clays and Clay Minerals, 60*(3), 300-314. doi:10.1346/ccmn.2012.0600307

Chang, K.-C., Chen, S.-T., Lin, H.-F., Lin, C.-Y., Huang, H.-H., Yeh, J.-M., & Yu, Y.-H. (2008). Effect of clay on the corrosion protection efficiency of PMMA/Na+-MMT clay nanocomposite coatings evaluated by electrochemical measurements. *European Polymer Journal, 44*(1), 13-23. doi:http://dx.doi.org/10.1016/j.eurpolymj.2007.10.011

Chen, X. X., Dam, M. A., Ono, K., Mal, A., Shen, H. B., Nutt, S. R., . . . Wudl, F. (2002). A thermally re-mendable cross-linked polymeric material. *Science, 295*(5560), 1698-1702. doi:10.1126/science.1065879

Choppin, G. R., Liljenzin, J.-O., Rydberg, J., & Ekberg, C. (2013). *Radiochemistry and nuclear chemistry* (4th edition / ed.). Amsterdam ; Boston: Elsevier/AP, Academic Press is an imprint of Elsevier.

Chung, C. M., Roh, Y. S., Cho, S. Y., & Kim, J. G. (2004). Crack healing in polymeric materials via photochemical 2+2 cycloaddition. *Chemistry of Materials, 16*(21), 3982-+. doi:10.1021/cm049394+

Collier, C. M. K., Jeffrey C. (2008). *A Cost-Effectiveness Analysis of Tactical Satellites, High-Altitude Long-Endurance Airships, and High and Medium Altitude Unmanned Aerial Systems for ISR and Communication Missions.* (Master Master's thesis), NAVAL POSTGRADUATE SCHOOL MONTEREY CA, (ADA488904)

DeBlois, B. M., Garwin, R. L., Kemp, R. S., & Marwell, J. C. (2004). Space weapons: crossing the US Rubicon. *International Security, 29*(2), 50-84.

Demir, F. (2010). Determination of mass attenuation coefficients of some boron ores at 59.54keV by using scintillation detector. *Applied Radiation and Isotopes, 68*(1), 175-179. doi:http://dx.doi.org/10.1016/j.apradiso.2009.09.003

Derun, E. M., & Kipcak, A. S. (2012). Characterization of some boron minerals against neutron shielding and 12 year performance of neutron permeability. *Journal of Radioanalytical and Nuclear Chemistry, 292*(2), 871-878. doi:10.1007/s10967-011-1528-6

Elashmawi, I. S., & Hakeem, N. A. (2008). Effect of PMMA addition on characterization and morphology of PVDF. *Polymer Engineering & Science, 48*(5), 895-901. doi:10.1002/pen.21032

Emmanuel, A., & Raghavan, J. (2016). Experimental validation of simulations of radiation shielding effectiveness of materials by MULASSIS. *Advances in Space Research, 58*(11), 2376-2384. doi:http://dx.doi.org/10.1016/j.asr.2016.08.018

Fadel, R. A., Tohme, S., & ieee. (2004). *Connection admission control cac for a mixed burst/packet service based on service differentiation in a Low Earth Orbit LEO satellite constellation*.

Fedrizzi, L., Fürbeth, W., Montemor, F. t., European Federation of Corrosion., & Institute of Materials Minerals and Mining. (2011). *Self-healing properties of new surface treatments*. Leeds: Published for the European Federation of Corrosion by Maney Pub. on behalf of the Institute of Materials, Minerals & Mining.

Ferguson, C. R. H., Douglas A. (2001). *High Altitude Long Endurance (HALE) Platforms for Tactical Wireless Communications and Sensor Use in Military Operations.* (Master's thesis), NAVAL POSTGRADUATE SCHOOL MONTEREY CA, (ADA397280)

F**ortescue, P. W., Stark, J., & Swinerd, G.** (2003). *Spacecraft systems engineering* (3rd ed.). New York: J. Wiley.

Frost, R. L., Xi, Y., Scholz, R., Belotti, F. M., & Cândido Filho, M. (2013). Infrared and Raman spectroscopic characterization of the borate mineral colemanite – CaB3O4(OH)3·H2O – implications for the molecular structure. *Journal of Molecular Structure, 1037*, 23-28. doi:http://doi.org/10.1016/j.molstruc.2012.11.047

Galante, N. (2001). NASA's Helios Prototype aircraft taking off from the Pacific Missile Range Facility, Kauai, Hawaii, for the record flight. Retrieved from http://www.dfrc.nasa.gov/Gallery/Photo/Helios/HTML/ED01-0230-1.html

Geckeler, K. E., & Nishide, H. (2009). *Advanced nanomaterials*: John Wiley & Sons.

Ghosh, B., & Urban, M. W. (2009). Self-Repairing Oxetane-Substituted Chitosan Polyurethane Networks. *Science, 323*(5920), 1458-1460. doi:10.1126/science.1167391

Ghosh, S. K. (2009). *Self-healing materials: fundamentals, design strategies, and applications*: John Wiley & Sons.

Gönen, M., Nyankson, E., & Gupta, R. B. (2016). Boric Acid Production from Colemanite Together with ex Situ CO2 Sequestration. *Industrial & Engineering Chemistry Research, 55*(17), 5116-5124. doi:10.1021/acs.iecr.6b00378

Griffin, M. D., & French, J. R. (2004). *Space vehicle design* (2nd ed.). Reston, VA: American Institute of Aeronautics and Astronautics, Inc.

Guzel, G., Sivrikaya, O., & Deveci, H. (2016). The use of colemanite and ulexite as novel fillers in epoxy composites: Influences on thermal and physico-mechanical properties. *Composites Part B: Engineering, 100*, 1-9. doi:https://doi.org/10.1016/j.compositesb.2016.06.054

Habault, D., Zhang, H. J., & Zhao, Y. (2013). Light-triggered self-healing and shape-memory polymers. *Chemical Society Reviews, 42*(17), 7244-7256. doi:10.1039/c3cs35489j

Hager, M. D., Greil, P., Leyens, C., van der Zwaag, S., & Schubert, U. S. (2010). Self-Healing Materials. *Advanced Materials, 22*(47), 5424-5430. doi:10.1002/adma.201003036

H**åkansson, E., Amiet, A., Nahavandi, S., & Kaynak, A.** (2007). Electromagnetic interference shielding and radiation absorption in thin polypyrrole films. *European Polymer Journal, 43*(1), 205-213. doi:http://dx.doi.org/10.1016/j.eurpolymj.2006.10.001

Hamilton, A. R., Sottos, N. R., & White, S. R. (2010). Self-Healing of Internal Damage in Synthetic Vascular Materials. *Advanced Materials, 22*(45), 5159-+. doi:10.1002/adma.201002561

Hamzah, N. H., Yaacob, S., Muthusamy, H., Hamzah, N., & Ghazali, N. (2013). The Study of Gravity Gradient Effect on Attitude of Low Earth Orbit Satellite. *Proceedings of the 20th National Symposium on Mathematical Sciences (Sksm20): Research in Mathematical Sciences: A Catalyst for Creativity and Innovation, Pts a and B, 1522*, 636-642. doi:10.1063/1.4801184

Hayes, S. A., Zhang, W., Branthwaite, M., & Jones, F. R. (2007). Self-healing of damage in fibre-reinforced polymer-matrix composites. *Journal of the Royal Society Interface, 4*(13), 381-387. doi:10.1098/rsif.2006.0209

Helvajian, H. (1999). *Microengineering aerospace systems*. El Segundo, CA
Reston, VA: Aerospace Press ;
American Institute of Aeronautics and Astronautics.

Herbst, F., Dohler, D., Michael, P., & Binder, W. H. (2013). Self-Healing Polymers via Supramolecular Forces. *Macromolecular Rapid Communications, 34*(3), 203-220. doi:10.1002/marc.201200675

Hsieh, H. C., Yang, T. J., & Lee, S. (2001). Crack healing in poly(methyl methacrylate) induced by co-solvent of methanol and ethanol. *Polymer, 42*(3), 1227-1241. doi:10.1016/s0032-3861(00)00407-9

Hu, W., Guo, H., Chen, Y., Xie, R., Jing, H., & He, P. (2016). Experimental investigation and modeling of the rate-dependent deformation behavior of PMMA at different temperatures. *European Polymer Journal, 85*, 313-323. doi:http://dx.doi.org/10.1016/j.eurpolymj.2016.10.036

Hughes, A. E., Cole, I. S., Muster, T. H., & Varley, R. J. (2010). Designing green, self-healing coatings for metal protection. *Npg Asia Materials, 2*(4), 143-151. doi:10.1038/asiamat.2010.136

Huth, F., Govyadinov, A., Amarie, S., Nuansing, W., Keilmann, F., & Hillenbrand, R. (2012). Nano-FTIR Absorption Spectroscopy of Molecular Fingerprints at 20 nm Spatial Resolution. *Nano Letters, 12*(8), 3973-3978. doi:10.1021/nl301159v

I**onov, L., & Synytska, A.** (2012). Self-healing superhydrophobic materials. *Physical Chemistry Chemical Physics, 14*(30), 10497-10502. doi:10.1039/c2cp41377a

Jenkinson, L. R., & Marchman, J. F. (2003). *Aircraft design projects : for engineering students*. Reston, VA
Oxford: American Institute of Aeronautics and Astronautics
Butterworth-Heinemann.

Kalay, S., Yilmaz, Z., & Çulha, M. (2013). Synthesis of boron nitride nanotubes from unprocessed colemanite. *Beilstein Journal of Nanotechnology, 4*(1), 843-851.

Kaynak, C., & Isitman, N. A. (2011). Synergistic fire retardancy of colemanite, a natural hydrated calcium borate, in high-impact polystyrene containing brominated epoxy and antimony oxide. *Polymer Degradation and Stability, 96*(5), 798-807.

Kim, B. W., Min, S. L., Yang, H. S., & Kim, C. S. (2000). A predictive call admission control scheme for low earth orbit satellite networks. *Ieee Transactions on Vehicular Technology, 49*(6), 2320-2335.

Kim, I. H., Cho, H. C., Bae, Y. C., Park, H. W., & Chung, K. S. (2003). Heat and radiation effect on the degradation behaviors of polymeric liquids. *European Polymer Journal, 39*(7), 1431-1435. doi:http://dx.doi.org/10.1016/S0014-3057(02)00384-1

Kleiman, J. I. (2006). *Protection of materials and structures from the space environment : ICPMSE-7*. Dordrecht: Springer.

Koo, J. H. (2006). *Polymer nanocomposites*: McGraw-Hill Professional Pub.

Korkut, T., Karabulut, A., Budak, G., Aygun, B., Gencel, O., & Hancerliogullari, A. (2012). Investigation of neutron shielding properties depending on number of boron atoms for colemanite, ulexite and tincal ores by experiments and FLUKA Monte Carlo simulations. *Applied Radiation and Isotopes, 70*(1), 341-345. doi:10.1016/j.apradiso.2011.09.006

Korkut, T., Ün, A., Demir, F., Karabulut, A., Budak, G., Şahin, R., & Oltulu, M. (2010). Neutron dose transmission measurements for several new concrete samples including colemanite. *Annals of Nuclear Energy, 37*(7), 996-998. doi:http://dx.doi.org/10.1016/j.anucene.2010.04.005

Kutz, M. (2002). *Handbook of materials selection*. New York: J. Wiley.

Lanzara, G., Yoon, Y., Liu, H., Peng, S., & Lee, W. I. (2009). Carbon nanotube reservoirs for self-healing materials. *Nanotechnology, 20*(33), 7. doi:10.1088/0957-4484/20/33/335704

Li, B., & Zhong, W.-H. (2011). Review on polymer/graphite nanoplatelet nanocomposites. *Journal of Materials Science, 46*(17), 5595-5614.

Li, L. H., Heymsfield, G. M., Racette, P. E., Tian, L., & Zenker, E. (2004). A 94-GHz cloud radar system on a NASA high-altitude ER-2 aircraft. *Journal of Atmospheric and Oceanic Technology, 21*(9), 1378-1388. doi:10.1175/1520-0426(2004)021<1378:agcrso>2.0.co;2

Li, S.-Y., & Wang, K.-Y. (2012). Application of maximum elevation angle probability density function to macroscopic selection diversity in low earth orbiting satellite constellation systems. *International Journal of Satellite Communications and Networking, 30*(5), 212-220. doi:10.1002/sat.1013

Lim, M. K. (2002). Cosmic rays: are air crew at risk? *Occupational and Environmental Medicine, 59*(7), 428-432. doi:10.1136/oem.59.7.428

Liu, Y. L., & Chuo, T. W. (2013). Self-healing polymers based on thermally reversible Diels-Alder chemistry. *Polymer Chemistry, 4*(7), 2194-2205. doi:10.1039/c2py20957h

Malkapur, S. M., Divakar, L., Narasimhan, M. C., Karkera, N. B., Goverdhan, P., Sathian, V., & Prasad, N. K. (2017). Neutron radiation shielding properties of polymer incorporated self compacting concrete mixes. *Applied Radiation and Isotopes, 125*, 86-93. doi:http://dx.doi.org/10.1016/j.apradiso.2017.03.029

McElroy, C. T. (1995). A SPECTRORADIOMETER FOR THE MEASUREMENT OF DIRECT AND SCATTERED SOLAR IRRADIANCE FROM ON-BOARD THE NASA ER-2 HIGH-ALTITUDE RESEARCH AIRCRAFT. *Geophysical Research Letters, 22*(11), 1361-1364. doi:10.1029/95gl01391

Mesbahi, A., Alizadeh, G., Seyed-Oskoee, G., & Azarpeyvand, A.-A. (2013). A new barite–colemanite concrete with lower neutron production in radiation therapy bunkers. *Annals of Nuclear Energy, 51*, 107-111. doi:http://dx.doi.org/10.1016/j.anucene.2012.07.039

Mourad, H. M., Al-Bassiouni, A. A. M., Emam, S. S., & Al-Hussaini, E. K. (2001). Generalized performance evaluation of Low Earth Orbit satellite systems. *Ieee Communications Letters, 5*(10), 405-407. doi:10.1109/4234.957376

Müller, A. H., & Matyjaszewski, K. (2010). Controlled and Living Polymerizations. In: Wiley Online Library.

Murphy, E. B., Bolanos, E., Schaffner-Hamann, C., Wudl, F., Nutt, S. R., & Auad, M. L. (2008). Synthesis and characterization of a single-component thermally remendable polymer network: Staudinger and Stille revisited. *Macromolecules, 41*(14), 5203-5209. doi:10.1021/ma800432g

Namouchi, F., Smaoui, H., Fourati, N., Zerrouki, C., Guermazi, H., & Bonnet, J. J. (2009). Investigation on electrical properties of thermally aged PMMA by combined use of FTIR and impedance spectroscopies. *Journal of Alloys and Compounds, 469*(1–2), 197-202. doi:http://doi.org/10.1016/j.jallcom.2008.01.148

Neuser, S., Michaud, V., & White, S. R. (2012). Improving solvent-based self-healing materials through shape memory alloys. *Polymer, 53*(2), 370-378. doi:10.1016/j.polymer.2011.12.020

Nikolaidis, A. K., Achilias, D. S., & Karayannidis, G. P. (2011). Synthesis and Characterization of PMMA/Organomodified Montmorillonite Nanocomposites Prepared by in Situ Bulk Polymerization. *Industrial & Engineering Chemistry Research, 50*(2), 571-579. doi:10.1021/ie100186a

O'Brien, T. K., Fibers, A. C. D.-o. H. M., & Composites, T. (1991). *Composite Materials: Fatigue and Fracture (third Volume)*: ASTM.

Okno ELINT complex in Tajikistan is becoming Russian. (2006). Retrieved from http://enews.ferganews.com/article.php?id=1390

Okuno, K. (2005). Neutron shielding material based on colemanite and epoxy resin. *Radiation Protection Dosimetry, 115*(1-4), 258-261. doi:10.1093/rpd/nci154

Orman, F., & Altınten, A. (2017). Sıcaklık kontrolü ile polistiren/kil nanokompozit sentezi ve karakterizasyonu. *Journal of the Faculty of Engineering and Architecture of Gazi University, 32*(2), 303-312.

Park, J. S., Darlington, T., Starr, A. F., Takahashi, K., Riendeau, J., & Hahn, H. T. (2010). Multiple healing effect of thermally activated self-healing composites based on Diels-Alder reaction. *Composites Science and Technology, 70*(15), 2154-2159. doi:10.1016/j.compscitech.2010.08.017

Patel, M. R. (2005). *Spacecraft power systems*. Boca Raton: CRC Press.

Pohl, L., & Britt, D. T. The radiation shielding potential of CI and CM chondrites. *Advances in Space Research*. doi:http://dx.doi.org/10.1016/j.asr.2016.12.028

Qu, X., Guan, T., Liu, G., She, Q., & Zhang, L. (2005). Preparation, structural characterization, and properties of poly (methyl methacrylate)/montmorillonite nanocomposites by bulk polymerization. *Journal of Applied Polymer Science, 97*(1), 348-357.

Ramesh, S., & Ang, G. P. (2010). Impedance and FTIR studies on plasticized PMMA–LiN(CF3SO2)2 nanocomposite polymer electrolytes. *Ionics, 16*(5), 465-473. doi:10.1007/s11581-009-0417-2

Ramesh, S., Leen, K. H., Kumutha, K., & Arof, A. K. (2007). FTIR studies of PVC/PMMA blend based polymer electrolytes. *Spectrochimica Acta Part A: Molecular and Biomolecular Spectroscopy, 66*(4–5), 1237-1242. doi:http://doi.org/10.1016/j.saa.2006.06.012

Sallı Bideci, Ö. (2016). The effect of high temperature on lightweight concretes produced with colemanite coated pumice aggregates. *Construction and Building Materials, 113*, 631-640. doi:https://doi.org/10.1016/j.conbuildmat.2016.03.113

Skorb, E. V., & Andreeva, D. V. (2013). Layer-by-Layer approaches for formation of smart self-healing materials. *Polymer Chemistry, 4*(18), 4834. doi:10.1039/c3py00088e

Slaba, T. C., Bahadori, A. A., Reddell, B. D., Singleterry, R. C., Clowdsley, M. S., & Blattnig, S. R. (2017). Optimal shielding thickness for galactic cosmic ray environments. *Life Sciences in Space Research, 12*, 1-15. doi:http://dx.doi.org/10.1016/j.lssr.2016.12.003

Swallowe, G. M. (1999). *Mechanical properties and testing of polymers : an A-Z reference*. Dordrecht ; Bosotn: Kluwer Academic.

Symolon, W. E. (2009). *High-Altitude Long Endurance UAVs vs Satellites Potential Benefits for U.S. Army Appications.* (Masters Masters), Masachusetts Institute of Technology,

Syrett, J. A., Becer, C. R., & Haddleton, D. M. (2010). Self-healing and self-mendable polymers. *Polymer Chemistry, 1*(7), 978-987. doi:10.1039/c0py00104j

Tabanli, S., Bilir, G., & Eryurek, G. (2017). Color tunable up-conversion emission from Er3+:Y2O3 nanoparticles embedded in PMMA matrix. *Journal of Luminescence, 182*, 146-153. doi:http://dx.doi.org/10.1016/j.jlumin.2016.10.009

Toohey, K. S., Sottos, N. R., Lewis, J. A., Moore, J. S., & White, S. R. (2007). Self-healing materials with microvascular networks. *Nature Materials, 6*(8), 581-585. doi:10.1038/nmat1934

Trask, R. S., Williams, G. J., & Bond, I. P. (2007). Bioinspired self-healing of advanced composite structures using hollow glass fibres. *Journal of the Royal Society Interface, 4*(13), 363-371. doi:10.1098/rsif.2006.0194

Uchihori, Y., Benton, E., Moeller, J., & Bendrick, G. (2003). Radiation measurements aboard NASA ER-2 high altitude aircraft with the Liulin-4J portable spectrometer. In D. F. Smart (Ed.), *Space Life Sciences: Structure and Dynamics of the Global Space Radiation Field at Aircraft Altitiudes* (Vol. 32, pp. 41-46). Kidlington: Pergamon-Elsevier Science Ltd.

Urban, M. W. (2012). Dynamic MaterialsThe chemistry of self-healing. *Nature Chemistry, 4*(2), 80-82. doi:10.1038/nchem.1249

Uysal, T., Mutlu, H. S., & Erdemoğlu, M. (2016). Effects of mechanical activation of colemanite (Ca2B6O11·5H2O) on its thermal transformations. *International Journal of Mineral Processing, 151*, 51-58. doi:https://doi.org/10.1016/j.minpro.2016.04.006

Vriezema, D. M., Aragones, M. C., Elemans, J., Cornelissen, J., Rowan, A. E., & Nolte, R. J. M. (2005). Self-assembled nanoreactors. *Chemical Reviews, 105*(4), 1445-1489. doi:10.1021/cr0300688

Waclawska, I., Stoch, L., Paulik, J., & Paulik, F. (1988). Thermal decomposition of colemanite. *Thermochimica Acta, 126*, 307-318.

Wang, H. P., Yuan, Y. C., Rong, M. Z., & Zhang, M. Q. (2010). Self-Healing of Thermoplastics via Living Polymerization. *Macromolecules, 43*(2), 595-598. doi:10.1021/ma902021v

Wang, X., Liu, F., Zheng, X. W., & Sun, J. Q. (2011). Water-Enabled Self-Healing of Polyelectrolyte Multilayer Coatings. *Angewandte Chemie-International Edition, 50*(48), 11378-11381. doi:10.1002/anie.201105822

Wang, Y. B., Joyce, H. J., Gao, Q. A., Liao, X. Z., Tan, H. H., Zou, J., . . . Jagadish, C. (2011). Self-Healing of Fractured GaAs Nanowires. *Nano Letters, 11*(4), 1546-1549. doi:10.1021/nl104330h

Was, G. S. (2007). *Fundamentals of radiation materials science : metals and alloys*. Berlin ; New York: Springer.

White, S. R., Sottos, N. R., Geubelle, P. H., Moore, J. S., Kessler, M. R., Sriram, S. R., . . . Viswanathan, S. (2001). Autonomic healing of polymer composites. *Nature, 409*(6822), 794-797. doi:10.1038/35057232

Wilkie, C. A., & Morgan, A. B. (2010). *Fire retardancy of polymeric materials* (2nd ed.). Boca Raton: CRC Press.

Williams, K. A., Dreyer, D. R., & Bielawski, C. W. (2008). The underlying chemistry of self-healing materials. *Mrs Bulletin, 33*(8), 759-765. doi:10.1557/mrs2008.162

Wu, D. Y., Meure, S., & Solomon, D. (2008). Self-healing polymeric materials: A review of recent developments. *Progress in Polymer Science, 33*(5), 479-522. doi:10.1016/j.progpolymsci.2008.02.001

Xiao, D. S., Yuan, Y. C., Rong, M. Z., & Zhang, M. Q. (2009). A Facile Strategy for Preparing Self-Healing Polymer Composites by Incorporation of Cationic Catalyst-Loaded Vegetable Fibers. *Advanced Functional Materials, 19*(14), 2289-2296. doi:10.1002/adfm.200801827

Yang, Y., & Dan, Y. (2003). Preparation of PMMA/SiO2 composite particles via emulsion polymerization. *Colloid and Polymer Science, 281*(8), 794-799. doi:10.1007/s00396-002-0845-2

Yang, Y., & Urban, M. W. (2013). Self-healing polymeric materials. *Chemical Society Reviews, 42*(17), 7446-7467. doi:10.1039/c3cs60109a

Yeh, J.-M., Liou, S.-J., Lin, C.-Y., Cheng, C.-Y., Chang, Y.-W., & Lee, K.-R. (2002). Anticorrosively enhanced PMMA− clay nanocomposite materials with quaternary alkylphosphonium salt as an intercalating agent. *Chemistry of Materials, 14*(1), 154-161.

Yu, D. R., & Lv, X. W. (2010). Configurations analysis for high-altitude/long-endurance airships. *Aircraft Engineering and Aerospace Technology, 82*(1), 48-59. doi:10.1108/00022661011028119

Zako, M., & Takano, N. (1999). Intelligent material systems using epoxy particles to repair microcracks and delamination damage in GFRP. *Journal of Intelligent Material Systems and Structures, 10*(10), 836-841. doi:10.1106/ye1h-qudh-fc7w-4qfm

Zhang, H. P., Zhang, P., Li, Z. H., Sun, M., Wu, Y. P., & Wu, H. Q. (2007). A novel sandwiched membrane as polymer electrolyte for lithium ion battery. *Electrochemistry Communications, 9*(7), 1700-1703. doi:http://doi.org/10.1016/j.elecom.2007.03.021

Zhang, L. Y., & Zhang, Y. F. (2016). In situ fast polymerization of graphene nanosheets-filled poly (methyl methacrylate) nanocomposites. *Journal of Applied Polymer Science, 133*(19).

Zhang, M. Q., & Rong, M. Z. (2011a). *Self-healing polymers and polymer composites*. Hoboken, N.J.: Wiley.

Zhang, M. Q., & Rong, M. Z. (2011b). *Self-healing polymers and polymer composites*: John Wiley & Sons.

Zhang, M. Q., & Rong, M. Z. (2012). Theoretical consideration and modeling of self-healing polymers. *Journal of Polymer Science Part B-Polymer Physics, 50*(4), 229-241. doi:10.1002/polb.22387

Zhang, Y., Broekhuis, A. A., & Picchioni, F. (2009). Thermally Self-Healing Polymeric Materials: The Next Step to Recycling Thermoset Polymers? *Macromolecules, 42*(6), 1906-1912. doi:10.1021/ma8027672

Zheng, P. W., & McCarthy, T. J. (2012). A Surprise from 1954: Siloxane Equilibration Is a Simple, Robust, and Obvious Polymer Self-Healing Mechanism. *Journal of the American Chemical Society, 134*(4), 2024-2027. doi:10.1021/ja2113257

Zhu, D. Y., Rong, M. Z., & Zhang, M. Q. (2015). Self-healing polymeric materials based on microencapsulated healing agents: From design to preparation. *Progress in Polymer Science, 49–50*, 175-220. doi:http://dx.doi.org/10.1016/j.progpolymsci.2015.07.002

ЗВЕЗДНЫЕ ВОЙНЫ НАЧИНАЮТСЯ В ПРЕДГОРЬЯХ ПАМИРА. (2014). Retrieved from http://www.trud.ru/article/12-03-2008/126754_zvezdnye_vojny_nachinajutsja_v_predgorjax_pamira.html

Россия прорубила новое «Окно» в космос. (2006). Retrieved from http://www.newizv.ru/world/2006-11-21/58560-rossija-prorubila-novoe-okno-v-kosmos.html

CURRICULUM VITAE

Name Surname :Tayfun BEL

Place and Date of Birth : Istanbul, 11-01-1981

E-Mail : tayfun@tayfunbel.com

EDUCATION **:**

- **B.Sc.:** 2007, ITU Faculty of Aeronautıcs and Astronautics, Meteorological Engineering Department
- **M.Sc.:** 2010, Energy Science and Technology at Energy Institute, ITU

PROFESSIONAL EXPERIENCE AND REWARDS:

- Scientific and Technological Research Council of Turkey rewarded my Ph.D. thesis with 1001 (biggest of its kind class academic) research project. The project title is " The Development of Mechanical Performance of Multi-Scale Self-Healing Nanocomposite Radiation Shielding Material for the use in Aerospace Applications."
- Personally, rewarded by Scientific and Technological Research Council of Turkey.
- National Center for High-Performance Computing Center granted 100.000,00 CPU hours at GPGPU systems for the modeling mechanical behavior of self-healing materials. Finding and optimizing the crack tip and path within the material.
- Istanbul Technical University Scientific Research Coordination Centre grants Tayfun BEL for the project of investigation of high energy

PUBLICATIONS AND PRESENTATIONS ON THE THESIS:

<u>Papers Published in Peer Reviewed International Journals</u>

- **T. Bel**, Cüneyt Arslan, Nilgün Baydoğan, PMMA/Mikroküre/Montmorillonite Nanokompozit ve PMMA/Mikroküre/Halloysite Nanokompozitin Atom Transfer Radikal Polimerizasyon Tekniği ile Üretilmesi ve Mekanik Özelliklerinin Karşılaştırmalı Olarak İncelenmesi, Journal of the Faculty of Engineering and Architecture of Gazi University, 2017 (SCI Index in TUBITAK Journal List) (article in press).
- **T.Bel**, H. Cakar, N. Yahya, C.Arslan, N.Baydogan, Investigation of the Bubble Effect in Lightweight PMMA Polymer, Defect and Diffusion Forum, 2017.

- **T.Bel**, G. Ulku, N. Kizilcan, H. Cimenoglu, N. Yahya, and N. Baydogan, Production of microencapsulate glycidyl methacrylate with melamine formaldehyde resin shell materials, 4th Internatıonal Conference On Fundamental and Applied Sciences (ICFAS2016), 15-17th August 2016, Kuala Lumpur, Malaysia, Published Online: December 2016, Book Series: AIP Conference Proceedings, Article Number: 050028-1 – 5 (2016)
- **T.Bel**, N.Baydogan, H. Cimenoglu, (2014), Effect of Curing Ambient on Poly (Methacrylate) Living Polymer, International Journal of Mechanical and Production Engineering, Volume- 2, Issue- 3, pp. 55-57, Indexed: Directory of Research Journal Indexing (DRJI), Open Academic Journals Index (OAJI).

Papers Published in International Conference Abstract Books

- **T.Bel**, M.Muhammettursun, S.Ulag, M.Ba Dughaish, N. Yahya, H. Cimenoglu, N.Baydogan**,** 'Preparatıon And Characterızatıon Of Pmma/Graphene Nanoplatelets Polymer Nanocomposıte, 13th International Conference on Diffusion in Solids and Liquids - DSL2017, Mass Transfer, Heat Transfer, Microstructure & Properties, Nanodiffusion & Nanostructured Materials, Alternative Energy, Abstract Book, pp. 103-104, 26-30 June, 2017 – Vienna, Austria.
- **T.Bel**, H. Cakar, M.Muhammettursun, S.Ulag, M.Ba Dughaish, N. Yahya, H. Cimenoglu, N.Baydogan**,** Investigation of the Bubble Effect in Lightweight PMMA Polymer, 13th International Conference on Diffusion in Solids and Liquids - DSL2017, Mass Transfer, Heat Transfer, Microstructure & Properties, Nanodiffusion & Nanostructured Materials, Alternative Energy, Abstract Book, pp. 101, 26-30 June, 2017 – Vienna, Austria.
- **T.Bel**, M.Muhammettursun, S.Ulag, H. Cimenoglu, N.Baydogan, Physical Properties of Poly(Methyl Methacrylate)/Graphene Nanoplatelets Nanocomposite, NanoTR-13 2017 - 13th Nanoscience & Nanotechnology Conference, Abstract Book, GRAP OR-01-2840 pp. 144Antalya, Turkey, 2017.
- **T.Bel**, S.Ulag, M.Muhammettursun, H. Cimenoglu, N.Baydogan, Preparation and Characterization of PMMA/MWCNT Polymer Nanocomposite, NanoTR-13 2017 - 13th Nanoscience & Nanotechnology Conference, Abstract Book, TUBES P-07-2811, pp. 403, Antalya, Turkey, 2017.
- **T.Bel**, N.Baydogan, H. Çimenoglu, (2014), Effect of Curing Time on Poly (Methacrylate) Living Polymer, Proceedings Book of International Conference on Energy and Management-ICEM 2014, pp. 114, Istanbul.
- **T.Bel**, N.Baydogan, H. Cimenoglu, (2014), Production of PMMA via living polymer with ATRP method, 1st International Semiconductor Science and Technology Conference, (ISSTC-2014), pp.167, Istanbul.

International Books (Chapters in Books)

- **T.Bel**, Nilgun Baydogan, Huseyin Cimenoglu, (2015), Chapter 18, Effect of Curing Time on Poly(methacrylate) Living Polymer, Energy Systems and Management, Springer 2015, pp 193-198.